TU Delft

Delft University of Technology

The accommodation of martensitic phase transformation strains by the ferritic matrix in dual-phase steels

Atreya, V.

DOI
10.4233/uuid:b57a9199-45ef-40d4-a4ed-a9a124fb39ed

Publication date
2023

Document Version
Final published version

Citation (APA)
Atreya, V. (2023). *The accommodation of martensitic phase transformation strains by the ferritic matrix in dual-phase steels.* [Dissertation (TU Delft), Delft University of Technology]. https://doi.org/10.4233/uuid:b57a9199-45ef-40d4-a4ed-a9a124fb39ed

Important note
To cite this publication, please use the final published version (if applicable).
Please check the document version above.

Copyright
Other than for strictly personal use, it is not permitted to download, forward or distribute the text or part of it, without the consent of the author(s) and/or copyright holder(s), unless the work is under an open content license such as Creative Commons.

Takedown policy
Please contact us and provide details if you believe this document breaches copyrights.
We will remove access to the work immediately and investigate your claim.

This work is downloaded from Delft University of Technology.
For technical reasons the number of authors shown on this cover page is limited to a maximum of 10.

THE ACCOMMODATION OF MARTENSITIC PHASE TRANSFORMATION STRAINS BY THE FERRITIC MATRIX IN DUAL-PHASE STEELS

Vibhor ATREYA

THE ACCOMMODATION OF MARTENSITIC PHASE TRANSFORMATION STRAINS BY THE FERRITIC MATRIX IN DUAL-PHASE STEELS

Dissertation

for the purpose of obtaining the degree of doctor at Delft University of Technology by the authority of the Rector Magnificus, Prof.dr.ir. T.H.J.J. van der Hagen, chair of the Board for Doctorates to be defended publicly on Tuesday, 14 March, 2023 at 12.30 hours

by

Vibhor ATREYA

Master of Science in Mechanical Engineering,
Delft University of Technology, the Netherlands,

born in Meerut, India.

This dissertation has been approved by the promotors.

Composition of the doctoral committee:

Rector Magnificus,	chairperson
Prof. dr. M.J. Santofimia Navarro,	Delft University of Technology, promoter
Dr. ir. C. Bos,	Delft University of Technology, copromoter
Independent members:	
Prof. dr.-ing. U. Prahl,	TU Freiberg, Germany
Prof .dr. ir. L. Kestens,	U. Ghent, Belgium
Prof. dr. rer. nat. F. Roters,	MPIE, Germany
Dr. F. Maresca,	RUG, The Netherlands
Prof.dr.ir. J. Sietsma,	Delft University of Technology
Reserve member:	
Prof.dr.ir. J.M.C. Mol,	Delft University of Technology

This research was carried out under project number T17019j in the framework of the Research Program of the Materials innovation institute (M2i) (www.m2i.nl) supported by the Dutch government.







Printed by: ProefschriftMaken (www.proefschriftmaken.nl)

Cover by: Vibhor Atreya

Copyright © 2023 by Vibhor Atreya

ISBN 978-94-6384-424-6

An electronic version of this dissertation is available at
http://repository.tudelft.nl/.

CONTENTS

Summary **9**

Samenvatting **13**

1 Introduction **17**

2 Characterisation and modelling of transformation-induced deformation of ferrite: State of the Art **23**

2.1 Background . . . 24
2.2 Effect of microstructure on the mechanical behaviour of DP steels . . . 27
2.3 Experimental characterisation of transformation-induced deformation of ferrite . . . 28
2.3.1 Dislocation density measurement using transmission electron microscopy (TEM) . . . 28
2.3.2 Strain hardening estimation using hardness and micropillar compression tests . . . 29
2.3.3 Crystal orientation mapping using electron backscatter diffraction . . . 29
2.4 Modelling approaches . . . 31
2.4.1 Analytical modelling . . . 31
2.4.2 Numerical modelling . . . 33
2.5 Conclusions and Outlook . . . 37

3 Cellular automata modelling of transformation-induced plastic deformation of ferrite in dual-phase steels **45**

3.1 Introduction . . . 46
3.2 Simulation tools . . . 47
3.2.1 Cellular automata based microstructure generation . . . 47
3.2.2 Crystal plasticity based micromechanical simulations . . . 48
3.3 Simulation settings . . . 48
3.4 Results . . . 50
3.5 Discussion . . . 51
3.6 Capabilities of a combined microstructure evolution and micromechanical modelling framework . . . 53
3.7 Conclusions . . . 53

4 Influence of martensitic microstructural characteristics on transformation-induced deformation of ferrite **59**
4.1 Introduction . . . 60
4.2 Experiments . . . 61
4.3 Results and Discussion . . . 61
4.3.1 Microstructural Analysis . . . 61
4.3.2 Long range (type I) and Short-range (type II) deformation of ferrite grains . . . 63
4.3.3 Slip-transmission from martensite into ferrite grains . . . 66
4.3.4 Relative frequency of type I and type II deformations . . . 68
4.4 Conclusions . . . 70

5 Effect of the anisotropy of martensitic transformation on ferrite deformation in Dual-Phase steels **75**
5.1 Introduction . . . 76
5.2 Approach and theoretical models . . . 77
5.2.1 Analysis of the ferrite/martensite microstructure (Step 1) . . . 78
5.2.2 Prior austenite grain reconstruction (Step 2) . . . 78
5.2.3 Determination of martensitic transformation deformation (Step 3) . . . 80
5.2.4 Micromechanical calculation of transformation-induced strains in ferrite (Step 4) . . . 82
5.3 Analysis of a dp steel microstructure using the proposed method . . . 82
5.3.1 Experimental procedure . . . 82
5.3.2 Application . . . 83
5.4 Discussion . . . 88
5.5 Conclusions . . . 91

6 Influence of self-accommodation in martensite on the transformation-induced deformation of ferrite **97**
6.1 Introduction . . . 98
6.2 Experimental Procedure . . . 99
6.3 Theory and Modelling Procedure . . . 100
6.3.1 PAG Reconstruction . . . 100
6.3.2 Micromechanical simulations . . . 100
6.4 Results . . . 101
6.4.1 Experiments . . . 101
6.4.2 Modelling . . . 102
6.5 Discussion . . . 106
6.5.1 Influence of carbon content in martensite on transformation dilatation and shear magnitudes . . . 106
6.5.2 Increased self-accommodation due to higher variant density in large PAGs . . . 107

6.5.3 Effective transformation-deformation due to self- accommodation in martensite . . . 108
6.5.4 The role of martensite sub-structure in causing deformation of ferrite matrix . . . 108
6.5.5 Comparison of simulated strain fields with the experimentally observed deformation of ferrite grains . . . 109
6.6 Conclusions . . . 109

7 Conclusions **113**
7.1 Key Takeaways . . . 114
7.2 Application of this study . . . 115
7.3 Recommendations for future works . . . 116
7.3.1 Using finite-strain and crystal plasticity based micromechanical model . . . 116
7.3.2 Prior austenite grain reconstruction based on 3D EBSD measurements . . . 117
7.3.3 Local variations in transformation strain and orientation relationships based on the carbon content of martensite . . . 118

A Appendix **121**

Acknowledgements **123**

Curriculum Vitæ **125**

List of Publications **127**

List of Conference Presentations **129**

SUMMARY

Advanced high-strength steels (AHSS) are multiphase steels which provide higher strength with good workability than conventional steels. They allow the manufacturing of lighter vehicles while maintaining safety and performance. More than 60% of the total body weight of modern-day automotive vehicles is made of AHSS and approximately half of this share belongs to Dual-Phase (DP) steels. DP steels are thus an important class of AHSS, which after their introduction in the 1970s, continue to be the mainstay of the automotive industry even today with many questions regarding their properties still unanswered. This work is an attempt to model the accommodation of the martensitic phase transformation strains by ferritic matrix in Dual-Phase (DP) steels and is a step toward better understanding and prediction of the mechanical behaviour of DP steels.

This thesis begins with Chapter 1 presenting a brief history of steel development and elucidates how the work presented in this PhD thesis fits in the overall steel research & development parlance. The microstructure of DP steels consists of hard martensite embedded in a soft ferritic matrix. The martensite results from the phase transformation of austenite upon rapid cooling. The volume increase and shape change associated with this phase transformation is majorly accommodated in the DP microstructure by the deformation of the soft ferritic matrix surrounding the newly formed martensite. This transformation-induced deformation of ferrite influences the local properties of ferrite and thus the global mechanical behaviour of DP steels.

Chapter 2 presents a critical review of the experimental and modelling techniques employed in previous works to study the transformation-induced deformation of ferrite. Although research articles highlighting the significant influence of transformation-induced deformation of ferrite on the global mechanical properties of DP steels appeared in the literature as early as the 1970s, till date there does not exist a model which accurately predicts the extent of local transformation-induced deformation of ferrite. Direct experimental measurements of transformation-induced deformation of ferrite are made difficult by the fact that martensite has a complex hierarchical microstructure resulting from the progressive formation of several structural sub-units (called laths) oriented differently in space. Moreover, martensitic transformation is displacive and proceeds at the speed of sound. Hence it is difficult to capture the deformation of ferrite caused by individual sub-units of martensite microstructure.

Several attempts have been made in the past to model the transformation-induced deformation of ferrite. The analytical models usually assumed martensite morphology to

be spherical and phase-transformation deformation to consist of only isotropic volumetric expansion. Since real-life microstructures consist of complex morphologies and martensitic phase-transformation strain is anisotropic, the existing analytical models are not suitable for the accurate prediction of transformation-induced deformation of ferrite. More recently, numerical models were employed to simulate the transformation-induced deformation of ferrite. However, the shear component of martensitic phase transformation strain was not considered in the simulations, thus possibly resulting in an underestimation of the transformation-induced deformation of ferrite. Despite the limitations and the assumptions involved, these modelling studies provided sufficient proof that transformation-induced deformation of ferrite significantly affects the global mechanical behaviour of DP steels.

The transformation-induced deformation of ferrite is expected to vary as per the local microstructural characteristics of DP steel. Therefore, accurate modelling of transformation-induced deformation of ferrite is only possible if the local crystallographic, morphological and compositional characteristics of the microstructure and their evolution are known. For this, a Cellular-Automata-based microstructure evolution model is used for generating virtual DP microstructures. The model can track the aforementioned characteristics. The plastically deformed ferrite regions were introduced as dislocations-rich regions (called interphase layer) of strain hardened ferrite at ferrite/martensite interfaces. The uniaxial tensile test response of the virtual microstructure was simulated using a crystal plasticity-based micromechanical simulation package. The combined microstructure evolution and micromechanics modelling framework is presented in Chapter 3.

Despite the modelling capability, the challenge remained to ascertain the extent of transformation-induced deformation of ferrite and the mechanisms explaining how it is influenced by local microstructural characteristics. This is addressed in Chapter 4, which discusses the findings of an electron backscatter diffraction (EBSD) experiments-based study, which was performed with a focus on investigating the relationship between the crystallographic orientations of ferrite and martensite, and the transformation-induced deformation of ferrite.

It was found that the transformation-induced deformation observed in ferrite grains can be distinguished as either a type I long-range (LR) deformation that spans most of the ferrite grain, or a type II short-range (SR) deformation in the form of a deformed ferrite region adjacent to the ferrite/martensite phase boundary. When prior austenite grain size (PAGS) is small, austenite may transform into a martensitic variant having a (110) close-packed plane-parallel (CPPP) relationship with neighbouring ferrite. This enables effective relaxation of transformation stresses by relatively easy deformation of ferrite via slip transmission and results in type I LR deformation. Type II SR deformation appears to be governed mostly by carbon content and degree of self-accommodation in martensite. This clearly showed that crystallographic orientations of ferrite and martensite variants play an important role in determining the extent of transformation-induced deformation

of ferrite.

Generally, the PAGS in DP steel microstructures is relatively small. Therefore, not all twenty-four martensite variants form out of a prior austenite grain (PAG). The modelling assumption that the martensitic transformation strain only involves isotropic dilatation, does not remain reasonable enough in the case of such small PAGS. The assumption of isotropic dilatation would imply that the shear deformation associated with the formation of martensitic variants, oriented differently in space, cancels each other out leaving only the unidirectional dilatation part for consideration in modelling studies. However, in the case of DP steels, the small prior austenite grain size (PAGS) allows only the formation of a few martensitic variants. This can be expected to result in sizeable shear strains which can not be neglected.

In Chapter 5, the disadvantages of simplifying the anisotropic transformation strain to isotropic dilatation are explained using a novel methodology comprising sequential experimental and numerical research on DP steels. This methodology combines the results of PAG reconstruction, phenomenological theory of martensite crystallography and electron backscatter diffraction orientation data to estimate variant-specific transformation deformation. Subsequently, the results of full-field micromechanical calculations on a virtual DP steel microstructure are compared with experimental EBSD kernel average misorientation and geometrically necessary dislocation measurement results. It is shown that neglecting the shear deformation associated with the martensitic transformation leads to significant underestimation in the prediction of transformation-induced strains in ferrite.

Chapter 6 investigates the influence of self-accommodation by martensite variant formation on transformation-induced deformation of ferrite via micromechanical modelling and verified using published EBSD experimental data. The results of the calculations revealed that the average von-Mises equivalent strain in ferrite decreases as more and more variants form from a PAG and reaches a minimum when all twenty-four variants form. An increase in the number of variants leads to a more localised strain field in ferrite. This is because of a decrease in the effective shear magnitude of the PAG, which cancels out completely when all twenty-four variants are formed.

Finally, Chapter 7 presents the key takeaways from the study. Possible applications of this study are also discussed and future research paths are suggested. This PhD thesis provides fresh perspectives to bridge the gaps in our understanding of transformation-induced deformation of ferrite. The scientific findings can be used for developing predictive tools for studying the mechanical behaviour of not only DP steels but any multiphase steels which exhibit plastic accommodation and residual stresses in their microstructure due to martensitic phase transformation.

SAMENVATTING

Geavanceerd hoge sterkte staal (AHSS) bestaat uit meerdere fases die samen sterker en beter vervormbaar zijn dan conventioneel staal. Dit staat de productie van lichtere voertuigen toe, terwijl de veiligheid en prestatie zijn gewaarborgd. Meer dan 60% van het totale gewicht van moderne voertuigen bestaat uit AHSS en ongeveer de helft daarvan is twee fase staal (DP). DP staal is dus een belangrijke groep binnen AHSS, die sinds zijn introductie in de jaren '70 nog steeds de hoeksteen van de automobielindustrie vormt. Er zijn nog steeds veel onbeantwoorde vragen over de eigenschappen van DP staal. Dit werk is een poging om de accommodatie in een ferritische matrix van de vervorming door de martensitische transformatie te modelleren. Daarnaast is dit werk een stap richting verdieping in kennis over en voorspelling van het mechanische gedrag van DP staal.

Dit proefschrift begint met hoofdstuk 1, dat een korte geschiedenis van de ontwikkeling van staal geeft. Daarnaast wordt verduidelijkt hoe dit proefschrift past in de algemene wetenschappelijk discussie met betrekking tot onderzoek en ontwikkelingen op het gebied van staal. De microstructuur van DP bestaat uit hard martensiet ingebed in een zachte ferritische matrix. Martensiet is het resultaat van een faseovergang van austeniet na snelle afkoeling. De volume-toename en vormverandering die daarbij horen, worden grotendeels geaccommodeerd in de DP microstructuur door de vervorming van de zachte ferritische matrix rondom nieuw gevormd martensiet. Deze door de transformatie veroorzaakte rekken in ferriet beïnvloeden lokale eigenschappen en dus het geobserveerde mechanische gedrag van DP staal.

Hoofdstuk 2 presenteert een kritisch overzicht van de experimentele en modelleer technieken in eerdere werken door de transformatie veroorzaakte rekken in ferriet bestuderen. Hoewel de eerste literatuur waarin het belang van de invloed van transformatie veroorzaakte rekken op de geobserveerde mechanische eigenschappen van DP beschreven wordt al in de jaren '70 verscheen, bestaat er tot nu toe geen model dat de omvang van lokale transformatie veroorzaakte rekken in ferriet nauwkeurig voorspelt. Directe experimentele meting van transformatie veroorzaakte rekken in ferriet wordt bemoeilijkt door het feit dat martensiet een complexe, hiërarchische microstructuur heeft. Dit is het resultaat van de progressieve vorming van verschillende structurele subeenheden ("laths" genaamd) met een variërende globale morfologie. Bovendien voltrekt de martensitische transformatie zich met de snelheid van het geluid. Het is daarom moeilijk om de rekken in het ferriet door individuele martensitische eenheden te observeren.

Er zijn verschillende pogingen gedaan om de transformatie veroorzaakte vervorming

van ferriet te modelleren. Analytische modellen nemen gewoonlijk aan dat martensiet bolvormig is en de fasetransformatie alleen bestaat uit isotrope expansie. Omdat de microstructuur in de werkelijkheid complexe morfologieën bevat en de martensitische transformatie rek anisotropisch is, zijn de bestaande analytische modellen niet geschikt voor de nauwkeurige voorspelling van de transformatie veroorzaakte rekken in ferriet. Recenter worden numerieke modellen ingezet om de transformatie veroorzaakte rekken in ferriet te simuleren. Echter, de afschuifcomponent van de martensitische transformatie rek wordt in deze simulaties niet betracht. Dit leidt mogelijk tot onderschatting van de transformatie veroorzaakte vervorming van ferriet. Desondanks hebben deze studies voldoende bewijs geleverd dat de transformatie veroorzaakte rekken in ferriet merkbaar invloed hebben op het geobserveerde mechanische gedrag van DP staal.

De vervorming van ferriet veroorzaakt door transformaties kan afhangen van de plaatselijke microstructuur eigenschappen van DP staal. Daarom is het nauwkeurig modelleren van de vervorming in ferriet door deze transformatie alleen mogelijk als de plaatselijke kristalstructuur, korrelvorm en samenstelling van de microstructuur, en hun evolutie bekend is. Daarom wordt een “Cellular-Automata” model van de evolutie van de microstructuur gebruikt om synthetische microstructuren van DP staal te genereren. Het model beschrijft de evolutie van de voorgenoemde microstructuur kenmerken. De plastisch vervormde regio's in ferriet worden geïntroduceerd als dislocatierijke lagen (’fasegrensvlak lagen’ genaamd) van verhard ferriet op de ferriet/martensiet grensvlakken. Enkele richtingstrekproeven van de virtuele microstructuren zijn gesimuleerd met behulp van een op ”crystal plasticity”-gebaseerd micromechanicsa simulatiepakket. Het gecombineerde raamwerk voor microstructuur evolutie en micromechanicamodel beschrijving wordt gepresenteerd in hoofdstuk 3.

Ondanks alles wat modellen kunnen blijft het een uitdaging om de omvang van transformatie-geïnduceerde rek van ferriet vast te stellen. Daarnaast moeten de verantwoordelijke mechanismes, en hoe deze beïnvloed worden door lokale microstructuur kenmerken, bepaald worden. Dit wordt behandeld in hoofdstuk 4 dat de bevindingen bespreekt van een onderzoek door middel van ”electron backscatter diffraction” (EBSD) experimenten. Het onderzoeksdoel is om de relatie tussen de kristal oriëntatie van ferriet en martensiet, en de transformatie-geïnduceerde rek in ferriet te onderzoeken.

Het is gebleken dat de transformatie-geïnduceerde vervorming gemeten in ferritische korrels kan worden gecategoriseerd in: type I lange-afstand (LR) vervorming die het grootste deel van het ferriet korrel bestrijkt; of, type II korte-afstand (SR) vervorming in de vorm van een vervormd ferriet volume aan het ferriet/martensiet grensvlak. Wanneer de initiële austenitische korrelgrootte (PAGS) klein is, kan austeniet transformeren in een martensitische variant met een (110) “parallelle dicht gestapelde vlakken” (CPPP) relatie met naburig ferriet. Hierdoor kan een directe transformatiespanningsreductie gerealiseerd worden door relatief makkelijke ferriet deformatie geïnduceerd door slip overdracht. Dit resulteert in type I LR vervorming. Type II SR vervorming hangt vooral af

van het koolstofgehalte en de mate van zelfaccommodatie in martensiet. Dit laat duidelijk zien dat de kristal oriëntatie van ferriet- en martensiet varianten een belangrijke rol spelen bij het bepalen van het bereik van de transformatie-geïnduceerde rekken in ferriet.

Over het algemeen zijn PAGSs in DP staal relatief klein. Daarom vormen niet alle vierentwintig martensiet varianten zich uit een initiële austenitische korrel (PAG). De modelaanname dat de martensitische transformatie rekken alleen uit isotrope expansie bestaat is onredelijk in kleine PAGS. De aanname van isotrope expansie zou betekenen dat de afschuivingen die samenhangen met de vorming van de martensiet varianten met verschillende oriëntaties, elkaar opheffen. Alleen expansie is dan van belang in model studies. Maar bij DP staal staat de kleine PAGS slechts de vorming van enkele varianten toe. Het is te verwachten dat dit resulteert in aanmerkelijke afschuiving die niet veronachtzaamd mag worden.

Hoofdstuk 5 beschrijft de beperking van het vereenvoudigen van de anisotrope transformatie tot isotrope uitzetting met behulp van een nieuwe methodologie. Deze methodologie bestaat uit experimenteel en opvolgend numeriek onderzoek in DP staal. Dit combineert de resultaten van PAG-reconstructie, fenomenologische theorie van martensiet kristallografie en oriëntaties uit EBSD metingen om de variant-specifieke transformatie rekken te schatten. Vervolgens worden de resultaten van ”full-field” micromechanische berekeningen op een virtuele DP microstructuur vergeleken met experimentele EBSD misorientatie en geometrische dislocatie metingen. Hieruit blijkt dat het niet in acht nemen van de afschuiving, geassocieerd met de martensitische transformatie, leidt tot een aanmerkelijke onderschatting van de transformatie-geïnduceerde rekken in ferriet.

Hoofdstuk 6 onderzoekt de invloed van zelfaccommodatie via de vorming van martensiet varianten op de rekken in ferriet door middel van een micromechanisch model. Deze invloed is geverifieerd met gepubliceerde EBSD data. Uit berekeningen blijkt dat de gemiddelde von-Mises equivalente rek in ferriet afneemt naarmate er meer varianten uit een gegeven PAG ontstaan. De equivalente rek minimaliseert met alle vierentwintig varianten. Een toename in het aantal varianten leidt tot meer lokale vorming van rek in ferriet. Dit komt door een afname van de effectieve afschuiving in de PAG, die volledig verdwijnt wanneer alle vierentwintig varianten zich vormen.

Tot slot presenteert hoofdstuk 7 de belangrijkste bevindingen van het onderzoek. Mogelijke toepassingen worden besproken en toekomstige onderzoeksrichtingen worden gesuggereerd. Dit proefschrift biedt nieuwe inzichten om de gaten in onze kennis van de transformatie-geïnduceerde rekken in ferriet te overbruggen. De wetenschappelijke bevindingen kunnen worden gebruikt om voorspelling te maken in studies van het mechanische gedrag van niet alleen DP staal; maar ook in elke ander meer-fase staal dat plastische accommodatie en residuele spanningen vertoont in diens microstructuur als gevolg van de martensitische fasetransformatie.

1

Introduction

Who really knows, and who can swear,
How creation came, when or where!
Even gods came after creation's day,
Who really knows and who can truly say,
When and how did creation start?
Did He do it? Or did He not?
Only He, up there, knows, maybe;
Or perhaps, not even He.

-Rig Veda 10:129

"The task is ... not so much to see what no one has yet seen;
but to think what nobody has yet thought,
about that which everybody sees."

-Erwin Schrodinger

The curiosity of humankind has known little bounds. Their relentless pursuit to gain a greater understanding of nature has unravelled great discoveries over thousands of years. Many of those discoveries were so revolutionary that they changed the course of human history and form the bedrock of modern-day society. The story of steel, the world's most important engineering material, shares similar attributes. It was rather a chance discovery by ancient blacksmiths, who found that iron hardens by absorbing carbon when left in charcoal furnaces. Now in the 21st century, a relative of the same carbon-containing iron, commonly called steel, finds utility in innumerable modern-day applications.

The history of steel can be understood by tracing the evolution of iron usage in different parts of the world. The use of wrought iron began in Mesopotamia and Anatolia in the 3rd millennium BCE, marking the beginning of the iron age [1]. Wrought iron is almost pure iron, malleable and tough. By the 8th century BCE, iron castings began to be produced regularly in China [1]. Cast iron contains 2-4 wt.% carbon and is hard and brittle. In southern India, an outstanding grade of steel called 'wootz steel' was first produced in the 4th century BCE and was used by middle-eastern blacksmiths to produce unprecedented steel weaponry known as 'Damascus steel' [2]. Steel generally contains 0.2-2 wt.% of carbon and has a superior combination of strength and ductility than both wrought and cast iron.

Blast furnaces began to be used in Europe for large-scale production of cast iron in the 12th century CE [1]. However, the impetus for the mass production of steel came from the invention of Bessemer's process in 1856 [3]. Since then, the steelmaking process has seen remarkable progress. The key feature of Bessemer's and all subsequent steelmaking processes is the removal of carbon and other elements by oxidation to obtain liquid iron with desired composition [4]. With the immense diversity of microstructures that can be produced, steel continues to meet the ever-increasing demands from several industries utilising steel in a variety of applications.

The second half of the 20th century saw a rapid increase in the application-specific microstructure design of steels. Most of the development was geared towards achieving higher corrosion resistance, tensile strength, ductility and fracture toughness. Figure 1.1 shows the global formability diagram (2021) [5], popularly known as the 'banana diagram', which classifies different steel grades depending upon their tensile strength and percentage elongation (ductility) into the following categories: (i) Conventional steels (ii) 1st (iii) 2nd and (iv) 3rd generation of advanced high strength steels (AHSS).

Conventional steels primarily contain ferrite, with some pearlite present occasionally. AHSS are multiphase steels containing one or more phases apart from ferrite, cementite and pearlite. The development of AHSS was majorly fuelled by the automotive industry as they provide much higher strength with good workability than conventional steel [6], thus allowing the manufacturing of lighter vehicles while maintaining safety and performance.

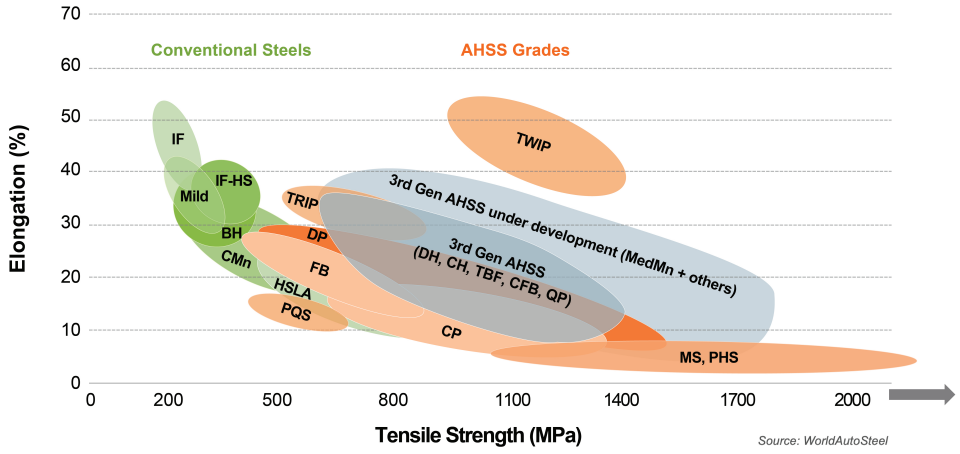

Figure 1.1: Global formability diagram 2021.

More than 60% of the total body weight of modern-day automotive vehicles is made of AHSS, with more than 30% made of Dual-phase (DP) steels [7]. DP steels belong to the 1st generation of AHSS [4], whereas the 2nd and 3rd generations of AHSS contain steel grades such as twinning induced plasticity (TWIP) steels, quenched and partitioned (Q&P) steels and carbide-free bainitic (CFB) steel.

The motive behind the development of successive generations of steel grades has been to impart high strength and large ductility to steels, at a reasonable cost. Much of the current efforts in the research and development of formable steels concern the 3rd generation of AHSS. Although there has been substantial advancement in our understanding of DP steels since their introduction in the 1970s [8], they continue to be the mainstay of the automotive industry even today with many fundamental questions regarding their properties still unanswered.

The microstructure of DP steels consists of hard martensite embedded in a soft ferrite matrix, which provides them with the combination of good strength and ductility for which they are widely known [9]. The DP steels are typically produced when steels kept at intercritical temperatures are rapidly cooled. The steel microstructure at an intercritical temperature consists of the ferrite and austenite phases. Rapid cooling causes a phase transformation from austenite to martensite resulting in a ferrite/martensite dual-phase microstructure.

The newly formed martensite has a higher volume and a different shape than the prior austenite [10]. Moreover, the formation of martensite occurs against the mechanical constraint imposed by the presence of ferrite in the surroundings. The transformation strain caused by volume and shape change must therefore be 'accommodated' in the

microstructure, majorly by the deformation of the softer ferrite matrix [11], [12]. This deformation alters the local mechanical properties of ferrite, which in turn influences the global mechanical properties of DP steel [13], [14].

A significant part of current research on DP steels is focused on creating models which accurately predict their performance during use in various applications. This helps in the development of advanced application-specific DP steel grades. Although research articles advocating the significant influence of transformation strain accommodation by ferrite on the global mechanical properties of DP steels appeared in the literature as early as the 1970s [15], till date there does not exist a model which accurately predicts the local variation in transformation-induced deformation of ferrite. Direct experimental measurement of transformation-induced deformation of ferrite is made difficult by the fact that the martensitic transformation is displacive and proceeds at the speed of sound.

Bridging the gaps in our understanding of transformation-induced deformation of ferrite needs fresh perspectives to improve existing experimental and modelling techniques. Through experiments and numerical modelling, this thesis identifies some crucial but commonly ignored aspects of martensitic microstructure and investigates their influence on the transformation-induced deformation of ferrite in DP steels.

In this thesis, Chapter 1 and 2 present a brief history of steel development and a review of the previous studies addressing characterisation and modelling of the transformation-induced deformation of ferrite in DP steels. In Chapter 3, a combined microstructure evolution and micromechanical modelling framework is presented to incorporate the effect of transformation-induced deformation of ferrite on overall mechanical behaviour of DP steels. The influence of local microstructure features on transformation-induced deformation of ferrite is investigated experimentally in Chapter 4. In Chapter 5, a sequential experimental and numerical research on DP steels is performed to estimate the deformation of ferrite grains induced by formation of various martensitic variant in their neighbourhood. In Chapter 6, the influence of self-accommodation by martensite variant formation on transformation-induced deformation of ferrite is investigated via micromechanical modelling and verified using published experimental research data. Finally, Chapter 7 presents the key takeaways from the study. Furthermore, practical applications of this study are discussed and future research paths are also suggested.

REFERENCES

[1] D. M. Stefanescu, "A History of Cast Iron," *Cast Iron Science and Technology*, vol. 1A, no. October, pp. 3–11, 2018. DOI: 10.31399/asm.hb.v01a.a0006320.

[2] S. Srinivasan and S. Ranganathan, *India's Legendary Wootz Steel*. Universities Press India Private Limited, 2013, ISBN: 8173717214.

[3] J. M. Swank, *History of the Manufacture of Iron in All Ages*. Cambridge University Press, 1892, ISBN: 9780511795374.

[4] G. Krauss, *Steels: processing, structure, and performance*, Second Edi. Materials Park, Ohio: ASM International, 2015, ISBN: 9781627080835. DOI: 10.5860/choice.43-6550.

[5] "Defining Steels - AHSS Guidelines," Tech. Rep. [Online]. Available: https://ahssinsights.org/metallurgy/defining-steels/.

[6] N. Baluch, Z. M. Udin, and C. S. Abdullah, "Advanced high strength steel in auto industry: an Overview," *Engineering, Technology & Applied Science Research*, vol. 4, no. 4, pp. 686–689, 2014, ISSN: 2241-4487. DOI: 10.48084/etasr.444.

[7] C. Du, J. P. Hoefnagels, S. Kölling, M. G. Geers, J. Sietsma, R. Petrov, V. Bliznuk, P. M. Koenraad, D. Schryvers, and B. Amin-Ahmadi, "Martensite crystallography and chemistry in dual phase and fully martensitic steels," *Materials Characterization*, vol. 139, no. October 2017, pp. 411–420, 2018, ISSN: 10445803. DOI: 10.1016/j.matchar.2018.03.011.

[8] W. G. Brazier and R. Stevenson, "Evaluation of a new, dual phase, cold rolled steel - Formability," *SAE Transactions*, vol. 87, pp. 544–551, 1978, ISSN: 26883627. DOI: 10.4271/780137.

[9] A. Nakagawa and G. Thomas, "Microstructure-mechanical property relationships of Dual-Phase steel wire," *Metallurgical Transactions A*, vol. 16A, pp. 831–840, 1985.

[10] J. S. Bowles and J. K. Mackenzie, "The crystallography of martensite transformations I," *Acta Metallurgica*, vol. 2, no. 1, pp. 129–137, 1954, ISSN: 00016160. DOI: 10.1016/0001-6160(54)90102-9.

[11] D. A. Korzekwa, D. K. Matlock, and G. Krauss, "Dislocation substructure as a function of strain in a dual-phase steel," *Metallurgical Transactions A*, vol. 15, no. 6, pp. 1221–1228, 1984, ISSN: 03602133. DOI: 10.1007/BF02644716.

[12] U. Liedl, S. Traint, and E. A. Werner, "An unexpected feature of the stress-strain diagram of dual-phase steel," *Computational Materials Science*, vol. 25, no. 1-2, pp. 122–128, 2002, ISSN: 09270256. DOI: 10.1016/S0927-0256(02)00256-2.

[13] T. Sakaki, K. Sugimoto, and T. Fukuzato, "Role of internal stress for the initial yielding of Dual-Phase steels.," *Acta Metallurgica*, vol. 31, pp. 455–460, 1983. DOI: 10.1016/b978-1-4832-8423-1.50076-6.

[14] D. L. Bourell and A. Rizk, "Influence of martensite transformation strain on the ductility of dual-phase steels," *Acta Metallurgica*, vol. 31, no. 4, pp. 609–617, 1983, ISSN: 00016160. DOI: 10.1016/0001-6160(83)90051-2.

[15] R. G. Davies, "Early stages of yielding and strain aging of a Vanadium-containing Dual-Phase steel," *Metallurgical Transactions A*, vol. 10A, 1979. DOI: https://doi.org/10.1007/BF02812021.

2

Characterisation and modelling of transformation-induced deformation of ferrite: State of the Art

This chapter is based on the scientific article: V. Atreya, C. Bos, and M. J. Santofimia, "Characterisation and modelling of transformation-induced deformation of ferrite: A Review." (To be submitted).

Ferrite-martensite dual-phase (DP) steels offer a good combination of strength and ductility due to a microstructure consisting of hard martensite embedded in a soft ferritic matrix. The martensite is formed via the phase transformation of austenite during quenching. The volume increase and shape change accompanying the phase transformation are accommodated by the deformation of the surrounding ferrite matrix in DP steels, generating high stresses and dislocation densities. Transformation-induced deformation of ferrite affects the subsequent mechanical behaviour of DP steels. Hence, for the rapid development of DP steels with application-specific mechanical properties, it is pertinent to experimentally characterise the transformation-induced deformation of ferrite and develop models to estimate the same. The experimental characterisation is usually performed using techniques such as transmission electron microscopy, electron backscatter diffraction and hardness measurement. Modelling techniques include analytical and numerical modelling, where the numerical modelling approaches consist of representative volume element-based computational micromechanics and phase-field modelling. A critical review of the aforementioned experimental and modelling techniques is presented herewith. Gaps in the understanding of transformation-induced deformation of ferrite are also discussed, along with the scope of further research.

2.1. BACKGROUND

DP steels generally constitute more than 30 wt.% of an automotive vehicle's body structure [1] and are used in the manufacturing of automotive parts such as dash cross member, A-pillar, B-pillar, front rail closeout, and roof structures [2], [3]. The reason for the widespread use of DP steels in the automotive industry is that they provide a good combination of strength and ductility due to their microstructure, in which 10-40 vol.% of the hard martensitic phase is dispersed in a soft ferrite matrix [4]–[6].

Martensite in DP steels forms upon phase transformation of austenite during quenching. The martensitic transformation is displacive and involves a macroscopic volume increase and shape change in the form of unidirectional dilatation perpendicular to the habit plane (also called the invariant plane of transformation) and shear parallel to the habit plane respectively, as schematically shown in figure 2.1(a) [7]. This volume increase and shape change is accommodated in the microstructure by the deformation of the ferrite matrix surrounding the martensite.

The microstructure of martensite is hierarchical. The basic structural unit in low-carbon martensite, called lath, can have one of the 24 Kurdjumov-Sachs (K-S) spatial orientations known as variants. Figure 2.1(b) is a schematic showing the hierarchical microstructure of martensite. The laths arrange themselves in groups called sub-blocks, blocks and packets depending on their orientation [8], [9]. Table 2.1 describes all 24 K-S variant orientations and the corresponding closed packed/bain group [10]. The formation of every martensitic variant involves the macroscopic volume increase and shape change shown in figure 2.1(a).

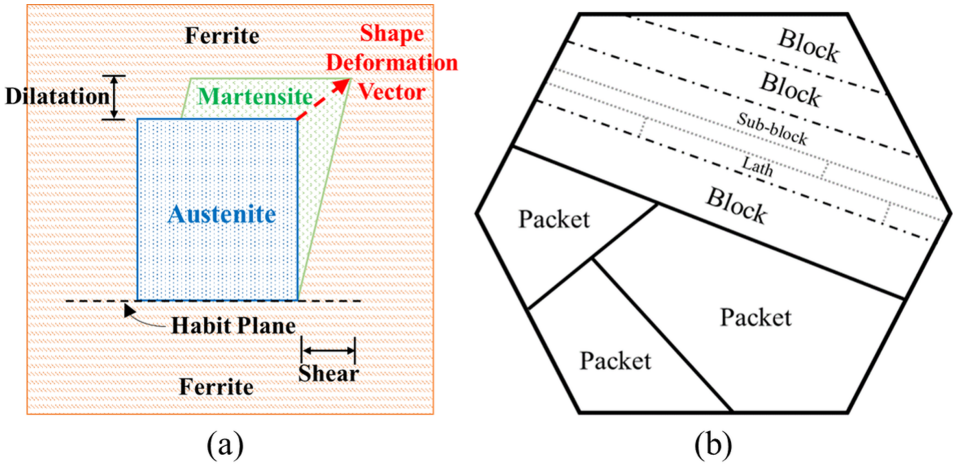

Figure 2.1: (a) A schematic showing the dilatation and shear involved in martensitic transformation (b) Hierarchical microstructure of martensite showing laths arranged in groups called sub-blocks, blocks and packets depending on spatial orientation.

Figure 2.2(a) shows a typical heat treatment schedule applied to an initial cold-rolled ferrite-pearlite microstructure to obtain the dual-phase microstructure. The heat treatment involves intercritical annealing between Ac1 and Ac3 temperatures, which are the critical temperatures indicating the start and finish of austenite formation during heating. During quenching, the martensitic transformation begins at the martensite start (M_s) temperature and progresses upon further cooling. The ferrite matrix undergoes deformation due to the progress of the martensite formation in this duration. This accommodation of the martensitic transformation gives rise to internal stresses in the microstructure. The stresses often exceed the elastic limit of ferrite locally, resulting in plastic flow and increased dislocation density in the ferrite regions near martensite [4], [11]–[13].

The transformation-induced deformation of ferrite can be considered as a pre-strain to which the ferrite is subjected before any external load is applied to the DP steel specimen. This pre-strain has a significant bearing on the mechanical behaviour of DP steels upon application of an external load. An earlier study reported that even at very low global strain values (10^{-6}), the dislocations in ferrite near inhomogeneities such as martensite can move relatively large distances ($> 60\,\mu$m) away from their source under localised stress concentrations [4].

Direct experimental measurements of transformation-induced deformation of ferrite either in the form of strains, stresses or accumulated dislocations in ferrite are rare. There are two reasons for this. First, martensite has a complex hierarchical microstructure resulting from the progressive formation of several structural sub-units oriented differently in space. Second, martensitic transformation is displacive and proceeds at the speed of

Table 2.1: Twenty-four martensite variants with the corresponding parallel planes and directions in the parent fcc austenite, along with the corresponding closed packed and bain groups [10]

Variant number	Plane parallel	Direction parallel	CP group	Bain group
V1	$(111)_\gamma \| \| (011)_\alpha$	$[\bar{1}01]_\gamma \| \| [\bar{1}\bar{1}1]_\alpha$	CP1	B1
V2		$[\bar{1}01]_\gamma \| \| [\bar{1}1\bar{1}]_\alpha$		B2
V3		$[01\bar{1}]_\gamma \| \| [\bar{1}\bar{1}1]_\alpha$		B3
V4		$[01\bar{1}]_\gamma \| \| [\bar{1}1\bar{1}]_\alpha$		B1
V5		$[1\bar{1}0]_\gamma \| \| [\bar{1}\bar{1}1]_\alpha$		B2
V6		$[1\bar{1}0]_\gamma \| \| [\bar{1}1\bar{1}]_\alpha$		B3
V7	$(1\bar{1}1)_\gamma \| \| (011)_\alpha$	$[10\bar{1}]_\gamma \| \| [\bar{1}\bar{1}1]_\alpha$	CP2	B2
V8		$[10\bar{1}]_\gamma \| \| [\bar{1}1\bar{1}]_\alpha$		B1
V9		$[\bar{1}\bar{1}0]_\gamma \| \| [\bar{1}\bar{1}1]_\alpha$		B3
V10		$[\bar{1}\bar{1}0]_\gamma \| \| [\bar{1}1\bar{1}]_\alpha$		B2
V11		$[011]_\gamma \| \| [\bar{1}\bar{1}1]_\alpha$		B1
V12		$[011]_\gamma \| \| [\bar{1}1\bar{1}]_\alpha$		B3
V13	$(\bar{1}11)_\gamma \| \| (011)_\alpha$	$[0\bar{1}1]_\gamma \| \| [\bar{1}\bar{1}1]_\alpha$	CP3	B1
V14		$[0\bar{1}1]_\gamma \| \| [\bar{1}1\bar{1}]_\alpha$		B3
V15		$[\bar{1}0[\bar{1}]_\gamma \| \| [\bar{1}\bar{1}1]_\alpha$		B2
V16		$[\bar{1}0\bar{1}]_\gamma \| \| [\bar{1}1\bar{1}]_\alpha$		B1
V17		$[110]_\gamma \| \| [\bar{1}\bar{1}1]_\alpha$		B3
V18		$[110]_\gamma \| \| [\bar{1}1\bar{1}]_\alpha$		B2
V19	$(11\bar{1})_\gamma \| \| (011)_\alpha$	$[\bar{1}10]_\gamma \| \| [\bar{1}\bar{1}1]_\alpha$	CP4	B3
V20		$[\bar{1}10]_\gamma \| \| [\bar{1}1\bar{1}]_\alpha$		B2
V21		$[0\bar{1}\bar{1}]_\gamma \| \| [\bar{1}\bar{1}1]_\alpha$		B1
V22		$[0\bar{1}\bar{1}]_\gamma \| \| [\bar{1}1\bar{1}]_\alpha$		B3
V23		$[101]_\gamma \| \| [\bar{1}\bar{1}1]_\alpha$		B2
V24		$[101]_\gamma \| \| [\bar{1}1\bar{1}]_\alpha$		B1

sound. Hence it is difficult to capture the deformation of ferrite caused by individual sub-units of martensite microstructure. Despite this, several attempts have been made in the past to measure and model the transformation-induced deformation of ferrite. This chapter collects and discusses experimental and modelling approaches previously used to understand the effect of martensitic transformation on the ferrite matrix in DP microstructures and, in general, on the overall mechanical behaviour of DP steels. Existing conceptual and technological challenges are also discussed, along with the scope of further research.

2.2. EFFECT OF MICROSTRUCTURE ON THE MECHANICAL BEHAVIOUR OF DP STEELS

The mechanical behaviour of steels is determined by the properties of the constituent phases and their interaction upon external loading. In this regard, several microstructural features play a key role in determining the mechanical behaviour of DP steels. The strength of DP steel increases as the ferrite or martensite grain size decreases [14]–[17], following the Hall-Petch relationship. For the same martensite volume fraction, finer DP microstructures exhibit higher work hardening rates and larger ductility limits [18], [19]. When the martensite volume fraction increases, the strength of DP steels increases [16], [20]–[22].

A comparison of flow curves of DP steel with other types of high-strength steel is shown in figure 2.2(b) [23]. The figure illustrates the important characteristics of a typical DP steel flow curve, namely, continuous yielding, low elastic limit, and high initial work hardening rate. These characteristics allow for a more uniform distribution of strain during the forming process, preventing any local thinning [24], [25]. DP steels provide larger formability at a high strength level than most steels.

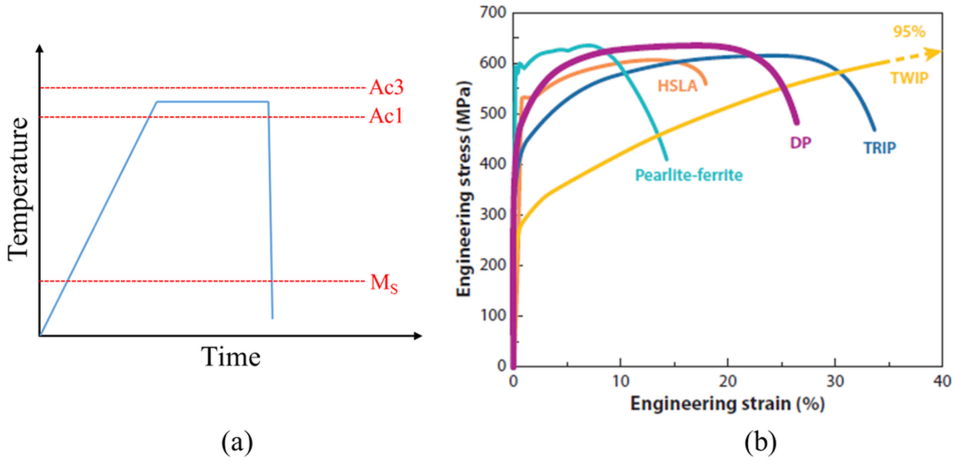

Figure 2.2: (a) Typical heat treatment schedule to obtain DP steel microstructure. (b) Comparison of flow curves of different types of steels: High-strength low-alloy (HSLA) steels, Pearlite-ferrite steels, Dual-Phase (DP) steels, Transformation-induced plasticity (TRIP) steels and Twinning-induced plasticity (TWIP) steels.

The aforementioned characteristics of the DP steel flow curve are closely linked to the transformation-induced deformation of ferrite [11]–[13], [26]. The process of accommodating newly formed martensite results in high stresses in the ferrite matrix which can easily exceed the elastic limit causing local plastic flow [4], [11]–[13], resulting in an increase in the yield strength of ferrite. High local elastic stresses persist in the ferrite matrix even after the plastic flow has ceased. A large amount of unpinned dislocations

are generated in the ferrite matrix due to plastic deformation [4], [27], [28].

With pre-existing local high elastic stresses in the ferrite matrix, the newly created unpinned dislocations need only a minor increment in local stresses to start moving. Usually, a small external load is sufficient to initiate local plastic deformation [4], [12], [13]. Thus the yielding of DP steels begins at stress levels much lower than the yield stress of constituent ferrite and it is difficult to locate a sharp yield point [12], [13]. The typical stress-strain curves of DP steels thus show continuously yielding.

2.3. EXPERIMENTAL CHARACTERISATION OF TRANSFORMATION-INDUCED DEFORMATION OF FERRITE

2.3.1. DISLOCATION DENSITY MEASUREMENT USING TRANSMISSION ELECTRON MICROSCOPY (TEM)

The transformation-induced deformation of ferrite can be observed using transmission electron microscopy (TEM) in the form of regions with high dislocation density in ferrite near phase boundaries as shown in figure 2.3(a) [29]. The dislocations are seen as thin thread-like structures and their density is highest near the phase boundary. Moving away from the phase boundary towards the ferrite grain interior reveals a drastic decrease in the dislocation density. Several previous studies have reported observing similar gradients of dislocation density [27], [28], [30], [31].

A few studies attempted to actually calculate the dislocation density using TEM micrographs [30], [31]. The dislocation density can be calculated by measuring the total dislocation line length in a unit volume of the crystal, providing an estimate in terms of length of $\frac{\mathrm{m}}{\mathrm{m}^3}$ [30]. Timokhina et al. [30] calculated the average dislocation density of ferrite in an intercritically annealed DP steel with 0.036 wt.% C and 15 vol.% martensite to be approximately 10^{14} m^{-2}. It was mentioned that the dislocation density near the phase boundary was higher than the aforementioned value. Cai et al. [31] estimated the dislocation density to be 10^{15} m^{-2} in the "tangles of highest density" within ferrite, for a DP steel with 0.11 wt.% C and 28.6 vol.% martensite.

It is difficult to compare dislocation densities reported in the aforementioned studies since the DP steel specimens they used had different carbon content, phase fractions and grain sizes. A drawback of using TEM measurements is that the specimens are very thin, and do not adequately represent the volume of the crystal. Moreover, TEM studies can only be performed on a relatively small area of interest ($< 1\ \mu$m). The observations therefore cannot be extended for the entire specimen, unless a large number of observations are made.

2.3.2. STRAIN HARDENING ESTIMATION USING HARDNESS AND MICROPILLAR COMPRESSION TESTS

The transformation-induced local plastic flow causes strain hardening of ferrite regions near phase boundaries. Figure 2.3(b) shows the micro-hardness measurements of four indents in a ferrite grain with increasing distance from martensite in a DP steel [32]. The hardness values continuously decrease with increasing distance from martensite.

Kadkhodapour et al.[33], through nano hardness measurements, reported that the strength of the deformed region was 75% higher than that of the ferrite matrix. However, Matsuno et al.[34], using the same technique, did not find any interfacial hardening of ferrite for a coarse-grain DP steel. All aforementioned works based on nano-hardness measurements showed in general considerable scatter due to the possible influences of other phase/grain boundaries, hidden martensite beneath the observed surface, or the difference in surface heights of ferrite and martensite [32], [34], [35].

Micropillar compression tests also reveal a higher strength of ferrite near martensite-ferrite phase boundaries. Using focused ion beam (FIB) milling, Armaki et al. [36] milled three small micropillars in a ferrite grain, one in the grain interior and two near the phase boundary. Compression tests on micropillars revealed that the grain interior was weaker. However, with few measurements, it is uncertain if the higher strength of the other two pillars was due to strain hardening caused by transformation-induced deformation, or a mere coincidence.

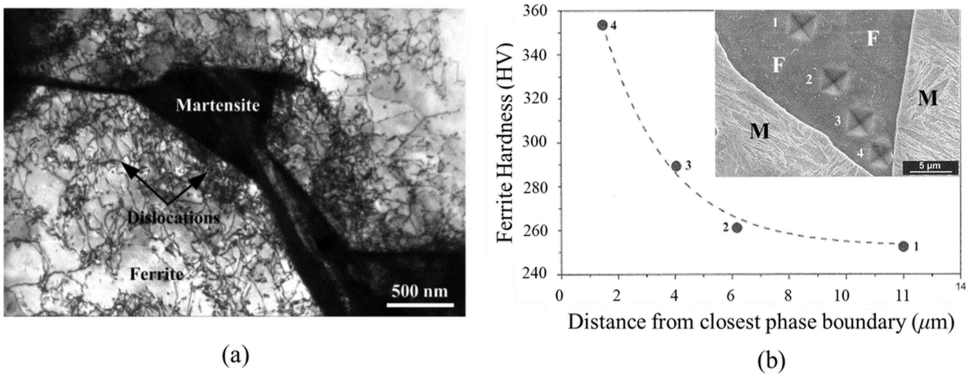

Figure 2.3: (a) Transmission electron microscopy (TEM) micrograph showing high dislocation density in ferrite close to martensite [29] (b) Decreasing hardness of ferrite matrix with increasing distance of nanoindents from the ferrite (F)/martensite (M) phase boundary [32].

2.3.3. CRYSTAL ORIENTATION MAPPING USING ELECTRON BACKSCATTER DIFFRACTION

Transformation-induced deformation of ferrite causes changes in the intra-grain unit-cell orientations. The difference in the unit-cell orientations of neighbouring points

within the ferrite grains can be estimated by electron backscatter diffraction (EBSD) measurements. EBSD provides information about the underlying unit cell orientation at every measurement point on the surface of the specimen. EBSD crystal orientation data can be used to calculate the misorientation metrics such as the Kernel Average Misorientation (KAM).

KAM is the average misorientation angle of nth nearest neighbours with respect to a measurement point in EBSD. The boundary formed by n^{th} nearest neighbours is called a kernel. Figure 2.4(a) shows 1st, 2nd and 3rd nearest neighbours cells used to calculate KAM using a hexagonal measurement grid. ω is the misorientation of the cell with respect to central hexagonal cell O in grey, and its superscript n represents the nth nearest neighbours used for calculation. The distance between two adjacent hexagonal cells is the measurement step size.

KAM is also often used to calculate geometrically necessary dislocation (GND) density in the qualitative study of transformation-induced deformation of ferrite grains [37], [38]. GNDs are the dislocations needed to maintain lattice continuity during deformation and account for the curvature of the grain [39]–[43]. As can be seen in figure 2.4(b), a non-uniform slip necessitates a curvature which is made possible by GNDs [44]. GNDs are different from statistically stored dislocations (SSDs) which are a result of random trappings of dislocations caused during uniform plastic strain. The simplest way to calculate GND density from KAM measurements is by using the model of Kubin and Mortensen [43]:

$$\rho_{GND} = \frac{2v}{ub}\,, \tag{2.1}$$

where ρ_{GND} is the GND density, v is the misorientation with respect to the neighbouring points, u is the distance between measurement points, and b is the magnitude of the Burgers vector. KAM can be used instead of v for calculating GND density.

Figures 2.5(a), 2.5(b) and 2.5(c) show the Image Quality (IQ), KAM and GND maps of a region containing ferrite-martensite phase boundaries in an intercritically annealed and quenched DP steel [37]. The ferrite grain is in the centre (light grey on IQ map), sharing a fraction of its boundary with martensite (black on IQ map). As expected, martensite has higher values of KAM and GND density. The ferrite grain shows a decreasing value of KAM and GND density along the arrow 'FM', indicating decreasing transformation-induced deformation going towards the ferrite grain interior. Such a trend is also reported in other EBSD-based studies [38], [45].

However, it has also been reported in the literature that in the case of coarse-grained DP steel, the deformation in ferrite grains near the ferrite-martensite phase boundary is so low that it could not be identified by KAM or GND maps [34], [45]. It was also noticed that some ferrite grains were deformed to a higher extent in their interior as well [34], [37],

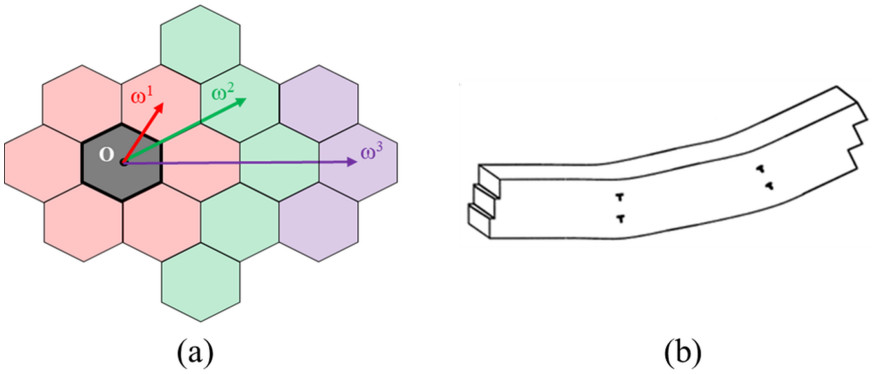

Figure 2.4: (a) 1st, 2nd and 3rd nearest neighbours used to calculate KAM; (b) GNDs facilitating the formation of curvature in a crystal [44].

[45]. Figure 2.5(d) shows the KAM map of a ferrite grain designated as 'F' showing such behaviour[45].

It should be noted that the calculated KAM and GND values are reasonably good for comparative analysis of transformation-induced deformation of ferrite among DP steel specimens of the same EBSD study. It is difficult to compare the values obtained from specimens belonging to different studies because the measurements depend on factors such as EBSD step size and the method employed to calculate KAM and GNDs which may differ among different studies.

2.4. MODELLING APPROACHES

The early experimental observations of transformation-induced deformation of ferrite near phase boundaries in DP steels led to the conjecture that the deformed ferrite must play a significant role in the overall mechanical behaviour of DP steels [4], [27], [28]. Several analytical models were developed to predict the mechanical behaviour of DP steels incorporating pre-existing stresses and strains in ferrite as a result of martensite formation. Constant improvements in computational power enabled fast solutions to numerical models for transformation-induced deformation. Henceforth, along with a brief description, the major advantages and disadvantages of relevant analytical and numerical models are discussed herewith.

2.4.1. ANALYTICAL MODELLING

DP steels can be considered a composite containing martensite particles with eigenstrain, embedded in a ferrite matrix. Eigenstrains are strains produced without external loads, such as during phase transformation or thermal expansion [46]. Considering martensite islands in DP steels as spherical particles, several authors estimated the deformation of

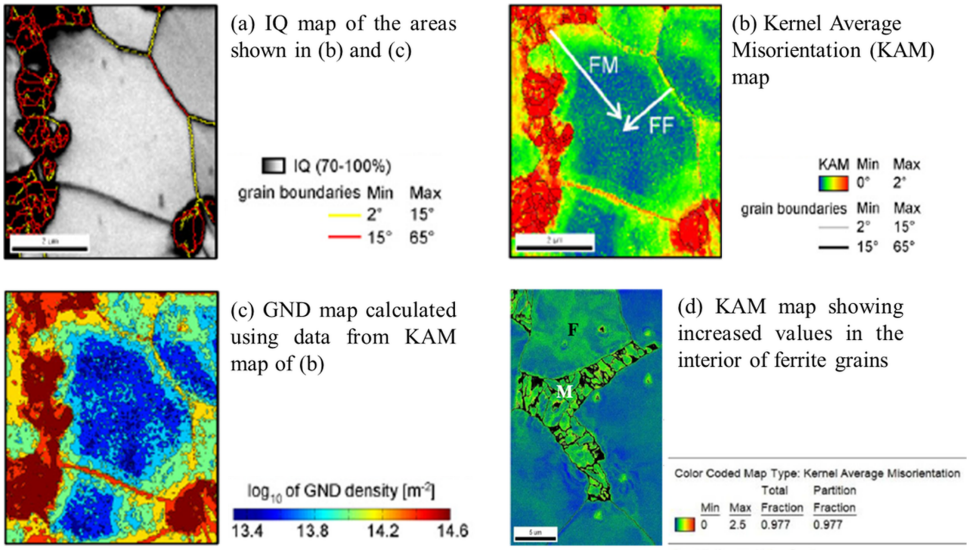

Figure 2.5: (a) Image Quality (IQ), (b) KAM, and (c) GND maps of a region containing ferrite-martensite phase boundary [37] (d) IQ and KAM maps showing ferrite grain F more deformed in the interior [34].

surrounding ferrite using micromechanics based on Eshelby's method [11], [26], [47].

Sakaki et al.[11] theoretically estimated equivalent plastic strain (ϵ) and equivalent stress ($\overline{\sigma}$) due to the formation of a spherical martensite of radius a from austenite in an infinite ferrite matrix. The transformation strain (δ) was assumed to be an isotropic volumetric strain whose magnitude varies linearly with the carbon content (X_C). Martensite was assumed to be elastic while ferrite was assumed to be elastic-plastic. Figure 6(a) shows the variation of equivalent strain with the distance r away from the ferrite/martensite interface, for $\delta = 0.026$ and ferrite yield strength, $\sigma_y = 200$ MPa. It can be seen that both (ϵ) and ($\overline{\sigma}$) reach a maximum value at the interface. Beyond a certain radial distance R away from the interface, ϵ becomes zero and only elastic strain remains. R, therefore, is the radius of the transformation-induced plastic zone, whose magnitude is given as:

$$R = \left[\frac{a^3 E \delta}{3(1-\nu)\sigma_y} \right]^{\frac{1}{3}}, \tag{2.2}$$

where a is the radius of the martensite island, E is Young's modulus and ν is Poisson's ratio. Bourell et al. [26] derived a theoretical expression for the "effective plastic strain" in ferrite, ϵ_e^{pl}, and used it for calculating the dislocation density, ρ, in plastically deformed ferrite based on the following power-law relation:

$$\rho = \rho_0 + C(\epsilon_e^{pl})^g, \tag{2.3}$$

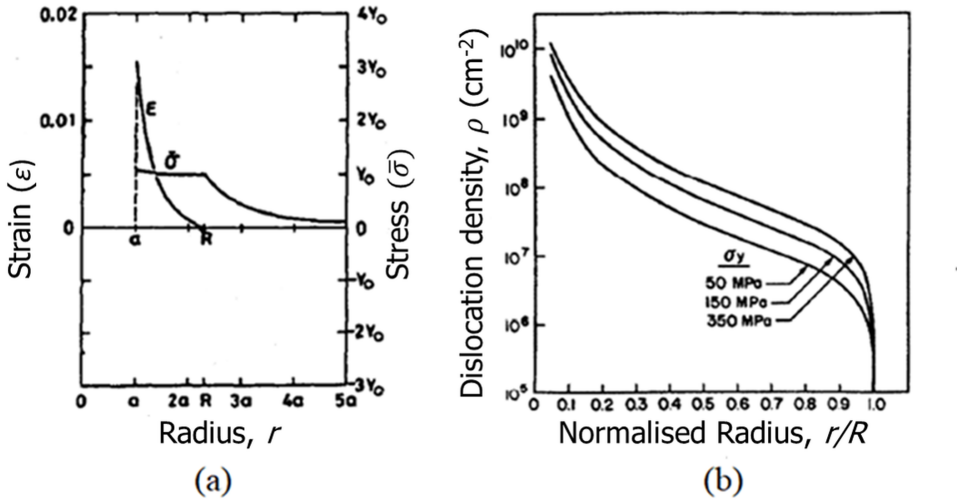

Figure 2.6: (a) Variation in equivalent plastic strain (ϵ) and equivalent stress ($\bar{\sigma}$) as a function of the distance r from the centre of a spherical martensite island [11]. 'a' represents the radius of the martensite island whereas 'R' represents the radius of the transformation-induced plastic zone (b) Variation in dislocation density of ferrite, ρ, as a function of normalized distance r/R from the centre of the martensite island and ferrite yield strength [26].

where C, ρ_0, and g are material parameters. Figure 2.6(b) shows that the dislocation density decreases with increasing normalised distance r/R away from the martensite island [26] for ferrite of different yield strengths σ_y. These results corroborate the experimental observations made using TEM and EBSD measurements.

Analytical models provide estimations of the transformation-induced deformation of ferrite and thus aid in improving the predictions of the overall mechanical behaviour of DP steels. However, accurate local distribution of transformation-induced strains and stresses cannot be obtained by considering simple spherical-shaped martensite islands in a ferrite matrix. Micromechanical modelling has shown that a simple change in the assumed shape of martensite islands from spherical to ellipse alters the work-hardening state of ferrite matrix post-transformation and significantly affects the subsequent mechanical behaviour of DP steels [47]. Since real DP microstructures have irregular morphologies, complex stress/strain fields result in the ferrite matrix due to the formation of martensite. Both fast and accurate solutions for these complex stress/strain fields cannot be obtained through available analytical approaches.

2.4.2. NUMERICAL MODELLING

As discussed, microstructural characteristics such as ferrite/martensite grain shape and sizes, composition, phase volume fractions, etc. determine the deformation field of

ferrite caused by martensite formation. Different combinations of aforementioned microstructural features can produce a large number of possible outcomes for the ferrite deformation field. In such a scenario, numerical models are preferred to find solutions for the ferrite deformation field.

MICROMECHANICAL MODELLING USING REPRESENTATIVE VOLUME ELEMENTS (RVES)

A commonly used approach to mimic deformed ferrite regions in DP steel RVEs is to consider an interphase layer of deformed and strain-hardened ferrite next to the ferrite/martensite interphase. The layer is considered the storage place of high GND density. This approach has its origin in the 'core and mantle' approach proposed by Meyersm and Ashworth [48] and Fu et al.[49] which has been used in previous studies to model the deformed ferrite regions [33], [50].

The inset in figure 2.7(a) shows a simple unit cell representing a DP microstructure based on the 'core and mantle' approach [33]. To elucidate the advantage of this approach, the mechanical response of the unit cell under a virtual tensile test was simulated for two different cases: with and without the interphase layer. The flow curves of ferrite and martensite were determined experimentally. The properties of the interphase layer, namely its strength and thickness, were estimated experimentally by performing nano hardness measurements in the ferritic surroundings of the martensite islands [33].

It is evident from figure 2.7(a) that the flow curve estimated by including the interphase layer is closer to the experimentally observed flow curve of DP steel. Figure 2.7(b) shows the interphase layer modelled in a more complex virtual DP microstructure [51]. Introducing the interphase layer has the effect equivalent to increasing the volume fraction of strain hardened ferrite. To gain true predictive capabilities, the properties of the interphase layer, namely its strength and thickness, should be ascertained beforehand. In the absence of any experimental evidence, both properties become free parameters that can be modified to fit the model flow curve to the experimental one.

Ramazani et al. [2], [52] performed a two-step simulation using an EBSD-based 2-dimensional RVE consisting of austenite and ferrite phases to obtain transformation-induced strains and stresses in the RVE. Figure 2.8(a) shows the EBSD scan and (b) shows the corresponding RVE built using the EBSD scan. In the first step, rapid cooling was simulated on the RVE resulting in austenite to martensitic transformation via an isotropic volumetric expansion, which results in accommodation deformation in the ferrite of the RVE. The resulting plastic strains in the ferrite matrix of the RVE are shown in figure 2.8(c).

In the second step, a finite element method-based virtual tensile test simulation was performed on the transformation-deformed RVE to obtain the flow curves as shown in figure 2.8(d). The figure shows that the simulated DP steel flow curves incorporating the transformation-induced deformation of ferrite (with GNDs) are in better agreement with experimental curves than curves obtained from simulations without deformed ferrite

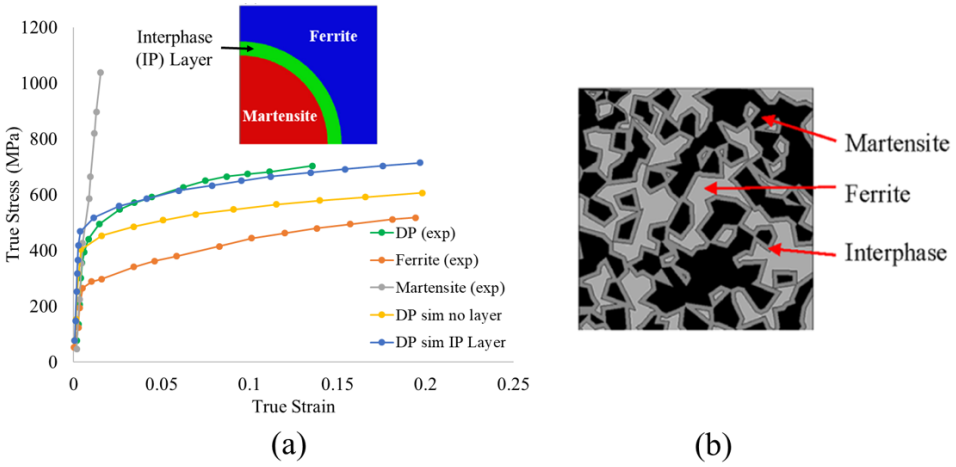

Figure 2.7: (a) True stress vs true strain graph shows the experimental flow curves of ferrite, martensite, DP steel and simulated flow curve of DP steel with and without interphase layer. Inset shows a simple virtual DP steel model used in the study, consisting of a spherical martensite island surrounded by the ferrite matrix with an interface layer of strain hardened ferrite in between [33] (b) Introduction of an interphase layer in a more complex and realistic virtual microstructure model of DP steel [51].

zones (without GNDs). From the results of the study, the authors concluded that deformed ferrite zones containing GNDs extend up to a distance of 0.25 times the size of martensite islands away from the ferrite/martensite interface, and the increased strength of ferrite in these zones is equal to 1.3 time the strength of ferrite grain interior [2], [52].

The advantage of such an approach is that there is no need to make any apriori assumption about the characteristics of the deformed ferrite region. Instead, the distribution of strains/stresses in ferrite is obtained as an intermediate result, to be used further in predicting the overall mechanical behaviour of DP steels. It should be kept in mind that the study only considered the volume increase during martensitic transformation, in the form of isotropic expansion of prior austenite, neglecting the shear part of transformation which causes the majority of shape change. Hence the good correspondence between the KAM map of figure 2.8(a) and the equivalent plastic strain map of figure 2.8(c) may only be a coincidence and not true for other locations in the microstructure.

From figures 2.7(a) and 2.8(d), it is seen that these studies gauge the success of modelling transformation-induced deformation of ferrite based on improvements in simulated DP steel flow curves. However, it should be kept in mind that the simulated stress-strain responses are also influenced by factors such as material composition, phase properties and the choice of strain hardening law.

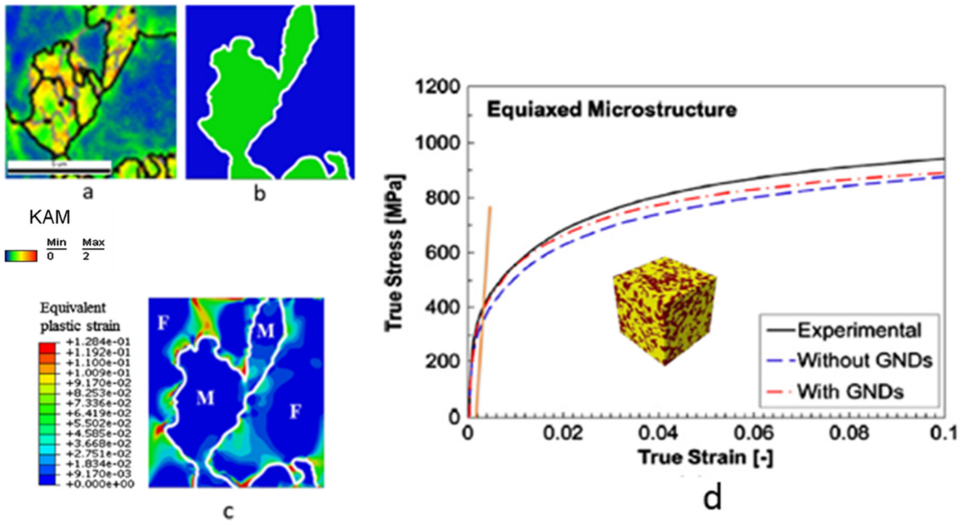

Figure 2.8: (a) EBSD scan of DP steel (b) Virtual RVE from EBSD scan (c) Plastic strain distribution after isotropic expansion of austenite (d) Uniaxial tensile test simulations with GNDs (i.e., with deformed ferrite zones) showing better match with experimental values [2].

PHASE-FIELD SIMULATIONS OF MARTENSITIC TRANSFORMATION IN DP STEEL

Phase-field modelling is a mathematical model to solve interfacial problems in which the interface is considered diffused, which means that the internal properties over the interface between two phases vary continuously. The advantage of a diffuse interface approach is that it avoids the need to explicitly track the position of a moving phase interface. There have been a number of studies in the past utilising phase-field models to study some key aspects of complex martensitic microstructure evolution.

Phase-field modelling was first applied to martensitic transformations by Khachaturyan and co-workers [53], [54], the theory is commonly referred to as the phase-field micro-elasticity theory. Later, Yamanaka and co-workers also included plasticity in the aforementioned theory to perform elastoplastic phase-field simulation of martensitic transformation [55]–[57]. Yeddu et al. employed phase-field modelling to study various aspects of 3-dimensional martensitic microstructure evolution such as stress-assisted transformation [58], the effect of martensite embryo potency [59], martensitic transformation in polycrystals [60], and the effect of austenite grain size on martensitic transformations [61].

Phase-field simulation of martensitic transformation in DP steel [62] reveals that the higher stress regions in ferrite lie along the longitudinal ends of martensite laths as shown in figures 2.9 (a) and (b). The simulations were carried out assuming purely elastic behaviour for both ferrite and martensite. However, only the dilatation strain associated with three Bain variants was considered instead of the shear and dilatation

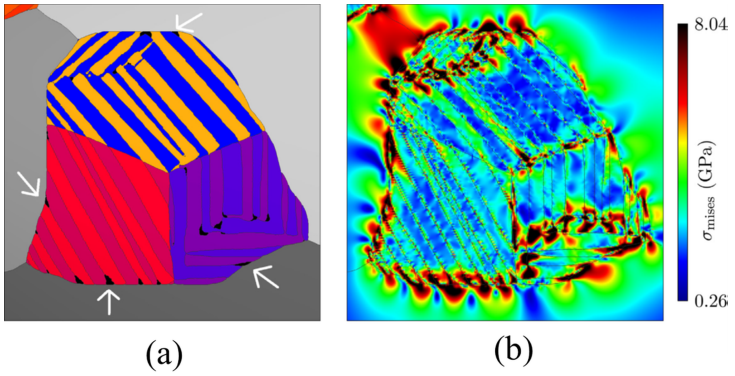

Figure 2.9: Phase-field simulation of (a) DP microstructure and (b) von Mises stress due to formation of martensite inclusion in a ferrite matrix [62].

strain corresponding to the well-known 24 K-S variants. In a recent work, the shear and dilatation strains were incorporated in phase-field modelling for studying the evolution of fully martensitic microstructures [63].

Phase-field may be useful in studying martensitic microstructural evolution on a length scale equivalent to the size of a single grain. For bigger microstructures containing hundreds of ferrite/austenite grains, studying transformation-induced deformation of ferrite by tracking austenite to martensite transformation, utilizing the phase-field approach will be computationally extremely expensive.

2.5. CONCLUSIONS AND OUTLOOK

The martensitic transformation in DP steels causes deformation of the surrounding ferrite matrix in the microstructure. The deformation results in local strain hardening and dislocation accumulation in ferrite, which are important factors determining the mechanical behaviour of DP steels. To accurately predict and improve the mechanical behaviour of DP steels, it is important to consider the transformation-induced deformation of the ferrite matrix in micromechanical calculations.

The experimental characterisation of transformation-induced deformation of ferrite carried out by measuring dislocation densities using TEM or EBSD does not provide an accurate quantitative measure of ferrite deformation. In TEM, the specimen used is very thin and small, therefore it does not adequately represent the 3D volume of the specimen. In EBSD, the results are dependent upon measurement conditions and instrument settings. Micropillar compression tests performed till now lack enough statistical evidence required to make any conclusions.

To model ferrite deformation due to martensitic transformation, several different ap-

proaches have been used in the past, starting with physics-based analytical approaches. Such analytical approaches assumed martensite morphology to be spherical and phase-transformation deformation to consist of only isotropic volumetric expansion. Since real-life microstructures consist of complex morphologies and martensitic phase-transformation deformation is anisotropic, the analytical models are not suitable for the accurate prediction of mechanical properties of DP steel specimens.

More realistic analyses were performed through numerical simulations using powerful computational capabilities. In one approach, transformation-induced ferrite regions were modelled as a layer of deformed ferrite near the ferrite-martensite interface in the DP steel RVE. In another, the formation of strain/stress fields in the ferrite of the DP steel RVE as a result of martensitic volume expansion was simulated using the finite element method. However, these approaches ignore the shear component of transformation strain, thus possibly resulting in an underestimation of the transformation-induced deformation of ferrite.

Phase-field modelling, which works on the minimization of Gibbs energy, has also been utilised to estimate the transformation-induced deformation of ferrite. However, it suffers from the difficulty of scaling up and modelling the transformation-induced deformation of ferrite for a multi-crystal microstructure in a reasonable amount of time.

In a nutshell, to model the transformation-induced deformation of ferrite and thus accurately predict the mechanical behaviour of DP steels, a modelling approach is required which captures the distribution of local deformation of ferrite matrix in DP steels accurately by incorporating the effects of crystallographic, morphological and compositional characteristics of martensite.

REFERENCES

[1] C. Du, J. P. Hoefnagels, S. Kölling, M. G. Geers, J. Sietsma, R. Petrov, V. Bliznuk, P. M. Koenraad, D. Schryvers, and B. Amin-Ahmadi, "Martensite crystallography and chemistry in dual phase and fully martensitic steels," *Materials Characterization*, vol. 139, no. October 2017, pp. 411–420, 2018, ISSN: 10445803. DOI: 10.1016/j.matchar.2018.03.011.

[2] A. Ramazani, K. Mukherjee, A. Schwedt, P. Goravanchi, U. Prahl, and W. Bleck, "Quantification of the effect of transformation-induced geometrically necessary dislocations on the flow-curve modelling of dual-phase steels," *International Journal of Plasticity*, vol. 43, pp. 128–152, 2013, ISSN: 07496419. DOI: 10.1016/j.ijplas.2012.11.003.

[3] T. Sirinakorn, S. Wongwises, and V. Uthaisangsuk, "A study of local deformation and damage of dual phase steel," *Materials and Design*, vol. 64, pp. 729–742, 2014, ISSN: 18734197. DOI: 10.1016/j.matdes.2014.08.009.

[4] R. G. Davies, "Early stages of yielding and strain aging of a Vanadium-containing Dual-Phase steel," *Metallurgical Transactions A*, vol. 10A, 1979. DOI: https://doi.org/10.1007/BF02812021.

[5] A. Nakagawa and G. Thomas, "Microstructure-mechanical property relationships of Dual-Phase steel wire," *Metallurgical Transactions A*, vol. 16A, pp. 831–840, 1985.

[6] G. Krauss, *Physical metallurgy of steels: An overview*. Elsevier Ltd, 2017, pp. 95–111, ISBN: 9780081006535. DOI: 10.1016/B978-0-08-100638-2.00004-3.

[7] H. Bhadeshia, *Worked Examples in the Geometry of Crystals*, Second. London: The institute of Metals, 1991. DOI: 10.1524/zkri.1991.195.1-2.155.

[8] H. Kitahara, R. Ueji, N. Tsuji, and Y. Minamino, "Crystallographic features of lath martensite in low-carbon steel," *Acta Materialia*, vol. 54, no. 5, pp. 1279–1288, 2006, ISSN: 13596454.

[9] G. Miyamoto, N. Iwata, N. Takayama, and T. Furuhara, "Mapping the parent austenite orientation reconstructed from the orientation of martensite by EBSD and its application to ausformed martensite," *Acta Materialia*, vol. 58, no. 19, pp. 6393–6403, 2010, ISSN: 13596454. DOI: 10.1016/j.actamat.2010.08.001.

[10] T. Furuhara, T. Chiba, T. Kaneshita, H. Wu, and G. Miyamoto, "Crystallography and Interphase Boundary of Martensite and Bainite in Steels," *Metallurgical and Materials Transactions A: Physical Metallurgy and Materials Science*, vol. 48, no. 6, pp. 2739–2752, 2017, ISSN: 10735623. DOI: 10.1007/s11661-017-4064-3.

[11] T. Sakaki, K. Sugimoto, and T. Fukuzato, "Role of internal stress for the initial yielding of Dual-Phase steels.," *Acta Metallurgica*, vol. 31, pp. 455–460, 1983. DOI: 10.1016/b978-1-4832-8423-1.50076-6.

[12] A. M. Sarosiek and W. S. Owen, "On the importance of extrinsic transformation accommodation hardening in Dual-Phase steels," *Scripta Metallurgica*, vol. 17, pp. 227–231, 1983. DOI: 10.1016/0036-9748(83)90103-5.

[13] R. Priestner, C. L. Aw, and G. Street, "On initial yielding in Dual-Phase steels," *Scripta Mt!TALLURG ICA*, vol. 18, pp. 133–136, 1984.

[14] C. Peng-Heng and A. G. Preban, "The effect of ferrite grain size and martensite volume fraction on the tensile properties of dual phase steel," *Acta Metallurgica*, vol. 33, no. 5, pp. 897–903, 1985, ISSN: 00016160. DOI: 10.1016/0001-6160(85)90114-2.

[15] M. Erdogan and S. Tekeli, "The effect of martensite particle size on tensile fracture of surface-carburised AISI 8620 steel with dual phase core microstructure," *Materials & Design*, vol. 23, no. 7, pp. 597–604, 2003, ISSN: 02613069. DOI: 10.1016/s0261-3069(02)00065-1.

[16] M. Erdogan and S. Tekeli, "The effect of martensite volume fraction and particle size on the tensile properties of a surface-carburized AISI 8620 steel with a dual-phase core microstructure," vol. 49, pp. 445–454, 2003. DOI: 10.1016/S1044-5803(03)00070-6.

[17] K. Park, M. Nishiyama, N. Nakada, and T. Tsuchiyama, "Effect of the martensite distribution on the strain hardening and ductile fracture behaviors in dual-phase steel," *Materials Science & Engineering A*, vol. 604, pp. 135–141, 2014, ISSN: 0921-5093. DOI: 10.1016/j.msea.2014.02.058.

[18] C. A. N. Lanzillotto and F. B. Pickering, "Structure–property relationships in dual-phase steels," *Metal Science*, vol. 16, no. 8, pp. 371–382, 1982, ISSN: 0306-3453. DOI: 10.1179/030634582790427433.

[19] M. H. Park, A. Shibata, and N. Tsuji, "Effect of grain size on mechanical properties of Dual-Phase steels composed of ferrite and martensite," *MRS Advances*, vol. 1, no. 12, pp. 811–816, 2016, ISSN: 20598521. DOI: 10.1557/adv.2016.230.

[20] R. G. Davies, "Influence of martensite composition and content on the properties of dual phase steels," *Metallurgical Transactions A*, vol. 9, no. 5, pp. 671–679, 1978, ISSN: 03602133. DOI: 10.1007/BF02659924.

[21] A. R. Marder, "Deformation characteristics of Dual-Phase steels.," *Metallurgical transactions. A, Physical metallurgy and materials science*, vol. 13 A, no. 1, pp. 85–92, 1982, ISSN: 03602133. DOI: 10.1007/BF02642418.

[22] A. Bag, K. K. Ray, and E. S. Dwarakadasa, "Influence of martensite content and morphology on tensile and impact properties of high-martensite Dual-Phase steels," vol. 30A, no. May, pp. 1193–1202, 1999.

[23] C. Tasan, M. Diehl, D. Yan, M. Bechtold, F. Roters, L. Schemmann, C. Zheng, N. Peranio, D. Ponge, M. Koyama, K. Tsuzaki, and D. Raabe, "An overview of Dual-Phase steels: Advances in microstructure-oriented processing and micromechanically guided design," *Annual Review of Materials Research*, vol. 45, no. 1, pp. 391–431, 2015, ISSN: 1531-7331. DOI: 10.1146/annurev-matsci-070214-021103.

[24] X. M. Chen, J. J. Drouin, D. R. Coopmans, R. D. Dell'Osso, and P. J. Belanger, "Stamping and crush performance of dual phase steel," in *SAE Technical Papers*, 2001. DOI: 10.4271/2001-01-3074.

[25] H. Mohrbacher, "Advanced Metallurgical Concepts for DP Steels With Improved Formability and Damage Resistance," *International Symposium on New Developments in Advanced High Strength Sheet Steels*, pp. 319–329, 2013.

[26] D. L. Bourell and A. Rizk, "Influence of martensite transformation strain on the ductility of dual-phase steels," *Acta Metallurgica*, vol. 31, no. 4, pp. 609–617, 1983, ISSN: 00016160. DOI: 10.1016/0001-6160(83)90051-2.

[27] U. Liedl, S. Traint, and E. A. Werner, "An unexpected feature of the stress-strain diagram of dual-phase steel," *Computational Materials Science*, vol. 25, no. 1-2, pp. 122–128, 2002, ISSN: 09270256. DOI: 10.1016/S0927-0256(02)00256-2.

[28] D. A. Korzekwa, D. K. Matlock, and G. Krauss, "Dislocation substructure as a function of strain in a dual-phase steel," *Metallurgical Transactions A*, vol. 15, no. 6, pp. 1221–1228, 1984, ISSN: 03602133. DOI: 10.1007/BF02644716.

[29] S. Li, C. Guo, L. Hao, Y. Kang, and Y. An, "In-situ EBSD study of deformation behaviour of 600 MPa grade dual phase steel during uniaxial tensile tests," *Materials Science and Engineering A*, vol. 759, no. March, pp. 624–632, 2019, ISSN: 09215093. DOI: 10.1016/j.msea.2019.05.083.

[30] I. B. Timokhina, P. D. Hodgson, and E. V. Pereloma, "Transmission electron microscopy characterization of the bake-hardening behavior of transformation-induced plasticity and dual-phase steels," *Metallurgical and Materials Transactions A: Physical Metallurgy and Materials Science*, vol. 38, no. 10, pp. 2442–2454, 2007, ISSN: 10735623. DOI: 10.1007/s11661-007-9258-7.

[31] X. L. Cai, J. Feng, and W. S. Owen, "The dependence of some tensile and fatigue properties of a dual-phase steel on its microstructure," *Metallurgical Transactions A*, vol. 16, no. 8, pp. 1405–1415, 1985, ISSN: 03602133. DOI: 10.1007/BF02658673.

[32] P. Tsipouridis, L. Koll, C. Krempaszky, and E. Werner, "On the strength of grain and phase boundaries in ferritic-martensitic dual-phase steels," *International Journal of Materials Research*, vol. 102, no. 6, pp. 674–686, 2011, ISSN: 18625282. DOI: 10.3139/146.110519.

[33] J. Kadkhodapour, S. Schmauder, D. Raabe, S. Ziaei-Rad, U. Weber, and M. Calcagnotto, "Experimental and numerical study on geometrically necessary dislocations and non-homogeneous mechanical properties of the ferrite phase in dual phase steels," *Acta Materialia*, vol. 59, no. 11, pp. 4387–4394, 2011, ISSN: 13596454. DOI: 10.1016/j.actamat.2011.03.062.

[34] T. Matsuno, R. Ando, N. Yamashita, H. Yokota, K. Goto, and I. Watanabe, "Analysis of preliminary local hardening close to the ferrite–martensite interface in dual-phase steel by a combination of finite element simulation and nanoindentation test," *International Journal of Mechanical Sciences*, vol. 180, no. March, 2020, ISSN: 00207403. DOI: 10.1016/j.ijmecsci.2020.105663.

[35] R. Ando, T. Matsuno, T. Matsuda, N. Yamashita, H. Yokota, K. Goto, and I. Watanabe, "Analysis of nano-hardness distribution near the ferritemartensite interface in a dual phase steel with factorization of its scattering behavior," *ISIJ International*, vol. 61, no. 1, pp. 473–480, 2021, ISSN: 09151559. DOI: 10.2355/isijinternational.ISIJINT-2020-546.

[36] H. Ghassemi-Armaki, R. Maaß, S. P. Bhat, S. Sriram, J. R. Greer, and K. S. Kumar, "Deformation response of ferrite and martensite in a dual-phase steel," *Acta Materialia*, vol. 62, no. 1, pp. 197–211, 2014, ISSN: 13596454. DOI: 10.1016/j.actamat.2013.10.001.

[37] M. Calcagnotto, D. Ponge, E. Demir, and D. Raabe, "Orientation gradients and geometrically necessary dislocations in ultrafine grained dual-phase steels studied by 2D and 3D EBSD," *Materials Science and Engineering A*, vol. 527, no. 10-11, pp. 2738–2746, 2010, ISSN: 09215093. DOI: 10.1016/j.msea.2010.01.004.

[38] J. Moerman, P. R. Triguero, C. Tasan, and P. van Liempt, "Evaluation of Geometrically Necessary Dislocations Density (GNDD) near Phase Boundaries in Dual Phase Steels by Means of EBSD," *Materials Science Forum*, vol. 702-703, pp. 485–488, 2011, ISSN: 1662-9752. DOI: 10.4028/www.scientific.net/MSF.702-703.485.

[39] M. F. Ashby, "The deformation of plastically non-homogeneous materials," *Philosophical Magazine*, vol. 21, no. 170, pp. 399–424, 1970. DOI: 10.1080/14786437008238426.

[40] N. A. Fleck, M. F. Ashby, and J. W. Hutchinson, "The role of geometrically necessary dislocations in giving material strengthening," *Scripta Materialia*, vol. 48, no. 2, pp. 179–183, 2003, ISSN: 13596462. DOI: 10.1016/S1359-6462(02)00338-X.

[41] D. Kuhlmann-Wilsdorf and N. Hansen, "Geometrically necessary, incidental and subgrain boundaries," *Scripta Metallurgica et Materiala*, vol. 25, no. 7, pp. 1557–1562, 1991, ISSN: 0956716X. DOI: 10.1016/0956-716X(91)90451-6.

[42] H. Gao and Y. Huang, "Geometrically necessary dislocation and size dependent plasticity," *Scripta mater.*, vol. 48, pp. 113–118, 2003. DOI: 10.1016/S1359-6462(02)00329-9.

[43] L. P. Kubin and A. Mortensen, "Geometrically necessary dislocations and strain-gradient plasticity: A few critical issues," *Scripta Materialia*, vol. 48, no. 2, pp. 119–125, 2003, ISSN: 13596462. DOI: 10.1016/S1359-6462(02)00335-4.

[44] A. Arsenlis and D. M. Parks, "Crystallographic aspects of geometrically-necessary and statistically-stored dislocation density," *Acta Materialia*, vol. 47, no. 5, pp. 1597–1611, 1999, ISSN: 13596454. DOI: 10.1016/S1359-6454(99)00020-8.

[45] V. Atreya, C. Bos, and M. J. Santofimia, "Understanding ferrite deformation caused by austenite to martensite transformation in dual phase steels," *Scripta Materialia*, vol. 202, p. 114 032, 2021, ISSN: 13596462. DOI: 10.1016/j.scriptamat.2021.114032.

[46] J. D. Eshelby, "The Determination of the Elastic Field of an Ellipsoidal Inclusion, and Related Problems," *Proceedings of the Royal Society A: Mathematical, Physical and Engineering Sciences*, vol. 241, no. 1226, pp. 376–396, 1957, ISSN: 1364-5021. DOI: 10.1098/rspa.1957.0133. arXiv: arXiv:1011.1669v3.

[47] A. Bhattacharyya, T. Sakaki, and G. J. Weng, "The influence of martensite shape, concentration, and phase transformation strain on the deformation behavior of stable dual-phase steels," *Metallurgical Transactions A*, vol. 24, no. 2, pp. 301–314, 1993, ISSN: 10735623. DOI: 10.1007/BF02657317.

[48] M. A. Meyersm and E. Ashworth, "A model for the effect of grain size on the yield stress of metals," *Philosophical Magazine A: Physics of Condensed Matter, Structure, Defects and Mechanical Properties*, vol. 46, no. 5, pp. 737–759, 1982, ISSN: 01418610. DOI: 10.1080/01418618208236928.

[49] H. Fu, D. J. Benson, and M. A. Meyers, "Analytical and Computational Description of Effect of Grain Size on Yield Stress of Metals," vol. 49, pp. 2567–2582, 2001, ISSN: 1469-1833. DOI: 10.1017/s1352465813000015.

[50] N. H. Abid, R. K. A. Al-rub, and A. N. Palazotto, "Computational modeling of the effect of equiaxed heterogeneous microstructures on strength and ductility of dual phase steels," *Computational Materials Science*, vol. 103, pp. 20–37, 2015, ISSN: 0927-0256. DOI: 10.1016/j.commatsci.2015.02.051.

[51] N. H. Abid, R. K. Abu Al-Rub, and A. N. Palazotto, "Micromechanical finite element analysis of the effects of martensite particle size and ferrite grain boundaries on the overall mechanical behavior of Dual Phase steel," *Journal of Engineering Materials and Technology*, vol. 139, no. 4, p. 041 006, 2017, ISSN: 0094-4289. DOI: 10.1115/1.4036687.

[52] A. Ramazani, K. Mukherjee, U. Prahl, and W. Bleck, "Transformation-induced, geometrically necessary, dislocation-based flow curve modeling of dual-phase steels: Effect of grain size," *Metallurgical and Materials Transactions A: Physical Metallurgy and Materials Science*, vol. 43, no. 10, pp. 3850–3869, 2012, ISSN: 10735623. DOI: 10.1007/s11661-012-1196-3.

[53] A. Artemev and A. Khachaturyan, "The phase field model and computer simulation of martensitic transformation under applied stresses," *Materials Science Forum*, vol. 327-328, pp. 347–350, 2000, ISSN: 1662-9752. DOI: 10.4028/www.scientific.net/MSF.327-328.347.

[54] A. Artemev, Y. Jin, and A. G. Khachaturyan, "Three-dimensional phase-field model of proper martensitic transformation," *Acta Materialia*, vol. 49, pp. 1165–1177, 2001.

[55] A. Yamanaka, T. Takaki, and Y. Tomita, "Elastoplastic Phase-Field Model of Martensitic Transformation," in *APCOM'07 in conjunction with EPMESC XI*, 2007.

[56] A. Yamanaka, T. Takaki, and Y. Tomita, "Elastoplastic phase-field simulation of self- and plastic accommodations in Cubic → tetragonal martensitic transformation," *Materials Science and Engineering A*, vol. 491, no. 1-2, pp. 378–384, 2008, ISSN: 09215093. DOI: 10.1016/j.msea.2008.02.035.

[57] A. Yamanaka, T. Takaki, and Y. Tomita, "International Journal of Mechanical Sciences Elastoplastic phase-field simulation of martensitic transformation with plastic deformation in polycrystal," *International Journal of Mechanical Sciences*, vol. 52, no. 2, pp. 245–250, 2010, ISSN: 0020-7403. DOI: 10.1016/j.ijmecsci.2009.09.020.

[58] H. K. Yeddu, A. Borgenstam, and A. John, "Stress-assisted martensitic transformations in steels : A 3-D phase-field study," *Acta Materialia*, vol. 61, pp. 2595–2606, 2013. DOI: 10.1016/j.actamat.2013.01.039.

[59] H. K. Yeddu, A. Borgenstam, and J. Agren, "Effect of martensite embryo potency on the martensitic transformations in steels — A 3D phase-field study," *Journal of Alloys and Compounds*, vol. 087, pp. 141–146, 2013. DOI: 10.1016/j.jallcom.2012.01.087.

[60] A. Malik, H. K. Yeddu, G. Amberg, A. Borgenstam, and J. Ågren, "Three dimensional elastoplastic phase field simulation of martensitic transformation in polycrystal," *Materials Science and Engineering A*, vol. 556, pp. 221–232, 2012, ISSN: 09215093. DOI: 10.1016/j.msea.2012.06.080.

[61] H. K. Yeddu, "Phase-field modeling of austenite grain size effect on martensitic transformation in stainless steels," *Computational Materials Science*, vol. 154, no. July, pp. 75–83, 2018, ISSN: 09270256. DOI: 10.1016/j.commatsci.2018.07.040.

[62] E. Schoof, D. Schneider, N. Streichhan, T. Mittnacht, M. Selzer, and B. Nestler, "Multiphase-field modeling of martensitic phase transformation in a dual-phase microstructure," *International Journal of Solids and Structures*, vol. 134, pp. 181–194, 2018, ISSN: 0020-7683. DOI: 10.1016/j.ijsolstr.2017.10.032.

[63] R. Ahluwalia, J. Mikula, R. Laskowski, and S. S. Quek, "Phase field simulation of martensitic-transformation-induced plasticity in steel," *Physical Review Materials*, vol. 4, no. 10, pp. 1–13, 2020, ISSN: 24759953. DOI: 10.1103/PhysRevMaterials.4.103607.

3

CELLULAR AUTOMATA MODELLING OF TRANSFORMATION-INDUCED PLASTIC DEFORMATION OF FERRITE IN DUAL-PHASE STEELS

.

This chapter is based on the scientific article: V. Atreya, C. Bos, and M. J. Santofimia, "Cellular Automata modelling of plastic deformation in ferrite during martensite formation in Dual-Phase steels", in Proceedings of the 8th International Conference on Modeling and Simulation of Metallurgical Processes in Steelmaking (STEELSIM 2019), Toronto, Canada, 2019 [1]

From previous experimental and modelling studies, it is understood that the transformation-induced deformation of ferrite is influenced by the crystallographic, morphological and compositional characteristics of martensite in Dual-phase (DP) steels. In this chapter, the effect of transformation-induced deformation of ferrite on the mechanical behaviour of DP steels is studied by modelling the plastically deformed regions in ferrite grains as a separate strain hardened ferrite phase. This strain hardened ferrite phase is present at the interface of regular ferrite and martensite in the virtual DP steel microstructures used in this study. A Cellular Automata (CA) based microstructure evolution model is used to create the virtual DP steel microstructure which also contains the strain hardened ferrite. The mechanical behaviour is studied using the multi-physics crystal plasticity simulation package called DAMASK. It was observed that the combined CA-DAMASK framework was able to reproduce the trends observed in the literature and can be used to study the effect of transformation-induced deformation of ferrite on the global mechanical properties of DP steels. In future, the variations in local crystallographic, morphological and compositional characteristics of martensite can also be incorporated into this framework.

3.1. INTRODUCTION

The transformation-induced deformation of ferrite grains is larger in the vicinity of ferrite/martensite phase boundaries than in the ferrite grain interiors. The resultant strain gradient necessitates the generation of geometrically necessary dislocations (GNDs) to maintain shape compatibility [2]–[5]. Therefore, the plastically deformed ferrite near the ferrite/martensite interface is generally considered the storehouse of GNDs. These GND-rich regions form a network of plastically deformed and strain-hardened regions of ferrite [6].

The effect of plastically deformed ferrite regions on the mechanical behaviour of DP steels can therefore be studied by introducing a GND-rich region (called interphase layer in this study) of strain hardened ferrite at ferrite/martensite interfaces in virtual DP microstructures for simulating the mechanical behaviour. This is similar to the 'core and mantle' model of grain boundary hardening during the yielding of metals, where the core is grain interior and the mantle is the strain-hardened region near grain boundaries [7], [8].

Previous studies introduced the interphase layer in virtual DP microstructures to be used in micromechanical calculations for simulating uniaxial tensile test of DP steels [9]–[12]. The properties of the interphase layer, namely the thickness (or volume in 3D) and strength, were estimated either by experiments (hardness measurements [9] and micropillar compression test[13]) or by micromechanical simulations of isotropic dilatation during austenite to martensite transformation and the resulting deformation in ferritic matrix [10], [11]. Although local variations were observed, a single value for interphase layer thickness and strength was selected for the DP microstructure under investigation to study the global mechanical behaviour of DP steels.

In this chapter, the effect of transformation-induced deformation of ferrite on the uniaxial tensile test response of DP steels is simulated. The interphase layer is introduced in the virtual DP representative volume element (RVE) obtained using a cellular automata (CA) based microstructure evolution modelling tool [14], [15]. An RVE is a volume of a heterogeneous material which is large enough to statistically represent the material [16]. The uniaxial tensile test response of the RVE is simulated using a multi-physics crystal plasticity simulation package called DAMASK [17], [18]. The development of a combined CA-DAMASK framework is carried out keeping in mind its potential to model the global mechanical behaviour of DP steels by incorporating the effects of local variations in the transformation-induced deformation of ferrite.

3.2. SIMULATION TOOLS

3.2.1. CELLULAR AUTOMATA BASED MICROSTRUCTURE GENERATION

A cellular automata (CA) based model was used to create several DP steel microstructures. For a complete description of the CA model, the reader is referred to references [14], [15]. Here, it is described in brief. The CA model works by discretising a polycrystalline material into a 2D or 3D grid of cubic cells (of size δ), where every cell belongs to a grain of a specific phase. In this study, the initial microstructures chosen for the simulations were Voronoi based and fully austenitic, with specific grain sizes. At any particular time, the cells at the interface transform according to the rules governing the metallurgical process taking place. The relevant metallurgical processes for this study are ferrite nucleation in austenite and ferrite growth, which are described briefly as follows. After the cooling is initiated from austenitising temperature, new ferrite grains nucleate when the temperature drops below Ae3, the local ferrite/austenite equilibrium temperature. The nucleation rate is given by [14], [15]:

$$\frac{dN}{dt} = K_N N_0 \frac{(k_B T)}{h} exp(\frac{-Q_d}{k_B T}) exp(\frac{\Delta G^*}{k_B T}) \ , \tag{3.1}$$

where N is the number of nuclei, t is the time, N_0 is the total number of potential nucleation sites, K_N is a dimensionless rate constant, k_B is the Boltzmann constant, h is the Planck's constant, Q_d is the activation energy for self-diffusion of iron, T is the temperature, and ΔG^* is the activation energy for nucleation. The growth of a ferrite grain at the expense of austenite is based on a mixed-mode model. Accordingly, the ferrite interface velocity is calculated as [14], [15]:

$$v_{\alpha\gamma} = M_0^{\alpha\gamma} exp(\frac{-Q}{RT}) \Delta G_{\alpha\gamma}(x_c^{\gamma,int}, T) \ , \tag{3.2}$$

where $M_0^{\alpha\gamma}$ is the pre-exponential factor, Q is the activation energy for interface mobility, $\Delta G_{\alpha\gamma}$ is the driving force for the transformation based on $x_c^{\gamma,int}$ - the carbon concentration

in the austenite phase at the interface. Every interface cell has a growth length L, which at any time $t+\Delta t$ is given by $(L(t+\delta t) = L(t)+\Delta t v_{\alpha\gamma})$. When the growth length exceeds δ, 2δ or 3δ, the transformation of first, second or third neighbour cells take place respectively. Once all the neighbours of the cell have transformed, its growth length becomes irrelevant since it ceases to be an interfacial cell. Now the growth length of new interfacial cells governs further transformation.

3.2.2. CRYSTAL PLASTICITY BASED MICROMECHANICAL SIMULATIONS

The uniaxial tensile test on output microstructure RVE of CA was simulated using the crystal plasticity (CP) simulation software, DAMASK [17], [18]. The phenomenological crystal plasticity formulation [19]–[21] was used in which the rate of change of slip resistance (or the critically resolved shear stress (CRSS)), $\dot{S}^{\alpha}$, for a slip system α is given by the relationship [20], [21]:

$$\dot{S}^{\alpha} = \sum_{\beta=1}^{24} \dot{\gamma}^{\beta} h_0 \left| 1 - \frac{S^{\beta}}{S^{\alpha}_{\infty}} \right|^{w} sgn\left(1 - \frac{S^{\beta}}{S^{\alpha}_{\infty}}\right) h_{\alpha\beta} \ , \tag{3.3}$$

where α and β are one of the twelve 110<111> or twelve 112<111> slip systems considered for bcc crystals, $h_{\alpha\beta}$ and (w, h_0) are interaction and fitting parameters respectively, $\dot{\gamma}$ is the shear rate and S_{∞} is the saturation shear stress. The shear on a slip system α evolves at the rate:

$$\dot{\gamma}^{\alpha} = \dot{\gamma}_0 \left| \frac{\tau^{\alpha}}{S^{\alpha}} \right|^{n} sgn(\tau^{\alpha}) \ , \tag{3.4}$$

where τ^{α} is the resolved shear stress, n is a measure of slip rate sensitivity and $\dot{\gamma}_0$ is the reference shear rate. The plastic velocity gradient is then determined by the superposition of shear on all slip systems [20], [21]. The material parameters for this work are obtained from the work of Tasan et al. [20], [21], where the authors obtained ferrite parameters by employing a nanoindentation-based optimisation procedure. For martensite, the parameters were found by fitting performed on the stress-strain curves of martensite polycrystals. All the parameters and their values used are listed in table 3.1.

3.3. SIMULATION SETTINGS

The starting microstructure was a Voronoi-based polycrystalline austenite microstructure at 1100° C. The 2D grid spacing and size of the simulation system were 0.5 μ and 125 × 125 μm^2 respectively. The number of austenite grains in the starting microstructure is inversely related to the average austenite grain size. As the microstructure cools and enters the intercritical region, ferrite grains begin to nucleate and grow. Here, heterogeneous corner nucleation of ferrite grains was considered. Smaller austenite grains result in

Table 3.1: Crystal plasticity parameters for ferrite and martensite used in this study [20], [21].

Property	Value(Ferrite)	Value(Martensite)	Unit
C11	233.3 x 10^9	417.4 x 10^9	Pa
C12	135.5 x 10^9	242.4 x 10^9	Pa
C44	118 x 10^9	211.1 x 10^9	Pa
$\dot{\gamma}_0$	1 x 10^{-3}	1 x 10^{-3}	ms^{-1}
$S_{0,\{110\}}$	96 x 10^6	406 x 10^6	Pa
$S_{\infty,\{110\}}$	222 x 10^6	873 x 10^6	Pa
$S_{0,\{112\}}$	96 x 10^6	457 x 10^6	Pa
$S_{\infty,\{112\}}$	412 x 10^6	971 x 10^6	Pa
h_0	1 x 10^9	563 x 10^9	Pa
$h_{\alpha\beta}$	1.0	1.0	
n	20	20	
w	2.25	2.25	

a higher density of ferrite nucleation sites. The ferrite nucleation rate is determined by the value of parameters used in the nucleation rate equation. After reaching an equilibrium state in the intercritical region, the microstructure was quenched to transform the remaining austenite into martensite. Now, the ferrite cells adjacent to martensite were assigned the properties of a strain-hardened ferrite phase and considered together as an interphase layer. The final simulated microstructure is shown in figure 3.1.

Previous nanoindentation studies and modelling works have shown that the strain hardened ferrite at the phase boundary has a yield strength which can be up to twice of that in ferrite grain interior [9], [22], [23]. The increased strength due to strain-hardened was incorporated in DAMASK as an increased critically resolved shear stress (CRSS) value which is twice the value of CRSS for phase boundary ferrite. This follows from the fact that the percentage increase in yield strength is comparable to the percentage increase in CRSS [24], [25]. In the current study, microstructural RVEs having 10 vol.% of martensite are used. Since only the interface cells are considered as part of the interphase layer, the thickness of the layer is equal to grid spacing, i.e., 0.5 μm. The effect of strain hardened ferrite layer is studied considering the following case studies:

- Case I: Effect of the interphase layer with varying prior austenite grain size. This is supposed to affect the size of final martensite particles formed only. The simulation sub-cases are identified by the letters SA for small austenite and LA as large austenite grains.

- Case II: Effect of the interphase layer with varying ferrite grain size. The sub-cases are identified as SF or LF for small and large ferrite grains, respectively. Note that this change also affects martensite particle size.

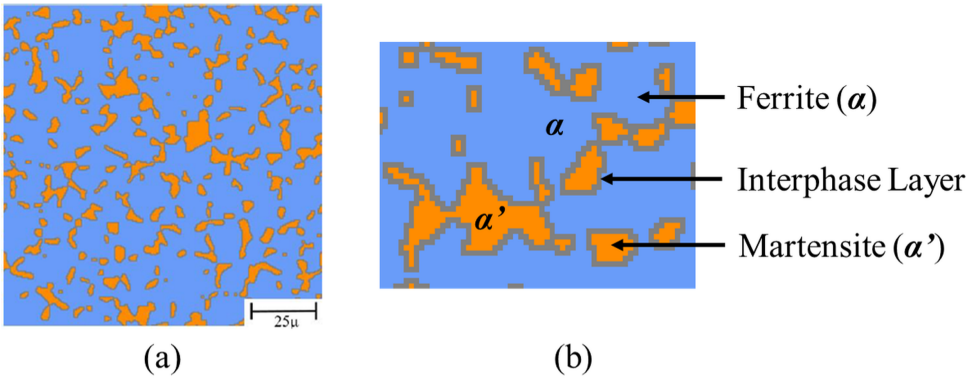

Figure 3.1: Development of a DP microstructure using CA. (a) Dual-phase polycrystalline microstructure with ferrite in blue and martensite in orange. Ferrite/ferrite grain boundaries are not shown (b) Magnified image of a small region in (a), showing the thin interphase layer of strain hardened ferrite in grey at ferrite/martensite interfaces.

The sizes of prior austenite grains, martensite particles and ferrite grains for all corresponding cases are shown in table 3.2. All conditions listed above can have an interphase layer (L) or no layer (NL). The simulation test sub-cases are therefore identified by three sets of letters: L/NL-SA/LA-SF/LF. For example, a sub-case with no layer (NL), small austenite (SA) and large ferrite (LF) grains is named NL-SA-LF. The microstructures corresponding to all cases are shown in figure 3.2, showing martensite (orange) in the ferrite matrix (blue). To study the mechanical behaviour, the microstructure RVE output of the CA model is provided as the input for simulation in DAMASK. The uniaxial tensile tests were simulated with a strain rate of $10^{-4}\,s^{-1}$.

Table 3.2: Average grain sizes (equivalent diameter in μm) of prior austenite, ferrite and martensite in DP steel microstructures for four different cases. Every case has a layer (L) or no-layer (NL) sub-case.

Case	Austenite	Ferrite	Martensite
LA/LF	4.5	16.1	3.5
SA/LF	3.2	15.6	3.0
LA/SF	4.5	7.0	3.0
SA/SF	3.2	5.7	2.4

3.4. RESULTS

Figure 3.3 shows the Von-Mises equivalent of true stress vs Von-Mises equivalent of true strain for all the sub-cases. Two bands of curves can be seen. The lower band is the grouping of all sub-cases without the interphase layer (NL-xx-xx). The curves are quite close to each other and it is difficult to observe them separately at this scale. The sub-cases with the interphase layer (L-xx-xx) show higher stress values and lie above the sub-cases

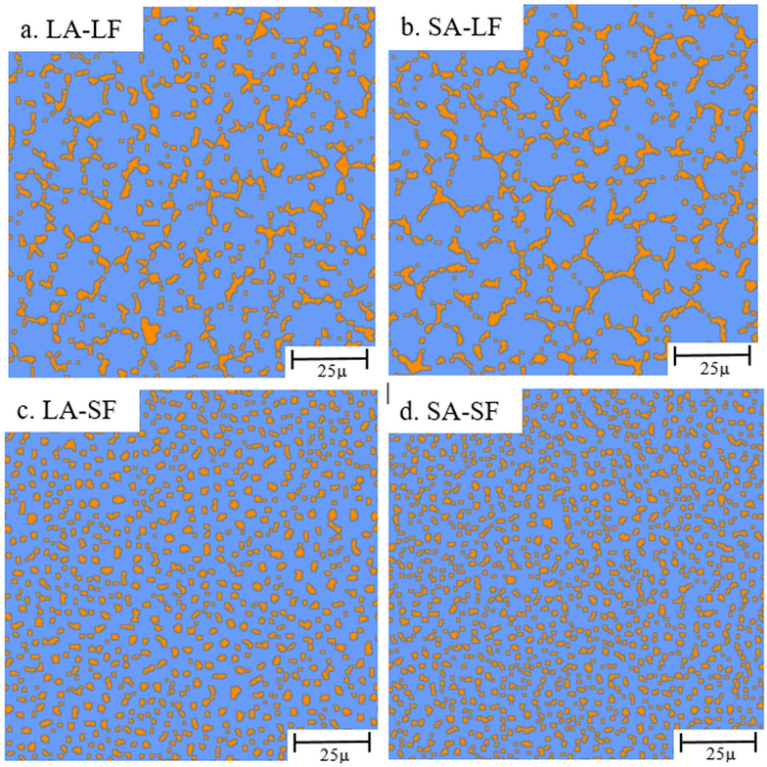

Figure 3.2: DP microstructures consisting of martensite (orange) in a matrix of ferrite (blue) for different case studies: (a) Large austenite/large ferrite (LA/LF) (b) Small austenite/large ferrite (SA/LF) (c) Large austenite/small ferrite (LA/SF) (d) Small austenite/small ferrite (SA/SF).

without the interphase layer (NL-xx-xx). Figure 3.4 shows a magnification of the initial part of curves in figure 3.3. All the sub-cases without the interphase layer show similar curves, but there are differences in the curves of microstructures with the interphase layer. The yield point is similar but the 0.2% offset yield stress increases in presence of the interphase layer, the highest increase being in SA-SF from 240 MPa to 290 MPa.

3.5. DISCUSSION

There is a distinct difference between the strengths of microstructures with an interphase layer and those without it. Introducing an interphase layer means a higher volume fraction of a stronger material than ferrite. With the increasing strength of the interphase layer, the flow curve is expected to move upwards.

If the ferrite grains are large, the size of prior austenite grains (or the final martensite particles) does not play a significant role and the strength increase by the interphase layer is the same with both large and small prior austenite grains, as can be seen by comparing

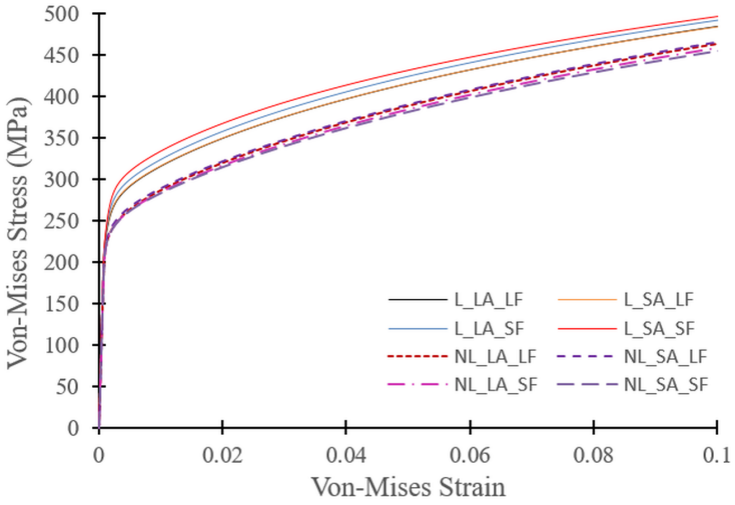

Figure 3.3: Von-Mises equivalent of true stress vs true strain curve for all sub-cases.

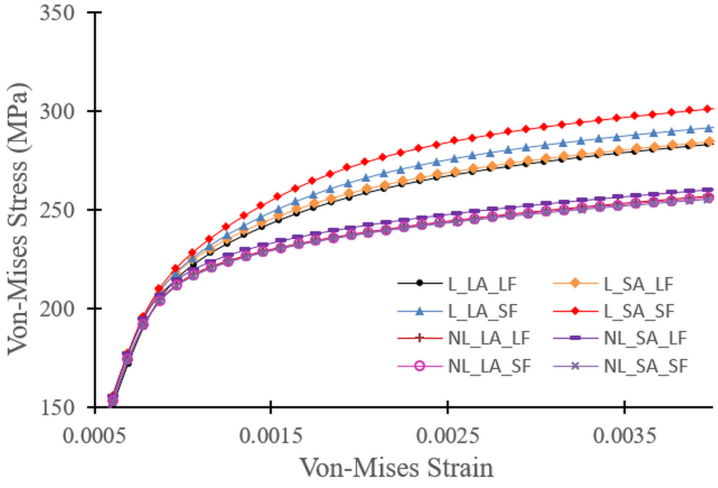

Figure 3.4: Von-Mises equivalent of true stress vs true strain curve for all sub-cases in the range of 0-0.4% strain.

the curves L-LA-LF and L-SA-LF with corresponding no-layer (NL) sub-cases in figure 3.4. The increase in strength due to the interphase layer is highest when the prior austenite grains and ferrite grains both are small as can be seen by observing the curves NL-SA-SF and L-SA-SF. This is because, in the case of small prior austenite and ferrite grain sizes, the volume fraction of the strain-hardened ferrite is highest compared to other grain size combinations.

The fact that all sub-cases with no layer (NL) have overlapping flow curves points to the fact that the crystal plasticity phenomenological power-law used in this work is insensitive to the grain size of constituent phases. In such cases, size effects can truly be captured if all the interfaces, including the ferrite-ferrite and martensite-martensite interfaces, are modelled as 'core and mantle'. However, the ferrite-martensite interfaces affect the mechanical behaviour the most. The modelling of the interphase layer enables us to observe the increase in strength with decreasing austenite (SA) or ferrite (SF) grain sizes, or in other words, by increasing the ferrite-martensite interface area.

This has an important implication: strength depends not only on grain (or particle) sizes of constituent phases but also on their spatial distribution which determines the fraction of the ferrite-martensite interface area. Therefore, the increase in strength due to ferrite-martensite interfaces using this approach may not be very pronounced if the microstructure contains only several clusters of ferrite or martensite instead of a more homogenous distribution.

3.6. CAPABILITIES OF A COMBINED MICROSTRUCTURE EVOLUTION AND MICROMECHANICAL MODELLING FRAMEWORK

The combined CA-DAMASK framework can model the transformation-induced deformation of ferrite and reproduce the trends regarding the resultant increase in strength of DP steels as reported in the literature [9]–[12]. An advantage of using the CA-based microstructure modelling tool, keeping in mind the future application, is that it also gives information about carbon content, grain orientation and morphology at any location in the microstructure [14], [15]. This allows the flexibility to assign strain hardening properties to the interphase layer (or the deformed ferrite region) depending upon local martensite characteristics such as carbon content, crystallographic orientations, etc. These characteristics can be used to obtain the magnitude and direction of the local transformation shear and dilatation. The induced deformation in ferrite can then be calculated using DAMASK.

3.7. CONCLUSIONS

In this work, martensitic transformation-induced deformation of ferrite in DP steels was modelled as an interphase layer of strain-hardened ferrite using a cellular automata-based microstructure evolution model and its tensile deformation response was simulated using DAMASK. It was observed that modelling the interphase layer increases the strength of DP steel microstructures. Moreover, the effect of the interphase layer is most prominent when the prior austenite grain size and ferrite grain size are both small as this results in maximum ferrite/martensite interface area. By modelling the interphase layer, it is also possible to reproduce the size effect of ferrite grains and martensite particles on strength of DP steels. Still, experimental investigations are required to identify important mi-

crostructural characteristics which determine the extent of local transformation-induced deformation of ferrite.

REFERENCES

[1] V. Atreya, C. Bos, and M. J. Santofimia, "Cellular automata modelling of plastic deformation in ferrite during martensite formation in Dual-Phase steels," in *Proceedings of the 8th International Conference on Modeling and Simulation of Metallurgical Processes in Steelmaking (STEELSIM 2019)*, Toronto, Canada, 2019. DOI: 10.33313/503/078.

[2] M. Calcagnotto, D. Ponge, E. Demir, and D. Raabe, "Orientation gradients and geometrically necessary dislocations in ultrafine grained dual-phase steels studied by 2D and 3D EBSD," *Materials Science and Engineering A*, vol. 527, no. 10-11, pp. 2738–2746, 2010, ISSN: 09215093. DOI: 10.1016/j.msea.2010.01.004.

[3] D. A. Korzekwa, D. K. Matlock, and G. Krauss, "Dislocation substructure as a function of strain in a dual-phase steel," *Metallurgical Transactions A*, vol. 15, no. 6, pp. 1221–1228, 1984, ISSN: 03602133. DOI: 10.1007/BF02644716.

[4] M. F. Ashby, "The deformation of plastically non-homogeneous materials," *Philosophical Magazine*, vol. 21, no. 170, pp. 399–424, 1970. DOI: 10.1080/14786437008238426.

[5] N. A. Fleck, M. F. Ashby, and J. W. Hutchinson, "The role of geometrically necessary dislocations in giving material strengthening," *Scripta Materialia*, vol. 48, no. 2, pp. 179–183, 2003, ISSN: 13596462. DOI: 10.1016/S1359-6462(02)00338-X.

[6] U. Liedl, S. Traint, and E. A. Werner, "An unexpected feature of the stress-strain diagram of dual-phase steel," *Computational Materials Science*, vol. 25, no. 1-2, pp. 122–128, 2002, ISSN: 09270256. DOI: 10.1016/S0927-0256(02)00256-2.

[7] M. A. Meyersm and E. Ashworth, "A model for the effect of grain size on the yield stress of metals," *Philosophical Magazine A: Physics of Condensed Matter, Structure, Defects and Mechanical Properties*, vol. 46, no. 5, pp. 737–759, 1982, ISSN: 01418610. DOI: 10.1080/01418618208236928.

[8] H. Fu, D. J. Benson, and M. A. Meyers, "Analytical and Computational Description of Effect of Grain Size on Yield Stress of Metals," vol. 49, pp. 2567–2582, 2001, ISSN: 1469-1833. DOI: 10.1017/s1352465813000015.

[9] J. Kadkhodapour, S. Schmauder, D. Raabe, S. Ziaei-Rad, U. Weber, and M. Calcagnotto, "Experimental and numerical study on geometrically necessary dislocations and non-homogeneous mechanical properties of the ferrite phase in dual phase steels," *Acta Materialia*, vol. 59, no. 11, pp. 4387–4394, 2011, ISSN: 13596454. DOI: 10.1016/j.actamat.2011.03.062.

[10] A. Ramazani, K. Mukherjee, U. Prahl, and W. Bleck, "Transformation-induced, geometrically necessary, dislocation-based flow curve modeling of dual-phase steels: Effect of grain size," *Metallurgical and Materials Transactions A: Physical Metallurgy and Materials Science*, vol. 43, no. 10, pp. 3850–3869, 2012, ISSN: 10735623. DOI: 10.1007/s11661-012-1196-3.

[11] A. Ramazani, K. Mukherjee, A. Schwedt, P. Goravanchi, U. Prahl, and W. Bleck, "Quantification of the effect of transformation-induced geometrically necessary dislocations on the flow-curve modelling of dual-phase steels," *International Journal of Plasticity*, vol. 43, pp. 128–152, 2013, ISSN: 07496419. DOI: 10.1016/j.ijplas.2012.11.003.

[12] N. H. Abid, R. K. Abu Al-Rub, and A. N. Palazotto, "Micromechanical finite element analysis of the effects of martensite particle size and ferrite grain boundaries on the overall mechanical behavior of Dual Phase steel," *Journal of Engineering Materials and Technology*, vol. 139, no. 4, p. 041 006, 2017, ISSN: 0094-4289. DOI: 10.1115/1.4036687.

[13] H. Ghassemi-Armaki, R. Maaß, S. P. Bhat, S. Sriram, J. R. Greer, and K. S. Kumar, "Deformation response of ferrite and martensite in a dual-phase steel," *Acta Materialia*, vol. 62, no. 1, pp. 197–211, 2014, ISSN: 13596454. DOI: 10.1016/j.actamat.2013.10.001.

[14] C. Bos, M. G. Mecozzi, and J. Sietsma, "A microstructure model for recrystallisation and phase transformation during the dual-phase steel annealing cycle," *Computational Materials Science*, vol. 48, no. 3, pp. 692–699, 2010, ISSN: 09270256. DOI: 10.1016/j.commatsci.2010.03.010.

[15] C. Bos, M. G. Mecozzi, D. N. Hanlon, M. P. Aarnts, and J. Sietsma, "Application of a three-dimensional microstructure evolution model to identify key process settings for the production of dual-phase steels," *Metallurgical and Materials Transactions A: Physical Metallurgy and Materials Science*, vol. 42, no. 12, pp. 3602–3610, 2011, ISSN: 10735623. DOI: 10.1007/s11661-011-0696-x.

[16] D. Jeulin, T. Kanit, and S. Forest, "Representative Volume Element: A Statistical Point of View," in *Continuum Models and Discrete Systems*, Kluwer Academic Publishers, 2004, pp. 21–27. DOI: 10.1007/978-1-4020-2316-3_5.

[17] F. Roters, P. Eisenlohr, C. Kords, D. D. Tjahjanto, M. Diehl, and D. Raabe, "DAMASK: The Dusseldorf advanced material simulation kit for studying crystal plasticity using an FE based or a spectral numerical solver," *Procedia IUTAM*, vol. 3, pp. 3–10, 2012, ISSN: 22109838. DOI: 10.1016/j.piutam.2012.03.001.

[18] F. Roters *et al.*, "DAMASK – The Düsseldorf Advanced Material Simulation Kit for modeling multi-physics crystal plasticity, thermal, and damage phenomena from the single crystal up to the component scale," *Computational Materials Science*, vol. 158, no. January 2018, pp. 420–478, 2019, ISSN: 09270256. DOI: 10.1016/j.commatsci.2018.04.030.

[19] F. Roters, P. Eisenlohr, L. Hantcherli, D. Tjahjanto, T. Bieler, and D. Raabe, "Overview of constitutive laws, kinematics, homogenization and multiscale methods in crystal plasticity finite-element modeling: Theory, experiments, applications," *Acta Materialia*, vol. 58, no. 4, pp. 1152–1211, 2009, ISSN: 13596454. DOI: 10.1016/j.actamat.2009.10.058.

[20] C. Tasan, J. Hoefnagels, M. Diehl, D. Yan, F. Roters, D. Raabe, M. Diehl, and D. Yan, "Strain localization and damage in dual phase steels investigated by coupled in-situ deformation experiments and crystal plasticity simulations," *International Journal of Plasticity*, vol. 63, no. 2014, pp. 198–210, 2014, ISSN: 07496419. DOI: 10.1016/j.ijplas.2014.06.004.

[21] C. C. Tasan, M. Diehl, D. Yan, C. Zambaldi, P. Shanthraj, F. Roters, and D. Raabe, "Integrated experimental-simulation analysis of stress and strain partitioning in multiphase alloys," *Acta Materialia*, vol. 81, pp. 386–400, 2014, ISSN: 13596454. DOI: 10.1016/j.actamat.2014.07.071.

[22] T. Matsuno, R. Ando, N. Yamashita, H. Yokota, K. Goto, and I. Watanabe, "Analysis of preliminary local hardening close to the ferrite–martensite interface in dual-phase steel by a combination of finite element simulation and nanoindentation test," *International Journal of Mechanical Sciences*, vol. 180, no. March, 2020, ISSN: 00207403. DOI: 10.1016/j.ijmecsci.2020.105663.

[23] T. Sakaki, K. Sugimoto, and T. Fukuzato, "Role of internal stress for the initial yielding of Dual-Phase steels.," *Acta Metallurgica*, vol. 31, pp. 455–460, 1983. DOI: 10.1016/b978-1-4832-8423-1.50076-6.

[24] S. J. Vachhani and S. R. Kalidindi, "Grain-scale measurement of slip resistances in aluminum polycrystals using spherical nanoindentation," *Acta Materialia*, vol. 90, pp. 27–36, 2015, ISSN: 13596454. DOI: 10.1016/j.actamat.2015.02.017.

[25] S. J. Vachhani, R. D. Doherty, and S. R. Kalidindi, "Studies of grain boundary regions in deformed polycrystalline aluminum using spherical nanoindentation," *International Journal of Plasticity*, vol. 81, pp. 87–101, 2016, ISSN: 0749-6419. DOI: 10.1016/j.ijplas.2016.01.001.

4

INFLUENCE OF MARTENSITIC MICROSTRUCTURAL CHARACTERISTICS ON TRANSFORMATION-INDUCED DEFORMATION OF FERRITE

.

This chapter is based on the scientific article: V. Atreya, C. Bos, and M. J. Santofimia, "Understanding ferrite deformation caused by austenite to martensite transformation in dual phase steels", Scripta Materialia, vol. 202, p. 114 032, 2021 [1]

The influence of morphological and compositional characteristics of martensite on transformation-induced deformation of ferrite has been studied in detail in previous works. However, relatively less attention has been given to investigating the influence of crystallographic orientations of the prior austenite grains, martensite variants and the ferrite grains neighbouring the martensite. Using electron backscatter diffraction measurements, this study identifies the crystallographic aspects which govern the extent of transformation-induced deformation of ferrite grains. It is found that small austenite grains tend to transform into martensitic variants having a close-packed plane parallel relationship with adjacent ferrite grains, thus achieving relatively easy slip transmission and resulting in a long-range deformation of ferrite grains. Additionally, it was also found that some ferrite grains exhibit a short-range deformation limited to the vicinity of the ferrite/martensite interface, which may be influenced by martensite carbon content or the degree of self-accommodation in martensite.

4.1. INTRODUCTION

Dual-Phase (DP) steels belong to the first generation of advanced high-strength steels (AHSS) [2] and are widely used in the automotive industry. DP steels consist of hard martensite particles dispersed in a soft ferritic matrix, leading to a good combination of strength and ductility [2]–[4]. In DP steels, martensite is typically formed from the austenite present in an intercritical ferrite-austenite microstructure during rapid cooling to room temperature. Martensite formation includes volume expansion and shape change, which takes place through dilatation and shearing of the prior austenite region.

To accommodate the volume expansion and shape change of newly formed martensite, the surrounding ferrite grains undergo deformation. Stresses generated as a result of this deformation usually exceed the elastic limit of ferrite, thus causing plastic deformation [5]–[8]. High elastic stresses can persist in the ferrite matrix even after the transformation-induced plastic deformation has ceased.

These plastically deformed ferrite regions contain mobile dislocations as reported by previous studies [2], [7]–[10]. These dislocations, aided by high internal elastic stresses, can move under low macroscopic stress and interact to produce a high initial work hardening rate. Thus, yielding in DP steels starts quite early in the form of localized plasticity. This leads to the absence of a sharp yield point in a typical uniaxial tensile stress-strain curve, a phenomenon known as continuous yielding [11]–[13]. The mechanical behaviour of DP steels thus depends upon the extent of transformation-induced deformation of ferrite.

Earlier investigations attempted to relate the extent of ferrite grain deformation to local microstructural aspects such as the fraction of ferrite/martensite phase boundary in the ferrite grain [14], its adjoining martensite island size, and the strength of the ferrite grain itself [15]–[18]. However, the difference in the extent to which various ferrite grains in the specimen deform could not be fully explained based on the aforementioned microstruc-

tural aspects only [19]. Several characteristics of martensite in DP steels need to be examined in order to fully understand how martensite formation causes the surrounding ferrite grains to deform.

In this work, electron backscatter diffraction (EBSD) measurements are used to study the influence of martensite microstructural characteristics such as the volume fraction, the carbon content, sub-structure size, and the relative orientation between deformed ferrite grains and their adjacent martensite on transformation-induced deformation of ferrite.

4.2. EXPERIMENTS

The starting material consisted of cold rolled steel with a ferrite-pearlite microstructure and composition 0.14C-1.8Mn-0.24Si by weight%. The microstructure revealed using optical microscopy post etching by Nital 5% solution is shown in figure 4.1. The microstructure consists of ferrite and dark-coloured pearlite nodules. Three specimens of dimensions 10 mm x 4 mm x 2 mm were cut from the raw material using electric discharge machining and heat-treated in a Bähr DIL 805 A/D dilatometer. Specimens were heated with a rate of 5 K/s and kept at three different intercritical temperatures for 5 min to obtain different phase fractions of austenite and ferrite, followed by quenching to fully transform the austenite to martensite. The heat treatment regimes are shown in figure 4.1(b) and the relative change in length of the specimens with temperature during the heat treatment is shown in figure 4.1(c).

The specimens are named IC750, IC775, and IC800 where the last three digits denote the intercritical annealing temperatures in Celsius. All specimens were then ground using SiC abrasive papers and polished with 3 μm and 1 μm diamond paste followed by electro-polishing using Struers electrolyte A2 at 35 V, 277 K for 6 s to prepare them for electron backscatter diffraction (EBSD) measurements. EBSD maps were taken on a Zeiss Ultra 55 machine equipped with a Field Emission Gun Scanning Electron Microscope (FEG-SEM) using Edax Pegasus XM 4 Hikari EBSD system. The scan area for this study was 50 μm x 50 μm, with a step size of 50 nm. The TSL OIM version 7 software was used to analyze the EBSD scans. EBSD data subsets from the regions of interest were cleaned using the neighbour confidence index (CI) correlation tool, and points with CI less than 0.1 were removed. Further cleaning was avoided.

4.3. RESULTS AND DISCUSSION

4.3.1. MICROSTRUCTURAL ANALYSIS

To quantify phase fractions in the DP microstructures, the grain average image quality (GAIQ) measure based on EBSD measurements was used. GAIQ is the average image quality value of all points belonging to a grain. Using a grain tolerance angle value between 0.5°-1.5° to demarcate grains for GAIQ calculation enables excellent identification of martensite particles in ferrite-martensite DP microstructures [20], [21]. Figure 4.1(d)

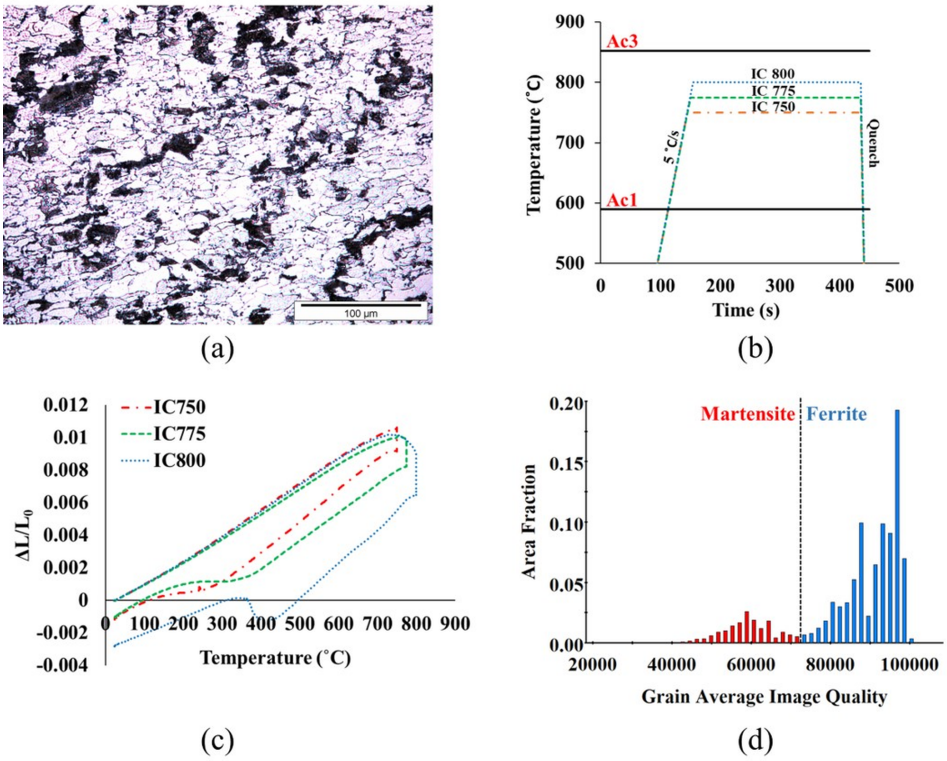

Figure 4.1: (a) Microstructure of the initial material containing ferrite (light) and pearlite (dark) as revealed by chemical etching using Nital 5% solution; (b) Heat treatment regimes applied to specimens. Ac1 and Ac3 refer to critical temperatures indicating the beginning and end of austenite formation, determined from the dilatometry curve of a steel specimen heated at 5 K/s to full austenitisation. The start of heating and the end of cooling occurs at room temperature. (c) Relative change in length of the specimens with temperature during the heat treatment; (d) Grain average image quality (GAIQ) distribution showing martensite and ferrite peaks obtained using data from EBSD scan of specimen IC750.

shows the area fraction distribution of ferrite and martensite GAIQ for specimen IC750. Two distinct peaks belonging to ferrite and martensite can be identified from the distribution, with ferrite exhibiting higher GAIQ. The phase fractions calculated by this method for analyzed EBSD locations are 0.33, 0.56, and 0.93 for IC750, IC775, and IC800 respectively.

Figure 4.2 (a, b, c) shows the image quality (IQ) maps of all specimens obtained via EBSD. Ferrite regions have better image quality and appear light grey in EBSD image quality (IQ) maps as compared to martensite regions which appear dark grey [2], [21]. The martensite particles resemble connected chains in IC750 and IC775, with the chains being bulkier in IC775.

Figure 4.2 (d, e, f) shows the kernel average misorientation (KAM) maps of all specimens.

The KAM measure gives an estimate of the extent of deformation within a grain [22]–[25]. The nth kernel average misorientation (KAM) at a measurement point is defined as the average misorientation of that point with respect to the n numbers of measured nearest neighbour points, neglecting those misorientations which are above a certain threshold. In the figure, KAM maps are shown for the 5th nearest neighbour and a maximum of 4° misorientation. The blue and the red end of the legend colour spectrum denote the minimum and maximum KAM values respectively. Martensite regions appear red in KAM maps due to very high misorientations, while the ferrite regions appear blue. There is a higher number of ferrite grains with deformation in IC750 and IC775 than in IC800. No prominent deformation is seen in the ferrite grains of IC800.

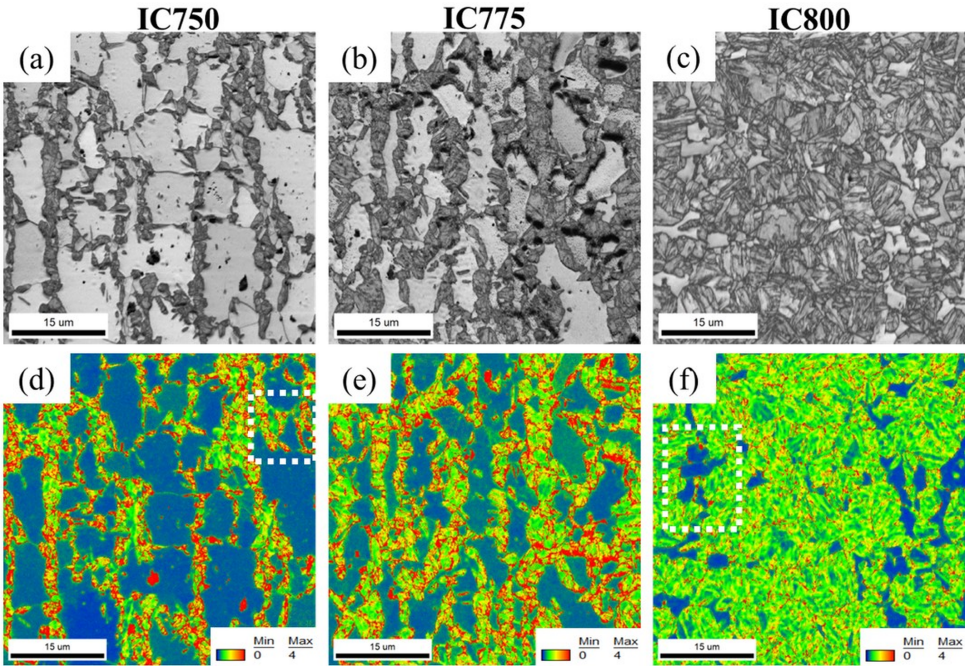

Figure 4.2: (a, b, c) EBSD image quality (IQ) maps for specimens IC750, IC775, and IC800 respectively; (d, e, f) EBSD kernel average misorientation (KAM) maps for specimens IC750, IC775, and IC800 respectively.

4.3.2. LONG RANGE (TYPE I) AND SHORT-RANGE (TYPE II) DEFORMATION OF FERRITE GRAINS

It is observed that some ferrite grains undergo long-range deformation, while in others deformation is limited to the vicinity of phase boundaries. This is evident from misorientation gradients present within the ferrite grains. Figure 4.3(a) shows the IQ and KAM maps of ferrite grains labelled F1 and F2 from the region of the IC750 specimen highlighted in figure 4.2(d). In the ferrite grain F1, KAM gradients cover the majority of

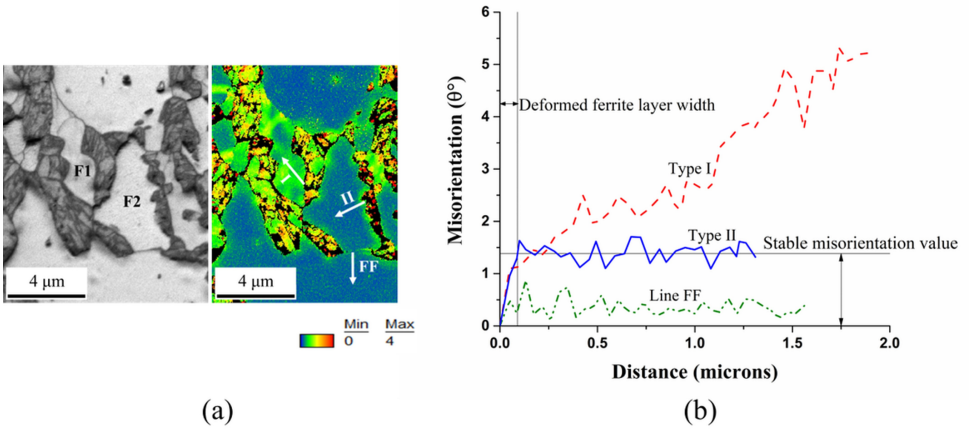

Figure 4.3: (a) IQ and KAM maps of ferrite grains F1 and F2 from the region of IC750 specimen highlighted in figure 4.2 with three profile lines. FF starts from the ferrite/ferrite phase boundary whereas lines I and II start from the ferrite/martensite phase boundary. Black regions in the KAM map represent pixels with low confidence index; (b) Change in point-to-origin misorientation angle while moving along profile line from phase/grain boundary towards ferrite grain interior.

the grain area. In the ferrite grain F2, higher KAM values are confined to the vicinity of the ferrite/martensite phase boundary in the form of a layer of deformed ferrite.

For a clear illustration, three misorientation profile lines are drawn in figure 4.3(a). Changes in misorientation angle with respect to the origin along the profile lines are plotted in figure 4.3(b). For the profile line which starts from the ferrite/ferrite grain boundary (FF), the misorientation angle in figure 4.3(b) first increases up to a certain distance and then becomes nearly stable. For the profile lines which start at the ferrite/martensite (FM) phase boundary, there are two scenarios: type I and II. In the type I profile line, the corresponding misorientation angle in figure 4.3(b) shows a continuously increasing trend even at a distance equal to half the grain size. This indicates that the grain has undergone significant deformation in its interior. Such deformation is henceforth called type I long-range (type I LR in short) ferrite deformation.

In the type II profile line, the misorientation angle change behaves similarly to that of the first case (FF), except that the stable misorientation value is significantly higher. This indicates that the deformation in ferrite grain is highest near the phase boundary and decreases up to a certain distance which represents the deformed ferrite layer width. The deformation remains confined to a small region near the phase boundary. This type of deformation is henceforth called type II short range (type II SR in short) ferrite deformation.

The occurrence of ferrite grains with type I LR deformation is common in EBSD scans of

IC750 and rare in IC775. Type II SR deformation can be spotted in several grains in both IC750 and IC775. However, in IC800, both type I LR and type II SR deformation appears to be absent which is indicated by very low values of KAM at all locations inside the ferrite grains.

Grains with type I LR deformation were quantified using the grain orientation spread (GOS) measure. It is used to estimate deformation in grains, especially to distinguish non-recrystallized grains from recrystallized ones [26]. For calculating GOS, the average orientation of the grain is calculated. Then the misorientations between this average orientation and the orientation of each measurement point within the grain are calculated. The average of these misorientations is the GOS value of that grain. Grains with type II SR deformation were quantified by identifying grains with a discernable width of deformed ferrite layer as illustrated in figure 4.3(b).

Volume fractions of ferrite grains with different types of deformation quantified from EBSD scans of figure 4.2 are shown in figure 4.4(a) together with the volume fraction of martensite. The deformed ferrite layer width for type II SR deformation measured for several randomly selected ferrite grains of IC750 and IC775 was found to be in the range 0.1 μm - 0.5 μm, while in IC800 it is absent, as evident from figure 4.4(b).

It is important to note that type II SR deformation in a ferrite grain can occur in addition to type I LR deformation. The large KAM gradients from type I LR deformation obfuscate the KAM gradients showing the type II deformation of ferrite near the ferrite/martensite interface. Therefore, it is highly likely that some fraction of ferrite grains exhibiting type I LR deformation contain type II SR deformation too.

To investigate its influence on transformation-induced ferrite deformation, the carbon content of martensite was calculated using the carbon mass balance equation, $C_0 = V_f C_f + V_m C_m$, where $C_0 = 0.13$ wt.% is the mean steel carbon content, V_f, V_m are the volume fractions of ferrite and martensite, C_f, C_m are the carbon contents of ferrite and martensite in wt.%, respectively. The values of C_f were approximated as the equilibrium carbon content in ferrite at different intercritical temperatures. This was calculated in ThermoCalc software using the TCFe9 database. The carbon content of martensite was observed to decrease with increasing martensite volume fraction.

Figure 4.4(c) shows the variation of average block size with carbon content in martensite for different martensite volume fractions. It shows that a higher carbon content in martensite reduces the sub-structure size, as reported in the literature [27], [28]. It can also be inferred that IC750 must have had the smallest average prior austenite grain size (PAGS) among all specimens since the average block size of martensite is directly proportional to the average PAGS of the specimen [29]–[31].

4.3.3. SLIP-TRANSMISSION FROM MARTENSITE INTO FERRITE GRAINS

A potential explanation for the transformation-induced type I-LR deformation of ferrite is slip transmission. Slip transmission from martensite to adjacent austenite [32] and ferrite grains [33] has been reported in the literature. Grain boundaries block dislocation movement, hence providing material strengthening [34], [35]. However, there can be partial or even full transmission of dislocations across the grain or phase boundaries under certain conditions.

The geometrical criteria used to estimate ease of slip transmission is called the slip transfer number λ which is a function of δ - the angle between the lines of intersection of slip planes with the boundary plane, and κ - the angle between slip directions, or Burgers vectors as shown in figure 4.4(d) [36], [37]. The smaller the values of δ and κ, the higher the value of λ and the larger the slip transmission. If the planes and directions of incoming and outgoing slip are nearly parallel, there is a higher chance of slip transmission [38].

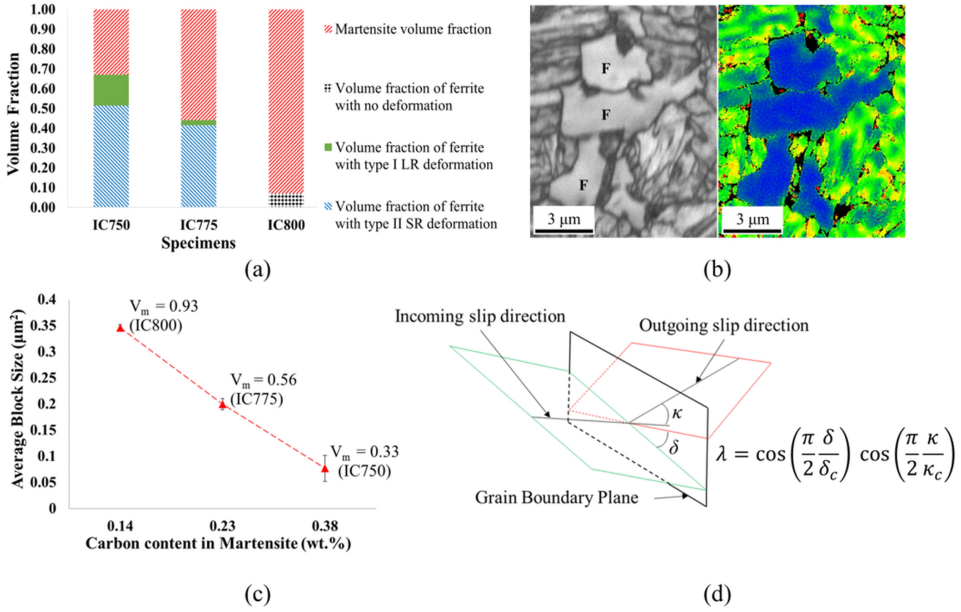

Figure 4.4: (a) Volume fraction of martensite and different types of ferrite deformation based on EBSD scans of figure 4.2; (b) IQ and KAM map of a region of IC800 highlighted in figure 4.2(f) with some ferrite grains indicated with 'F'. Both type I and type II deformation are absent; (c) Variation in average block size and carbon content of martensite for specimens with different martensite volume fraction (V_m); (d) Geometrical configuration of slip planes during slip transmission. Incoming and outgoing slip planes are indicated in green and red colours respectively. The equation for slip transfer number λ is shown, where δ is the angle between the lines of intersection of slip planes with the boundary plane, κ is the angle between slip directions, δ_c and κ_c are the limiting values of δ and κ beyond which slip transmission not possible.

Since the (110) plane is the most active slip plane for bcc crystal structures, the (110) pole

figures were plotted for ferrite grains F1 and F2 as shown in figure 4.5 and overlaid on (110) pole figures of adjacent martensite blocks to check for parallel plane relationships [33], [39]. Overlap in pole figures (highlighted by black circles) shows that the (110) planes of the ferrite grains with type I LR deformation exhibit a parallel relationship with the (110) planes of adjacent martensite blocks. Such a relationship is henceforth referred to as (110) close-packed plane parallel (CPPP) relationship. The martensite blocks which show (110) CPPP relationship with the ferrite grain are coloured.

Five out of a total of ten martensite blocks with a CPPP relationship have at least one <111> direction parallel to the <111> direction of ferrite grain F1, indicated by the black circle in (111) pole figures shown in figure 4.5(a). The rest of the blocks have a misorientation of 5°-15° between their <111> direction and <111> direction of ferrite, which is lower than the generally used critical value of $\kappa(\kappa_c = 45°)$, above which slip transmission is not possible [36]. Such blocks are indicated by a dotted black circle in (111) pole figure shown in figure 4.5(a).

Ferrite grain F2 which shows type II SR deformation only has one small martensite block with (110) CPPP relationship as shown in figure 4.5(b). On the contrary, a higher number of martensite blocks with (110) CPPP relationships are present adjacent to type I LR deformed ferrite grain F1. The quantification of grains that show CPPP relation for all three specimen scans is given in table 1. The volume fraction of ferrite grains with type I LR deformation and also exhibiting CPPP relation is highest in IC750.

In 2D micrographs, it is always a concern whether observations may have been influenced by features below the surface. The amount of ferrite exhibiting type I LR deformation as a percentage of total ferrite is 24%, 7%, and 0% for IC750, IC775, and IC800 respectively. This indicates that observations of type I LR deformation cannot be caused solely by the presence of martensite beneath the ferrite grain observed in the 2D scan as in that case an equal fraction of ferrite grains should have exhibited type I LR deformation in all specimens.

Table 4.1: Quantification of type I LR ferrite grains with CPPP relationship in EBSD scans of the specimens shown in figure 4.2

Specimen	Volume fraction of ferrite	Total no. of ferrite grains	Volume fraction of ferrite with type I LR deformation	Number of ferrite grains with type I LR deformation	Volume fraction of ferrite with type I LR deformation and CPPP relationship
IC750	0.67	124	0.16	21	0.14
IC775	0.44	79	0.03	4	0.01
IC800	0.07	42	-	-	-

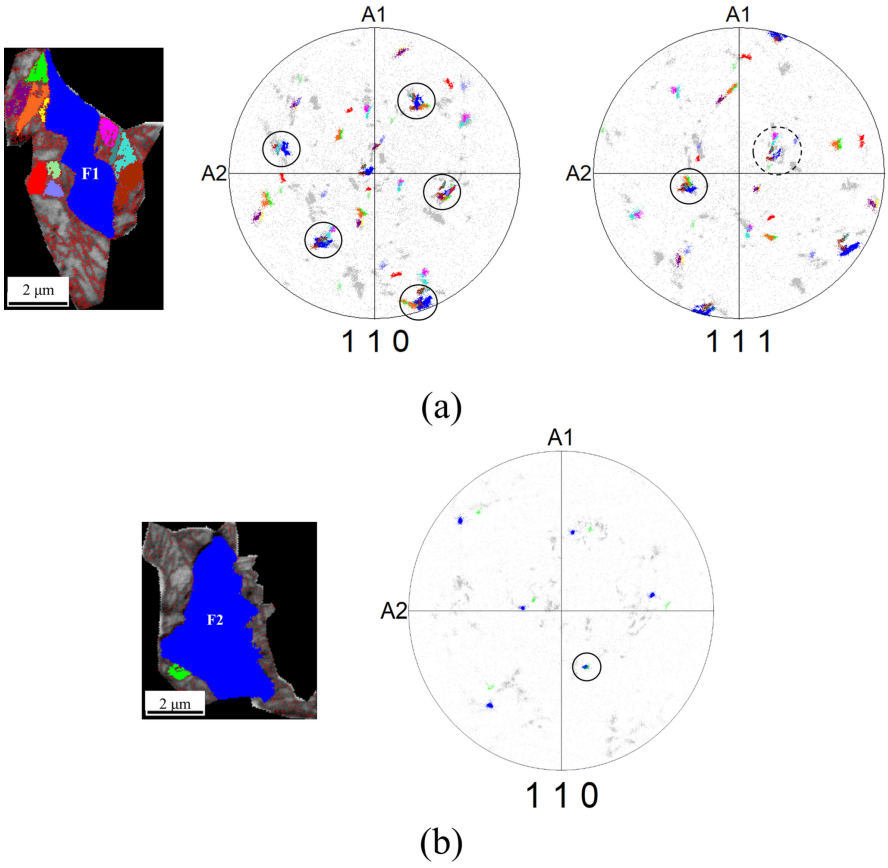

Figure 4.5: IQ maps and (110) pole figures of ferrite grains (a)F1 and (b) F2 (both highlighted in blue in IQ maps above) in specimen IC750 exhibiting type I and type II deformations respectively, overlaid on (110) pole figures of surrounding martensite blocks (grey coloured points). The blocks showing the CPPP relationship with ferrite are coloured in IQ maps along with corresponding points on the pole figure. Black circles indicate overlapping 110 planes of ferrite and martensite blocks. In (a), (111) pole figures show the <111> directions in ferrite grain F1 overlaid on those of highlighted martensite blocks. Black circle indicates overlapping <111> directions for effective slip transfer. Dotted black circle indicate those blocks which have 5°- 15° misorientation between their <111> direction and <111> direction of ferrite.

4.3.4. RELATIVE FREQUENCY OF TYPE I AND TYPE II DEFORMATIONS

The highest frequency of type I LR deformed ferrite grains in IC750 can be explained as follows. IC750 has the minimum average block size and hence the minimum average PAGS as evident from figure 4.4(c). Small prior austenite grains show a lack of formation of an adequate number of variants for self-accommodation, and hence generate the greatest elastic stresses upon transformation [29], [30], [32], [33]. This causes the surrounding microstructure to undergo plastic deformation to relax those stresses.

Limited freedom to choose variants for self-accommodation due to small PAGS forces the austenite to transform into martensite variants having CPPP relation with adjacent ferrite grains. This achieves relatively easy slip transmission while relaxing high transformation stresses resulting in type I LR deformation. An important implication of this is that ferrite grain orientation can affect the variant selection during the transformation of an adjacent small PAG [33], [39].

The existence of the CPPP relation indicates an orientation relationship (OR) between intercritical ferrite and the austenite present before the transformation. As the intercritical temperature increases, the propensity of nucleating austenite to have Kurdjumov-Sachs (K-S) OR with multiple ferrite neighbours decreases [40]. Since boundaries without K-S OR grow faster [41], [42], higher intercritical temperatures eventually result in microstructure with decreasing probability of austenite grains having K-S OR with ferrite neighbours. Therefore, a ferrite grain in DP steel has a higher probability of having K-S OR with multiple prior austenite grains and hence CPPP relation with multiple martensite blocks if lower intercritical temperatures are used.

Ferrite-martensite interface boundary length may also explain the frequency of type I LR deformation since a larger interaction area between ferrite and martensite provides more opportunities for the occurrence of the CPPP relationship. However, the interface boundary length decrease from 3195 μm in IC750 to 2970 μm in IC775 is very minimal and hence does not explain the drastic decrease in the frequency of type I LR deformation observed in IC775.

The fraction of ferrite grains with type II SR deformation is also higher in IC750 than in IC775, but absent in IC800. This probably means that type II SR deformation decreases with increasing martensite volume fraction. Since in specimens IC750 and IC775 type II SR deformation is observed in almost all ferrite grains where type I LR deformation is not observed, it can be better explained by an overall average characteristic of the microstructure, rather than a local characteristic such as the fulfilment of CPPP relation.

No type II SR deformation is observed in IC800, which can be explained by the fact that the volumetric expansion of martensitic transformation increases with the increasing carbon content of martensite [40]. This causes increased deformation in surrounding ferrite resulting in type II SR deformation. It seems that below a certain threshold carbon content, transformation strain is so low that the deformed ferrite layer is indistinguishable. Moreover, IC800 probably has a higher number of martensitic variants formed from a single prior austenite grain, as it has the largest prior austenite grain size. A higher number of variants can cancel the shear part of austenite-to-martensite transformation strain more effectively and significantly reduce the magnitude of deformation in ferrite [15], [16].

4.4. CONCLUSIONS

In summary, there are two types of deformation observed in ferrite grains: a type I long-range (LR) deformation that spans the complete ferrite grain, and a type II short-range (SR) deformation in the form of a deformed ferrite region at the ferrite/martensite boundary.

The fraction of ferrite grains with type I LR deformation was highest in specimen IC750 which has the smallest martensite block sizes, and hence the smallest PAGS. When PAGS is small, austenite may transform into martensitic variants having a (110) CPPP relationship with neighbouring ferrite. This enables effective relaxation of transformation stresses by relatively easy deformation of ferrite and results in type I LR deformation. It was observed that most ferrite grains with type I LR deformation also possess a (110) CPPP relationship with several surrounding martensite blocks.

At the locations where type I LR deformation and the CPPP relation are not present, type II SR deformation is observed. Type II SR deformation is encountered more often as the PAGS increases. Type II SR deformation is observed only in IC750 and IC775 and is absent in IC800. This may either be because the carbon content in the martensite of IC800 is low, which causes small transformation-induced deformation of ferrite unable to be captured by EBSD KAM measurements. Or, a higher number of variants form in PAGs of IC800, which cancels the shear part of the transformation strain more effectively.

REFERENCES

[1] V. Atreya, C. Bos, and M. J. Santofimia, "Understanding ferrite deformation caused by austenite to martensite transformation in dual phase steels," *Scripta Materialia*, vol. 202, p. 114 032, 2021, ISSN: 13596462. DOI: 10.1016/j.scriptamat.2021.114032.

[2] G. Krauss, *Steels: processing, structure, and performance*, Second Edi. Materials Park, Ohio: ASM International, 2015, ISBN: 9781627080835. DOI: 10.5860/choice.43-6550.

[3] A. Nakagawa and G. Thomas, "Microstructure-mechanical property relationships of Dual-Phase steel wire," *Metallurgical Transactions A*, vol. 16A, pp. 831–840, 1985.

[4] R. G. Davies, "Early stages of yielding and strain aging of a Vanadium-containing Dual-Phase steel," *Metallurgical Transactions A*, vol. 10A, 1979. DOI: https://doi.org/10.1007/BF02812021.

[5] T. Sakaki, K. Sugimoto, and T. Fukuzato, "Role of internal stress for the initial yielding of Dual-Phase steels.," *Acta Metallurgica*, vol. 31, pp. 455–460, 1983. DOI: 10.1016/b978-1-4832-8423-1.50076-6.

[6] D. L. Bourell and A. Rizk, "Influence of martensite transformation strain on the ductility of dual-phase steels," *Acta Metallurgica*, vol. 31, no. 4, pp. 609–617, 1983, ISSN: 00016160. DOI: 10.1016/0001-6160(83)90051-2.

[7] D. A. Korzekwa, D. K. Matlock, and G. Krauss, "Dislocation substructure as a function of strain in a dual-phase steel," *Metallurgical Transactions A*, vol. 15, no. 6, pp. 1221–1228, 1984, ISSN: 03602133. DOI: 10.1007/BF02644716.

[8] U. Liedl, S. Traint, and E. A. Werner, "An unexpected feature of the stress-strain diagram of dual-phase steel," *Computational Materials Science*, vol. 25, no. 1-2, pp. 122–128, 2002, ISSN: 09270256. DOI: 10.1016/S0927-0256(02)00256-2.

[9] M. Nouroozi, H. Mirzadeh, and M. Zamani, "Effect of microstructural refinement and intercritical annealing time on mechanical properties of high-formability dual phase steel," *Materials Science and Engineering A*, vol. 736, pp. 22–26, 2018, ISSN: 09215093. DOI: 10.1016/j.msea.2018.08.088.

[10] H. Mirzadeh, M. Alibeyki, and M. Najafi, "Unraveling the Initial Microstructure Effects on Mechanical Properties and Work-Hardening Capacity of Dual-Phase Steel," *Metallurgical and Materials Transactions A: Physical Metallurgy and Materials Science*, vol. 48, no. 10, pp. 4565–4573, 2017, ISSN: 10735623. DOI: 10.1007/s11661-017-4246-z.

[11] A. Karimi, S. Kheirandish, and M. Mahmoudiniya, "Effect of bainite volume fraction on mechanical properties of a ferrite-bainite-martensite steel," *Kovove Materialy*, vol. 55, no. 3, pp. 175–182, 2017, ISSN: 0023432X. DOI: 10.4149/km2017-3-175.

[12] B. G. Prusty and A. Banerjee, "Structure-property correlation and constitutive description of structural steels during hot working and strain rate deformation," *Materials*, vol. 13, no. 3, p. 556, 2020, ISSN: 19961944. DOI: 10.3390/ma13030556.

[13] Z. Xiong, A. G. Kostryzhev, Y. Zhao, and E. V. Pereloma, "Microstructure evolution during the production of dual phase and transformation induced plasticity steels using modified strip casting simulated in the laboratory," *Metals*, vol. 9, no. 4, pp. 1–14, 2019, ISSN: 20754701. DOI: 10.3390/met9040449.

[14] M. Calcagnotto, D. Ponge, E. Demir, and D. Raabe, "Orientation gradients and geometrically necessary dislocations in ultrafine grained dual-phase steels studied by 2D and 3D EBSD," *Materials Science and Engineering A*, vol. 527, no. 10-11, pp. 2738–2746, 2010, ISSN: 09215093. DOI: 10.1016/j.msea.2010.01.004.

[15] A. Ramazani, K. Mukherjee, U. Prahl, and W. Bleck, "Transformation-induced, geometrically necessary, dislocation-based flow curve modeling of dual-phase steels: Effect of grain size," *Metallurgical and Materials Transactions A: Physical Metallurgy and Materials Science*, vol. 43, no. 10, pp. 3850–3869, 2012, ISSN: 10735623. DOI: 10.1007/s11661-012-1196-3.

[16] A. Ramazani, K. Mukherjee, A. Schwedt, P. Goravanchi, U. Prahl, and W. Bleck, "Quantification of the effect of transformation-induced geometrically necessary dislocations on the flow-curve modelling of dual-phase steels," *International Journal of Plasticity*, vol. 43, pp. 128–152, 2013, ISSN: 07496419. DOI: 10.1016/j.ijplas.2012.11.003.

[17] A. Ramazani, K. Mukherjee, H. Quade, U. Prahl, and W. Bleck, "Correlation between 2D and 3D flow curve modelling of DP steels using a microstructure-based RVE approach," *Materials Science and Engineering A*, vol. 560, pp. 129–139, 2013, ISSN: 09215093. DOI: 10.1016/j.msea.2012.09.046.

[18] J. Kadkhodapour, S. Schmauder, D. Raabe, S. Ziaei-Rad, U. Weber, and M. Calcagnotto, "Experimental and numerical study on geometrically necessary dislocations and non-homogeneous mechanical properties of the ferrite phase in dual phase steels," *Acta Materialia*, vol. 59, no. 11, pp. 4387–4394, 2011, ISSN: 13596454. DOI: 10.1016/j.actamat.2011.03.062.

[19] T. Matsuno, R. Ando, N. Yamashita, H. Yokota, K. Goto, and I. Watanabe, "Analysis of preliminary local hardening close to the ferrite–martensite interface in dual-phase steel by a combination of finite element simulation and nanoindentation test," *International Journal of Mechanical Sciences*, vol. 180, no. March, 2020, ISSN: 00207403. DOI: 10.1016/j.ijmecsci.2020.105663.

[20] J. Moerman, P. R. Triguero, C. Tasan, and P. van Liempt, "Evaluation of Geometrically Necessary Dislocations Density (GNDD) near Phase Boundaries in Dual Phase Steels by Means of EBSD," *Materials Science Forum*, vol. 702-703, pp. 485–488, 2011, ISSN: 1662-9752. DOI: 10.4028/www.scientific.net/MSF.702-703.485.

[21] L. Ryde, "Application of EBSD to analysis of microstructures in commercial steels Application of EBSD to analysis of microstructures in commercial steels," *Material Science and Technology*, vol. 0836, 2006. DOI: 10.1179/174328406X130948.

[22] D. Jorge-Badiola, A. Iza-Mendia, and I. Guti´errez, "Evaluation of intragranular misorientation parameters measured by EBSD in a hot worked austenitic stainless steel," *Journal of Microscopy*, vol. 228, no. July, pp. 373–383, 2007. DOI: 10.1111/j.1365-2818.2007.01850.x.

[23] M. Kamaya, A. J. Wilkinson, and J. M. Titchmarsh, "Measurement of plastic strain of polycrystalline material by electron backscatter diffraction," vol. 235, pp. 713–725, 2005. DOI: 10.1016/j.nucengdes.2004.11.006.

[24] M. Kamaya, A. J. Wilkinson, and J. M. Titchmarsh, "Quantification of plastic strain of stainless steel and nickel alloy by electron backscatter diffraction," *Acta Materialia*, vol. 54, no. 2, pp. 539–548, 2006, ISSN: 13596454. DOI: 10.1016/j.actamat.2005.08.046.

[25] M. Kamaya, "Assessment of local deformation using EBSD: Quantification of local damage at grain boundaries," *Materials Characterization*, vol. 66, pp. 56–67, 2012, ISSN: 10445803. DOI: 10.1016/j.matchar.2012.02.001.

[26] S. Cheong and H. Weiland, "Understanding a microstructure using GOS (Grain Orientation Spread) and its application to recrystallization study of hot deformed Al-Cu-Mg alloys," *Materials Science Forum*, vol. 558-559, pp. 153–158, 2007. DOI: 10.4028/www.scientific.net/MSF.558-559.153.

[27] X. L. Wang, X. P. Ma, Z. Q. Wang, S. V. Subramanian, Z. J. Xie, C. J. Shang, and X. C. Li, "Carbon microalloying effect of base material on variant selection in coarse grained heat affected zone of X80 pipeline steel," *Materials Characterization*, vol. 149, no. October 2018, pp. 26–33, 2019, ISSN: 10445803. DOI: 10.1016/j.matchar.2019.01.005.

[28] S. Morito, H. Yoshida, T. Maki, and X. Huang, "Effect of block size on the strength of lath martensite in low carbon steels," *Materials Science and Engineering A*, vol. 438-440, no. SPEC. ISS. Pp. 237–240, 2006, ISSN: 09215093. DOI: 10.1016/j.msea.2005.12.048.

[29] S. Morito, H. Saito, T. Ogawa, T. Furuhara, and T. Maki, "Effect of Austenite Grain Size on the Morphology and Crystallog- raphy of Lath Martensite in Low Carbon Steels," *Acta Materialia*, vol. 63, no. 9, pp. 202–214, 2005, ISSN: 13596454. DOI: 10.1177/0309324715596700.

[30] C. Celada-Casero, J. Sietsma, and M. J. Santofimia, "The role of the austenite grain size in the martensitic transformation in low carbon steels," *Materials and Design*, vol. 167, 2019. DOI: 10.1016/j.matdes.2019.107625.

[31] J. Hidalgo and M. J. Santofimia, "Effect of Prior Austenite Grain Size Refinement by Thermal Cycling on the Microstructural Features of As-Quenched Lath Martensite," *Metallurgical and Materials Transactions A: Physical Metallurgy and Materials Science*, vol. 47, no. 11, pp. 5288–5301, 2016, ISSN: 10735623. DOI: 10.1007/s11661-016-3525-4.

[32] S. Takaki, K. Fukunaga, J. Syarif, and T. Tsuchiyama, "Effect of Grain Refinement on Thermal Stability of Metastable Austenitic Steel," *Materials Transactions*, vol. 45, no. 7, 2004. DOI: http://dx.doi.org/10.2320/matertrans.45.2245.

[33] S. Sakai, S. Morito, T. Ohba, H. Yoshida, and S. Takagi, "Connectivity of slip systems between different phases in ferrite-martensite dual-phase steels," *Journal of Alloys and Compounds*, vol. 577, no. SUPPL. 1, S597–S600, 2013, ISSN: 09258388. DOI: 10.1016/j.jallcom.2012.02.027.

[34] J. P. Hirth, "The Influence of Grain Boundaries," *Metallurgical Transactions*, vol. 3, no. December, pp. 3047–3067, 1972. DOI: 10.1007/bf02661312.

[35] E. Hall, "The Deformation and Ageing of Mild Steel: III Discussion of Results," *Proc. Phys.Soc. B*, vol. 64, p. 747, 1951.

[36] E. Werner and W. Prantl, "Slip transfer across grain and phase boundaries," *Acta Metallurgica Et Materialia*, vol. 38, no. 3, pp. 533–537, 1990.

[37] I. J. Beyerlein, N. A. Mara, J. Wang, J. S. Carpenter, S. J. Zheng, W. Z. Han, R. F. Zhang, K. Kang, T. Nizolek, and T. M. Pollock, "Structure-property-functionality of bimetal interfaces," *JOM*, vol. 64, no. 10, pp. 1192–1207, 2012, ISSN: 10474838. DOI: 10.1007/s11837-012-0431-0.

[38] L. Patriarca, W. Abuzaid, H. Sehitoglu, and H. J. Maier, "Slip transmission in bcc FeCr polycrystal," *Materials Science and Engineering A*, vol. 588, pp. 308–317, 2013, ISSN: 09215093. DOI: 10.1016/j.msea.2013.08.050.

[39] H. Yoshida, S. Takagi, S. Sakai, S. Morito, and T. Ohba, "Crystallographic analysis of lath martensite in Ferrite-Martensite dual phase steel sheet annealed after cold-rolling," *ISIJ International*, vol. 55, no. 10, pp. 2198–2205, 2015, ISSN: 09151559. DOI: 10.2355/isijinternational.ISIJINT-2014-641.

[40] H. Sharma, J. Sietsma, and S. E. Offerman, "Preferential nucleation during polymorphic transformations," *Scientific Reports*, vol. 6, no. August, pp. 1–7, 2016, ISSN: 20452322. DOI: 10.1038/srep30860.

[41] K. Chattopadhyay, "The Role of Interfaces in Diffusional Growth," *Materials Science Forum*, vol. 3, pp. 231–246, 1985, ISSN: 1662-9752. DOI: 10.4028/www.scientific.net/msf.3.231.

[42] H. Dong, Y. Zhang, G. Miyamoto, H. Chen, Z. Yang, and T. Furuhara, "A comparative study on intrinsic mobility of incoherent and semicoherent interfaces during the austenite to ferrite transformation," *Scripta Materialia*, vol. 188, pp. 59–63, 2020, ISSN: 13596462. DOI: 10.1016/j.scriptamat.2020.07.007.

5

Effect of the anisotropy of martensitic transformation on ferrite deformation in Dual-Phase steels

This chapter is based on the scientific article: V. Atreya, J. S. Van Dokkum, C. Bos, and M. J. Santofimia, "Effect of the anisotropy of martensitic transformation on ferrite deformation in Dual-Phase steels", Materials & Design, vol. 219, p. 110805, 2022 (2022) [1]

The results of the investigations in Chapter 4 indicated that the extent of transformation-induced deformation of ferrite depends upon the crystallographic orientation of the martensite variants formed. The martensitic transformation deformation, composed of dilatation and shear, is anisotropic and variant-specific. However, the transformation deformation is generally considered equivalent to an isotropic dilatation while modelling the transformation-induced deformation of ferrite in Dual-phase (DP) steels. This chapter aims to illustrate the disadvantages of simplifying the anisotropic transformation deformation of martensite to isotropic dilatation. A novel methodology is developed comprising sequential experimental and numerical research on DP steels to quantify transformation-induced deformation and the resulting strains in ferrite. This methodology combines the results of PAG reconstruction, phenomenological theory of martensite crystallography and electron backscatter diffraction (EBSD) orientation data to estimate variant-specific transformation deformation. Subsequently, full-field micromechanical calculation results on a virtual DP steel microstructure are compared with experimental EBSD kernel average misorientation and geometrically necessary dislocation measurement results. It is shown that neglecting the shear deformation associated with the martensitic transformation leads to significant underestimation in the prediction of transformation-induced strains in ferrite.

5.1. INTRODUCTION

The martensite in DP steels is typically formed when austenite present in the microstructure at intercritical conditions transforms into martensite upon rapid cooling. This phase transformation is accompanied by a volume increase and a shape change [2], [3] which, at the macroscopic level, is observed as a unidirectional dilatation and shear deformation of the transforming region. To accommodate the newly formed martensite in the microstructure, the ferritic matrix undergoes deformation resulting in plastic flow and subsequent strain hardening [4], [5].

The transformation-induced plastic deformation of ferrite generates a high density of unpinned dislocations near the ferrite/martensite interface [6]–[8]. Because of the high local stresses already present in the ferrite matrix, the newly formed dislocations start to move and interact even at a relatively low value of global flow stress [9], [10], which results in the typical characteristics of DP steels such as a low elastic limit, continuous yielding, and a high initial work hardening rate [11], [12]. Moreover, the extent of transformation-induced deformation of ferrite significantly influences the yield strength and hardening behaviour of DP steels [4], [5], which highlights the need of estimating the transformation-induced deformation of ferrite to understand the global mechanical behaviour of DP steels.

In Chapter 4, the results of the EBSD experimental study showed that the crystallographic orientation of martensite variants has a strong influence on the transformation-induced deformation of ferrite grains. This is because the direction of dilatation and shear deformations associated with a variant formation depends upon the crystallographic orientation

of the variant and the prior austenite grain (PAG) it belongs to. Post-transformation experimental observation using EBSD does not provide any direct information about PAG orientation and hence it is difficult to accurately estimate the transformation-induced deformation field in ferrite based on such experimental results alone.

Continuum mechanics-based analytical models for transformation-induced deformation of ferrite have been formulated in the past, but only for ideal martensite island shapes [9], [10]. While Sakaki et al. [9] estimated the spatial extent of plastic deformation, Bourell and Rizk [10] estimated the dislocation density increase in the deformed ferrite matrix surrounding a spherical martensite island. For microstructures consisting of martensite with more complex shapes, the transformation-induced deformation of ferrite has been described with a micromechanics-based numerical modelling approach [4], [5], [13]. Naturally, the anisotropic character of the transformation deformation comprising the shear and dilatation deformation associated with every martensite variant is expected to have a strong influence on the transformation-induced deformation of ferrite. However, in the aforementioned works, the transformation deformation was assumed to be comprised only of isotropic dilatation of the prior austenite grains.

The assumption of isotropic dilatation implies that the shear deformation associated with the formation of martensitic variants, oriented differently in space, cancel each other out leaving only the unidirectional dilatation part for consideration. The volume average deformation of all variants combined is then considered equivalent to the isotropic dilatation of the PAG. This assumption is reasonable when the prior austenite grain size is sufficiently large to allow the formation of a maximum of twenty-four martensitic variants with different orientations. However, in the case of DP steels, the small prior austenite grain size (PAGS) allows only the formation of a few martensitic variants [14]–[16]. Hence the volume average shear of all variants is non-zero, and the volume average deformation of all variants combined is less likely to be equal to the isotropic dilatation of the PAG.

This study aims to show the disadvantages of simplifying the anisotropic transformation deformation of martensite to isotropic dilatation for studying the transformation-induced deformation of ferrite in the case of relatively small PAGS, such as in DP steels. Quantification of the transformation-induced deformation of ferrite is proposed using a novel methodology comprising sequential experimental and numerical research on DP steels.

5.2. APPROACH AND THEORETICAL MODELS

The approach to model the transformation-induced deformation of ferrite is schematically presented in figure 5.1. It is divided into four steps and starts with an EBSD scan of the DP steel microstructure to obtain lattice orientations of ferrite and martensite, followed by prior austenite grain reconstruction to estimate the morphology and lattice orientation of prior austenite grains. The anisotropic transformation deformation is then determined by using the phenomenological theory of martensite crystallography (PTMC)

[3], [17], [18]. As per the authors' knowledge, the application of a crystallographic theory (such as the PTMC) to calculate the magnitude of shear and dilatation components of transformation deformation is missing in the previous modelling works concerning the transformation-induced deformation of ferrite in DP steels. Subsequently, the transformation is mimicked by subjecting all reconstructed prior austenite grains, constrained by an initially undeformed ferrite matrix, to the anisotropic deformation associated with the transformation. The resulting transformation-induced deformation of ferrite is calculated using a micromechanical model (Appendix A)[19]. A detailed explanation of every step follows.

5.2.1. ANALYSIS OF THE FERRITE/MARTENSITE MICROSTRUCTURE (STEP 1)

The EBSD scan of a selected location within the DP steel specimen is carried out to obtain information about the distribution of phases and crystal orientations. Although both ferrite and martensite are recognized in the EBSD as bcc crystal structures, martensite regions exhibit low image quality in the EBSD scans. Therefore the grain average image quality measure is used to distinguish martensite from ferrite regions [20]. The identified martensite data points are used as input for the PAG reconstruction.

5.2.2. PRIOR AUSTENITE GRAIN RECONSTRUCTION (STEP 2)

The PAG reconstruction was performed using Mtex, a freely available Matlab toolbox [21], [22]. Only the measurement points corresponding to martensite in the EBSD scan were considered for reconstruction. The reconstruction involves determination of the experimentally observed orientation relationship (OR) between austenite and martensite, which usually deviate slightly from the Kurdjumov-Sachs (K-S) OR [23]. The procedure followed in Mtex to determine the experimentally observed OR is described as follows.

The misorientation matrix, $\mathbf{M}_{ij}$, between two martensitic variants, i and j, formed from the same prior austenite grain can be represented as [24], [25]

$$\mathbf{M}_{ij} = \mathbf{C}_j^{-1}\,\mathbf{T}^{-1}\,\mathbf{S}_j^{-1}\,\mathbf{S}_i\,\mathbf{T}\,\mathbf{C}_i\,, \tag{5.1}$$

where $\mathbf{S}_i$ and $\mathbf{S}_j$ are one of the 24 cubic symmetry matrices for the prior austenite grains of ith and j^{th} martensitic variants respectively, $\mathbf{C}_i$ and $\mathbf{C}_j$ are one of the 24 cubic symmetry matrices for i^{th} and j^{th} martensitic variants as well, $\mathbf{T}$ is the austenite-martensite orientation relationship matrix, and superscript $\bullet^{-1}$ denotes the inverse. Here, the subscripts are not index notations. The term $\left(\mathbf{T}^{-1}\,\mathbf{S}_j^{-1}\,\mathbf{S}_i\,\mathbf{T}\right)$ results in 24 distinct rotations [24]. If the experimentally observed misorientation matrix $\mathbf{M}_{\text{exp}}$, between the two martensitic variants, i and j, is found to be close to one of the predicted 24^3 misorientation matrices according to equation 5.1, the two variants are assigned to the same PAG. However, prior to this calculation, the OR matrix $\mathbf{T}$ should be ascertained. Manipulating equation 5.1, we find that:

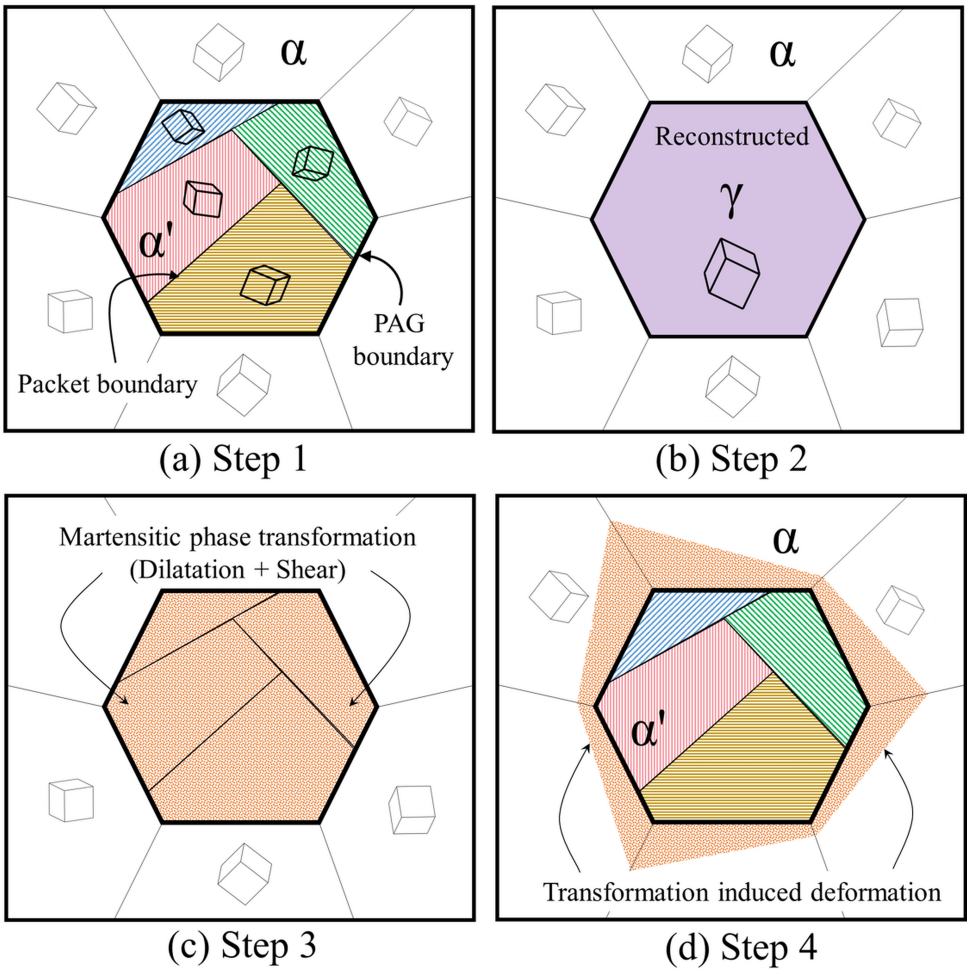

Figure 5.1: Illustration of the four steps involved in the calculation of transformation-induced deformation of ferrite. (a) The crystal orientations of ferrite and martensite phases in the specimen are obtained from EBSD measurements (b) A PAG reconstruction algorithm provides the shape and the crystal orientation of the PAGs. (c) The anisotropic transformation deformations are calculated using the phenomenological theory of martensite crystallography (PTMC) (d) The reconstructed PAGs are subjected to the calculated anisotropic and variant-specific transformation deformations and the resulting transformation-induced deformation of ferrite is calculated via micromechanical modelling.

$$\mathbf{T} = \left(\mathbf{T}^{-1}\,\mathbf{S}_j^{-1}\,\mathbf{S}_i\right)^{-1}\mathbf{C}_j\,\mathbf{M}_{\text{exp}}\,\mathbf{C}_i^{-1}\,. \tag{5.2}$$

Since the OR matrix $\mathbf{T}$ appears on both sides of equation 5.2, the equation can only be solved iteratively. Equation 5.2 then becomes:

$$\mathbf{T}_{n+1} = \left(\bar{\mathbf{T}}_n^{-1}\,\mathbf{S}_j^{-1}\,\mathbf{S}_i\right)^{-1}\mathbf{C}_j\,\mathbf{M}_{\text{exp}}\,\mathbf{C}_i^{-1}\,, \tag{5.3}$$

where n is the iterator, $\mathbf{T}_{n=0}$ is the initial guess for $\mathbf{T}_n$ equal to the OR matrix corresponding to the theoretical K-S OR, $\mathbf{T}_{n+1}$ is the OR matrix calculated from $\mathbf{M}_{\text{exp}}$, and $\bar{\mathbf{T}}_n$ is the OR matrix corresponding to average of all ORs determined in the previous iterations. The iterative process is based on determining correct symmetry matrices by using $\mathbf{T} = \bar{\mathbf{T}}_n$ in equation 5.1 and comparing all predicted values of misorientation matrix $\mathbf{M}_{ij}$ with $\mathbf{M}_{\text{exp}}$. When there is no change in the calculated symmetry matrices in subsequent iterations, the final OR matrix $\bar{\mathbf{T}}_n$ is concluded to be the observed experimental orientation relationship for the specimen under study.

The application of this reconstruction algorithm not only predicts the PAG shape but also helps in identifying the martensitic variants and provides an estimate for PAG crystal orientation. This information is further used to determine the anisotropic, variant-specific transformation deformation.

5.2.3. DETERMINATION OF MARTENSITIC TRANSFORMATION DEFORMATION (STEP 3)

The austenite to martensite phase transformation comprises of dilatation and shear deformation [3], [17], [26]. The transformation is an invariant plane strain (IPS) deformation, where the invariant plane is also called the habit plane. The dilatation part is perpendicular to the invariant plane of martensitic transformation, while the shear part is parallel to the invariant plane. According to the phenomenological theory of martensite crystallography (PTMC), the IPS can be expressed in the form of the following equation [3], [17], [18]:

$$\mathbf{Z} = \mathbf{R}\,\mathbf{B}\,\mathbf{P}\,, \tag{5.4}$$

where $\mathbf{Z}$ is the IPS shape deformation gradient matrix, $\mathbf{R}$ is the rotation matrix representing a rigid body rotation, $\mathbf{B}$ is the Bain strain matrix, and $\mathbf{P}$ is the lattice invariant shear matrix. The lattice invariant shear is either in the form of slip, resulting in the formation of laths in low carbon martensite, or in the form of twinning in high carbon martensite [27]. Since martensitic transformation is an invariant plane strain deformation, $\mathbf{Z}$ can also be written in the following form [26]

$$\mathbf{Z} = \mathbf{I} + m\,\hat{\boldsymbol{d}} \otimes \hat{\boldsymbol{p}}, \tag{5.5}$$

where m is the magnitude of displacements in the direction of displacement unit vector $\hat{\boldsymbol{d}}$, $\hat{\boldsymbol{p}}$ is the habit plane unit normal vector, and $\otimes$ is the outer product. The slip plane and direction for the lattice invariant shear matrix $\mathbf{P}$ are assumed to be $\{112\}\langle 111\rangle_{\text{bcc}}$ since it

is common to observe {112} striations on the martensite surface [28]. The shape deformation gradient matrix **Z** and the rotation matrix **R** are now calculated from equations 5.4 and 5.5. The Bain strain matrix **B** is calculated from lattice parameters of martensite and prior austenite [26]. In this work, PTC lab software [29] is used to obtain the solution for the shape deformation gradient matrix **Z** by providing lattice parameters of austenite and martensite as inputs.

Apart from the shape deformation gradient matrix **Z**, the PTMC also enables the calculation of orientation transformation matrix **T** using the PTC lab software [29]. The change in crystallographic orientation due to martensitic transformation can be expressed in the form of the following matrix equation [30], [31]:

$$\mathbf{M} = \mathbf{T}\,\mathbf{A}, \tag{5.6}$$

where **M** and **A** are the orientation matrices consisting of three orthogonal unit vectors representing the crystal orientation of martensite and austenite respectively. The orientation transformation matrices of all 24 K-S variants of martensite are

$$\mathbf{T}_k = \mathbf{C}_k\,\mathbf{T}\,{\mathbf{C}_k}^{\mathrm{T}}, \tag{5.7}$$

where **C** is the cubic symmetry matrix, k=1$\cdots$24, and $\bullet^T$ is the transpose of the matrix. Plugging equation 5.7 into 5.6, we have

$$\mathbf{M}_k = \mathbf{C}_k\,\mathbf{T}\,{\mathbf{C}_k}^{\mathrm{T}}\,\mathbf{A}, \tag{5.8}$$

which gives the orientation matrices of all 24 variants formed from a prior austenite grain. Similarly, the IPS solution **Z** for all 24 variants formed from a single prior austenite grain is calculated using the following equation:

$$\mathbf{Z}_k = \mathbf{C}_k\,\mathbf{Z}\,{\mathbf{C}_k}^{\mathrm{T}}, \tag{5.9}$$

where $\mathbf{Z}_k$ is the variant-specific deformation matrix which can only be obtained if the correct symmetry matrix $\mathbf{C}_k$ is identified. The symmetry matrix $\mathbf{C}_k$ which results in the minimum misorientation angle between $\mathbf{M}_k$ and the experimentally measured orientation matrix of a variant is concluded to be the correct symmetry matrix for that variant present at a specific martensite location in the EBSD scan.

The deformation gradient matrix $\mathbf{Z}_k$ is calculated with respect to the reference frame of the prior austenite grain. Any given PAG has an arbitrary orientation with respect to the specimen coordinates. The correct IPS deformation gradient matrix for any martensitic variant is [32]:

$$\mathbf{Z}_{kl} = \mathbf{A}_l \left(\mathbf{C}_k \mathbf{Z} {\mathbf{C}_k}^{\mathrm{T}} \right) {\mathbf{A}_l}^{\mathrm{T}}, \tag{5.10}$$

where $\mathbf{A}_l$ is the orientation matrix of lth prior austenite grain. The variant-specific deformation gradient matrices, $\mathbf{Z}_{kl}$, are used to calculate the variant-specific eigenstrains $\boldsymbol{\epsilon}^*_{kl}$. Eigenstrains are the strains developed in the material due to inelastic processes such as phase transformation and thermal expansion in the absence of any external mechanical stress. The variant-specific eigenstrains $\boldsymbol{\epsilon}^*_{kl}$ are then used as input in the micromechanical model to calculate the transformation-induced strains in ferrite.

5.2.4. MICROMECHANICAL CALCULATION OF TRANSFORMATION-INDUCED STRAINS IN FERRITE (STEP 4)

In the last step of the proposed procedure, micromechanical calculations are performed to estimate the transformation-induced strains in the ferrite matrix in response to austenite undergoing variant-specific deformation while transforming into martensite. A Fast Fourier Transform (FFT)-based micromechanical modelling software, CraFT 1.0, is used to perform the calculations (Appendix A) [19]. The inputs for the calculations are: a representative volume element (RVE) based on a microstructural image of DP steel, a behaviour law for each phase involved in the RVE, the boundary conditions imposed on the RVE, and the eigenstrains corresponding to martensitic transformation deformation.

In the present micromechanical model calculations, the strains are assumed to be infinitesimal. This means that the second-order terms from the definition of finite strain are neglected. Therefore any significant transformation-induced rotation in the material contributes to the error in calculated transformation-induced strains. A comparative analysis of the transformation-induced deformation of ferrite is performed, in response to two different assumptions regarding martensite transformation deformation, i.e., isotropic and anisotropic transformation deformation. The trends observed are considered representative given the absence of local *a priory* known rotations. The intention here is to use the simplest numerical method to elucidate the importance of considering the anisotropy of martensitic transformation deformation in modelling studies.

5.3. ANALYSIS OF A DP STEEL MICROSTRUCTURE USING THE PROPOSED METHOD

5.3.1. EXPERIMENTAL PROCEDURE

Cold-rolled steel with composition Fe-0.14C-1.8Mn-0.24Si by weight % and with an initial microstructure consisting of pearlite and ferrite was cut into a specimen of dimensions 10 mm x 4 mm x 2 mm using electrical discharge machining. Using a Bähr DIL A/D dilatometer, the specimen was heated at 5 K/s, kept at 775°C for 5 min, and then quenched to obtain a ferrite-martensite dual-phase microstructure. The specimen was ground

using SiC abrasive papers and subsequently polished using 3 and 1 μm diamond paste. Further, it was electropolished using Struers A2 electrolyte at 35V, 277 K for 6 s. EBSD measurements were made on a Zeiss Ultra 55 scanning electron microscope (SEM) using the Edax Pegasus XM 4 Hikari EBSD system. The step size of the scan was 50 nm. The EBSD scans were analyzed using the TSL OIM version 7 software.

5.3.2. APPLICATION

ANALYSIS OF THE FERRITE/MARTENSITE MICROSTRUCTURE

The microstructure of the specimen used in this work was investigated in detail in a previous study [33] elaborated in Chapter 4. Figure 5.2(a) shows the image quality (IQ) map of the specimen obtained via EBSD scan, which is a part of the full IQ map shown in figure 4.2(b). The dark-coloured martensite is present in the form of connected, chain-like structures. The sub-region used for PAG reconstruction and RVE generation for micromechanical calculations is highlighted in red and shown enlarged in figure 5.2(b). The RVE hence generated based on the IQ map is shown in figure 5.2(c) where blue and red colours represent ferrite and martensite respectively.

The martensite volume fraction for the specific scanned location of the specimen was calculated to be 0.56 [33], based on phase identification using grain average image quality (GAIQ) measurements [20], [33]. GAIQ is the average image quality of all measurement points within a grain. Using an angular tolerance value between 0.5-1.5° to identify the grains followed by an application of GAIQ measure enables excellent identification and quantification of martensite in a DP steel microstructure [20], [33]. The equilibrium carbon content in ferrite at the intercritical temperature calculated using ThermoCalc software is 0.006 wt.%. Consequently, the carbon content in martensite was calculated to be 0.23 wt.% [33] after the application of carbon mass balance. The lattice parameters used in this study to calculate transformation-deformation are a = 2.858 nm and c = 2.885 nm for martensite and a = 3.565 nm for prior austenite based on calculated carbon content [34].

The nth neighbour kernel average misorientation (KAM) at an EBSD measurement point is the average misorientation of the nth nearest neighbour points with respect to that measurement point. Since intra-grain misorientations arise due to dislocations, KAM values can be used to study the level of deformation within individual grains [35]. Figure 5.2(d) shows the KAM maps of the region of interest for the 5th nearest neighbors and a maximum 3° misorientation. As expected, the highest KAM values are observed for the martensite regions. The KAM magnitude is higher in ferrite grains near the phase boundary than in the grain interior. This becomes apparent in figure 5.2(e), where the KAM values are grouped into five uniformly spaced ranges and overlaid on the IQ map. The regions near the phase boundary which show higher KAM are highlighted in dashed white ellipses.

A local geometrically necessary dislocation (GND) density map is calculated using MTex software [21], [22], [36], following the approach given by Pantleon [37]. This approach involves the calculation of the dislocation density tensor at every measurement point of the EBSD scan, whose components are determined using the lattice curvature tensor. The lattice curvature tensor is calculated from the misorientations between neighbouring points in an EBSD scan. Figure 5.2(f) shows the result for the GND density calculations, with some regions of relatively high GND densities highlighted with black dashed ellipses.

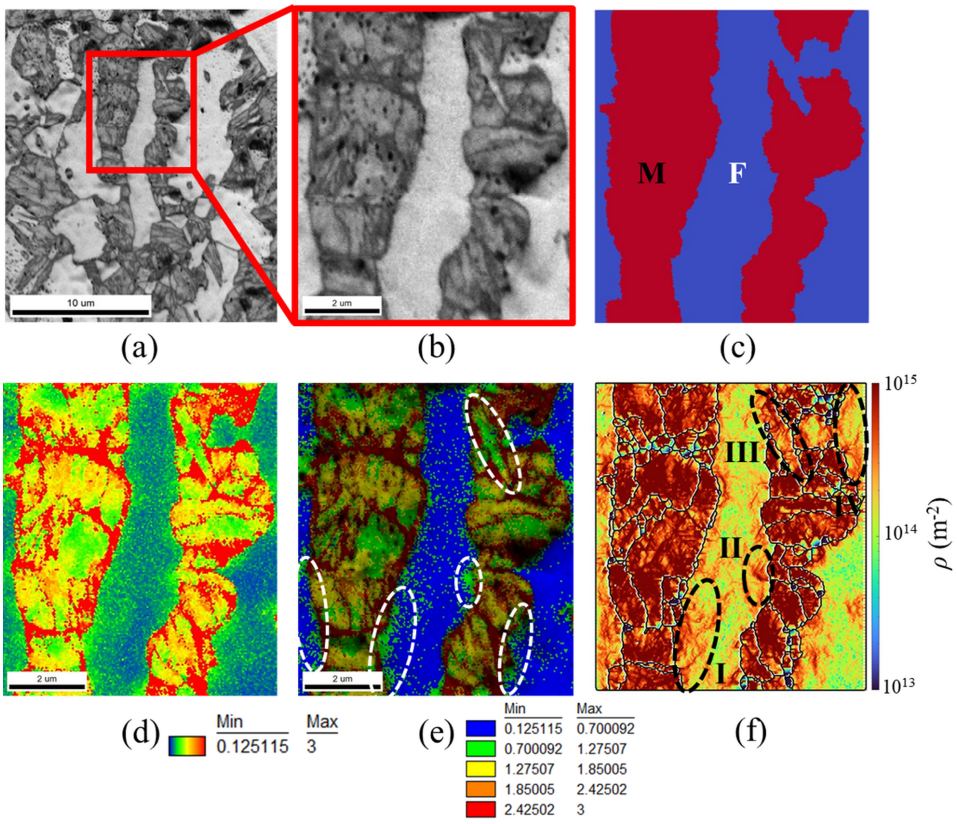

Figure 5.2: (a) Image quality (IQ) map of the specimen region scanned with EBSD (b) Specific area selected for this study (c) Generation of an RVE consisting of ferrite and martensite (d) Kernel average misorientation (KAM) map for the selected region. KAM values are in degrees (e) KAM map for the selected region with values grouped into specific ranges. Areas within the white dashed white ellipses indicate higher KAM regions in ferrite (f) Geometrically necessary dislocations (m^{-2}) calculated for the region of interest. Some regions of higher GND density are highlighted with black dashed ellipses.

PRIOR AUSTENITE GRAIN RECONSTRUCTION

To carry out the prior austenite grain (PAG) reconstruction, the bcc ferrite phase data points in the EBSD maps were identified using the grain average image quality (GAIQ) criterion and then removed from the EBSD scan data. Reconstruction was then performed

on the remaining martensite data points. Mtex version 5.6 toolbox available in Matlab [21] was used for carrying out the PAG reconstruction.

Figure 5.3(a) shows the reconstructed parent grain boundaries overlaid on the IQ map of the region of interest shown in figure 5.2(b). Figures 5.3(b) and 5.3(c) show the packet and variant map of all the PAGs shown in figure 5.3(a). The PAGs are very small and with a mean diameter of 1.6 μm. The average number of martensite variants in PAGs is 6.

Figure 5.4(a) shows the pole figure orientation of the largest prior austenite grain, named 'PAG 1', indicated in figure 5.3(a). Figure 5.4(b) shows the pole figures of identified variants of 'PAG 1'. The theoretical pole figure of all 24 variants according to the OR identified during the reconstruction is shown in figure 5.4(c). Experimental pole figures of the variants match very well with the expected theoretical pole figures. The experimental OR was found to be 1.1 degrees off from the theoretical K-S relationship.

A comparison of the pole figures of martensitic variants according to theoretical K-S and those obtained via PTMC is shown in figure 5.4(d). The misorientation between predictions of variant orientation by K-S OR and that by PTMC is 3.22°. Neither the PTMC nor the K-S OR predicts the experimentally observed ORs accurately.

As per the prediction of PTMC, the deviation between close-packed planes of austenite $(111)_\gamma$ and martensite $(110)_\alpha$ decreases from 0.4°to 0.3° when the carbon content increases from 0.1 wt.% to 0.4 wt.%. This is also corroborated in experiments where the decrease in angular deviation for close-packed planes is from 0.8° to 0.3° for the same increase in carbon content [38]. This shows that even though PTMC may not capture the experimentally observed OR, it can predict the changes in OR with varying carbon content in austenite/martensite.

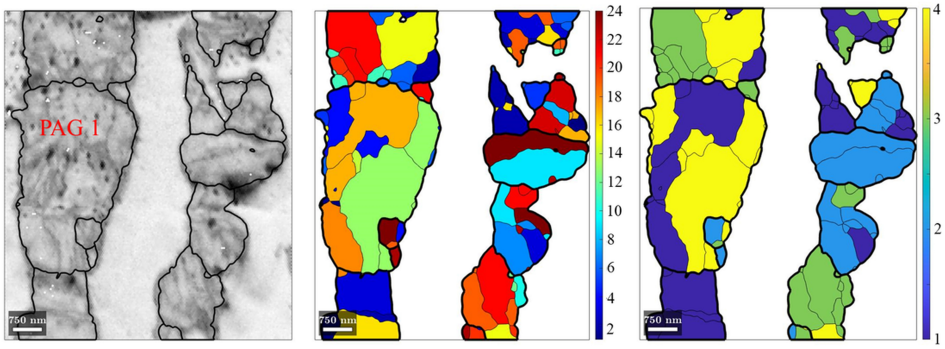

Figure 5.3: (a) Reconstructed prior austenite grain boundaries in black overlaid on image quality map of the region of interest (b) Variants of every PAG coloured differently, with a maximum of 24 variants per PAG (c) Packets of every PAG coloured differently, with a maximum of 4 packets per PAG.

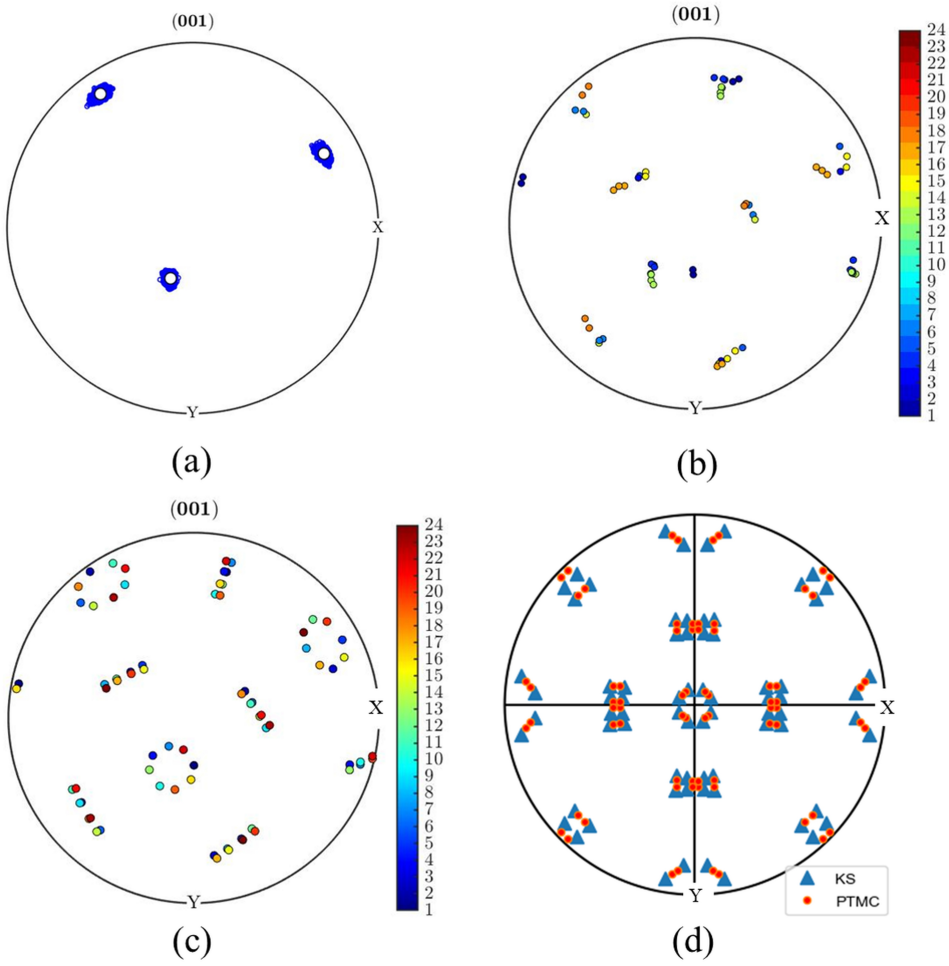

Figure 5.4: (a) Pole figure of the largest prior austenite grain (PAG 1) indicated in figure 5.3(a); (b) The pole figures of identified variants. (c) The theoretical pole figure of all 24 variants according to the OR identified during the reconstruction (d) A comparison of the pole figures of martensitic variants according to theoretical K-S and those obtained via PTMC.

DETERMINATION OF MARTENSITIC TRANSFORMATION DEFORMATION

The anisotropic transformation eigenstrain for martensite, $\boldsymbol{\epsilon}^{*,\text{aniso}}_{kl}$, for the kth variant of the lth austenite grain is calculated from the anisotropic transformation deformation matrix, $\mathbf{Z}_{kl}$ of equation 5.9 using the definition of Green-Lagrange strain (appendix A). The value of m in equation 5.5 as calculated using PTMC theory is 0.26. The transformation eigenstrain matrix for isotropic dilatation of martensite, $\boldsymbol{\epsilon}^{*,\text{iso}}$, is of the form $\boldsymbol{\epsilon}^{*,\text{iso}} = (\boldsymbol{\Delta}/3)\,\boldsymbol{\delta}_{ij}$, where $\boldsymbol{\Delta}$ is the volumetric strain for austenite to martensite transformation

and $\boldsymbol{\delta}_{ij}$ is the Kronecker delta representing the identity matrix. The volumetric strain accompanying martensitic phase transformation depends on the carbon content as [2], [9]:

$$\boldsymbol{\Delta} = \left(\frac{\Delta V_{\gamma\rightarrow\alpha}}{V_\gamma}\right)_{\mathrm{M_s}} = 0.017 + 0.013 X_\mathrm{C}\,, \tag{5.11}$$

where $\Delta V_{\gamma\rightarrow\alpha}$ is the change in specific volume due to phase transformation from austenite (γ) to martensite (α), V_γ is the specific volume of austenite, and X_C is the carbon content of austenite in wt.%. For $X_\mathrm{C} = 0.23$, $\boldsymbol{\Delta}$ is calculated to be 2.0×10^{-2}. In equation 5.11, all transformation is assumed to occur at the martensite start temperature ($\mathrm{M_S}$).

MICROMECHANICAL CALCULATION OF TRANSFORMATION-INDUCED STRAINS IN FERRITE

Following PAG reconstruction, the micromechanical model calculations are performed on the EBSD-based RVE to calculate transformation-induced strains in ferrite. Depending upon the variant identity, the corresponding eigenstrain is applied at the locations of transformation. The lattice-invariant shear between the martensitic laths is a part of the macroscopic shape deformation and therefore does not need to be considered separately in the micromechanical calculations. Assuming a fixed room-temperature value of linear thermal expansion coefficient, the thermal strain in ferrite due to quenching is in the order of 10^{-3} [39]. The strains induced in ferrite by anisotropic martensitic transformations are expected to be higher in magnitude (in the order of 10^{-1}) than the thermal strains, hence thermal strains are not considered in this study.

The material behaviour of martensite was assumed to be isotropic elastic, while ferrite was considered isotropic elastic-plastic with linear hardening in the following form:

$$\sigma_0 = \sigma_\mathrm{Y} + H\epsilon_\mathrm{vM}\,, \tag{5.12}$$

where σ_0 is the flow stress, $\sigma_\mathrm{Y} = 283$ MPa is the uniaxial ferrite yield strength, $H = 595$ MPa is the plastic modulus [19]-a parameter which determines the level of strain hardening depending upon strain magnitude, and ϵ_vM is von-Mises equivalent strain. The values of σ_Y and H were chosen in such a way that the flow curve resulting from equation 5.12 is the best linear fit for the experimentally observed uniaxial tensile flow curve of ferrite with a similar carbon concentration as shown in figure 5.5 [40]. The elastic modulus and Poisson's ratio for martensite (E=203.5 GPa, ν=0.292) and ferrite (E=209 GPa, ν=0.289) are obtained from the literature [41].

For the EBSD-based RVE, the spatial discretization in the x, y and z directions is 332 × 291 × 1, equal to the number of measurement points in the area selected to study from the EBSD scan. Periodic boundary conditions are applied in the plane of the 2D surface. No information is available on grain morphology out of the plane. Therefore, a mechanical

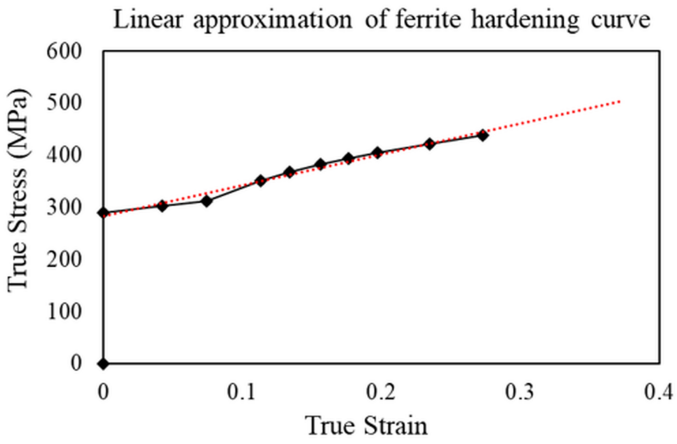

Figure 5.5: (a) Linear approximation of ferrite hardening curve (in red dotted line) based on experimental flow curves of ferrite presented in reference [40]

limit is applied and the average far-field strain orthogonal to the 2D surface is set to zero, i.e., plane strain condition was considered for the in-plane direction. The convergence of the numerical iterative process was evaluated by comparison with the required accuracy of 10^{-5} m^{-1}.

Figure 5.6 shows the von-Mises equivalent map of (a) transformation-induced strains in ferrite due to isotropic transformation eigenstrains, $\epsilon_{vM}^{iso,tr\text{-}ind}$, and (b) transformation-induced strains in ferrite due to anisotropic transformation eigenstrains, $\epsilon_{vM}^{aniso,tr\text{-}ind}$. The magnitude of deformation at all locations in ferrite is found to be higher in figure 5.6(b) than in 5.6(a). The high strain regions highlighted with black dashed circles at the top and bottom edge of both figures 5.6(a) and 5.6(b), arise because of the imperfect periodicity of the microstructural region selected for this study. It is to be noted that the elastic lattice strains within martensite are numerically obtained but are not shown in the strain maps as they hamper the visibility of strains in ferrite.

5.4. DISCUSSION

Figures 5.2(d) and 5.2(e) show that some regions of ferrite near the phase boundary have higher KAM values, indicating higher deformation. These regions are highlighted by dashed white ellipses in figure 5.2(e). As reported in Chapter-4, the spatial extent of type II SR ferrite deformation lies approximately in the range of 0.1 μm – 0.5 μm from the ferrite/martensite interface [33]. It is important to note that this distance is not a single fixed value. Previous micromechanical modelling studies assuming isotropic dilatation during transformation assume that a continuous deformed ferrite region of specific width exists along the phase boundaries [4], [13], [42]. The results of the present modelling

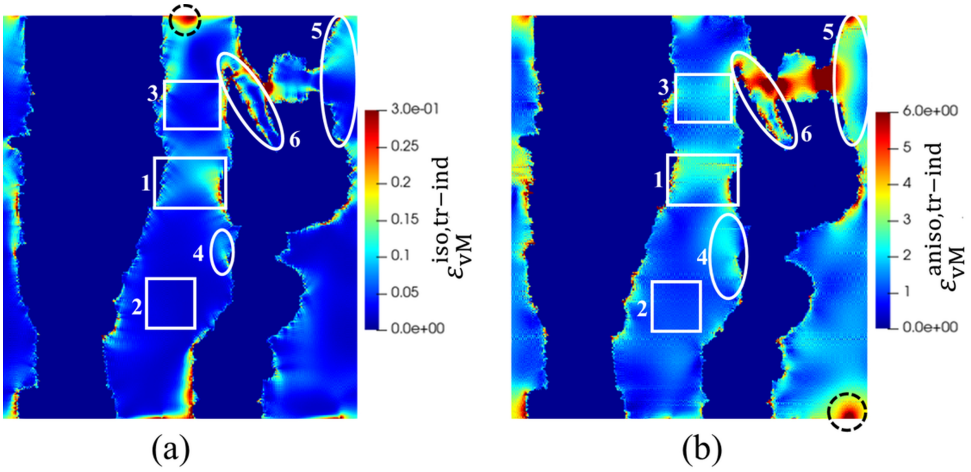

Figure 5.6: von-Mises equivalent map of (a) transformation-induced strain in ferrite due to isotropic transformation eigenstrains, $\epsilon_{vM}^{iso,tr-ind}$, and (b) transformation-induced strain in ferrite due to anisotropic transformation eigenstrains, $\epsilon_{vM}^{aniso,tr-ind}$

study, shown in figure 5.6(a) and 5.6(b), corroborate previous experimental results that the deformed ferrite region is discontinuous and the extent of deformation varies from one location to another [33].

The PAG reconstruction results shown in figure 5.3 reveal that the PAGs in the current DP steel specimen are very small with a mean diameter of 1.6 μm and an average of 6 variants within every PAG. As mentioned earlier, several previous studies assumed that the shear component of transformation for differently oriented variants cancel each other leaving only the dilatation part as the effective transformation deformation [4], [9], [10], [42] However, present results suggest that such an assumption should be avoided wherever small PAGs with much less than 24 variants are present. For instance, the prior austenite grain marked 'PAG 1' in figure 5.3(a) consist of 14 variants. The magnitude of ferrite deformation adjacent to 'PAG 1' for the case of isotropic dilatation (figure 5.6(a)) is less than that of anisotropic deformation (figure 5.6(b)). This proves that the shear deformations accompanying the formation of 14 variants do not cancel out, otherwise, the transformation-induced deformation of ferrite would have been similar in both cases. Therefore, the average transformation deformation in DP steels with small PAGS cannot be considered equivalent to an isotropic dilatation of prior austenite.

The micromechanical model calculation results in figures 5.6(a) and 5.6(b) show that the transformation-induced deformation of ferrite is non-homogenous throughout the microstructure, regardless of the assumption of isotropic or anisotropic transformation deformation. This non-homogeneity is more pronounced in figure 5.6(b) since the varia-

tion in magnitude of transformation-induced strains is larger in this case. For example, the strain in the region marked '1' is significantly higher in magnitude compared to that of the region marked '2'.

The assumption of isotropic or anisotropic transformation deformation in the micromechanical calculations affects the distribution of transformation-induced strains in ferrite. Large strains are present at different locations depending on the choice of the assumption. For instance, in figure 5.6(b), the area marked '3' shows a relatively larger strain compared to its surroundings, whereas in figure 5.6(a) the same area shows comparatively smaller strain. Similarly, the areas marked '4' and '5' also show relatively large strain in figure 5.6(b) than in figure 5.6(a). In general, at most locations, the strain in ferrite due to anisotropic transformation deformation is larger by a factor of up to 10 than that induced by isotropic dilatation.

In the case of isotropic transformation deformation, the dilatation is the same for all the variants. Therefore the non-homogeneity in the transformation-induced deformation of ferrite, in this case, is because of complex grain shapes. In the case of anisotropic transformation deformation, the non-homogeneity in the transformation-induced deformation of ferrite is not only because of complex grain shapes but also because of the martensite variants formed within PAGs. This is because the magnitude and direction of shear and dilatation deformation differ for every martensitic variant. As a consequence, every variant uniquely deforms the surrounding ferrite matrix.

On comparing the results of the present micromechanical model calculations to the GND density map, it is observed that the regions of high GND density marked 'II', 'III', and 'IV' in figure 5.2(f) correspond to the regions of high strain '4', '6', and '5' respectively in figures 5.6(a) and (b). This correspondence is stronger in figure 5.6(b), i.e., in the case of anisotropic transformation. There are also some regions of high GND density, such as the one marked 'I' in figure 5.2(f), which do not have high strain at the corresponding locations in the strain maps. This is perhaps because the transformation-induced deformation of ferrite observed on the surface is also contributed to by the martensite formation below the observed surface, while the present study is carried out on a 2D EBSD-based RVE. Region '3' with high strain in figure 5.6(b) does not have a corresponding region of high GND density in figure 5.2(f), which may be because of incorrect identification of martensite variants adjacent to this region.

This study elucidates the importance of including the anisotropy of martensitic transformation deformation in modelling the mechanical behaviour of DP steels. However, it also reveals that indirect measures of in-grain deformation in the form of experimental KAM or GND values are insufficient to validate the transformation-induced deformation of ferrite estimated via the current modelling approach. Hence, the following aspects of this study can be considered in future investigations: (i) Instead of PTMC, more advanced theories such as the double shear theory [43], and parameter-free double shear theory [44] can

be used to calculate anisotropic transformation strains with even more accuracy, (ii) the local variations in the carbon content of the martensite should be taken into account while using PTMC and PAG reconstruction, (iii) 3D PAG reconstruction based on 3D EBSD measurement should be carried out to take into account the anisotropic transformation strains associated with martensite formation beneath the observed surface, (iv) The use of finite strain definition in micromechanical calculations should provide more accurate quantification of transformation-induced strains in ferrite.

5.5. CONCLUSIONS

The martensitic transformation-induced deformation of ferrite has a profound effect on the mechanical behaviour of DP steels. In previous studies modelling the transformation-induced deformation of ferrite, the anisotropy of transformation deformation was ignored. Rather, isotropic dilatation alone was considered to induce the deformation of the surrounding ferrite matrix. In this work, the validity of the assumption of isotropic dilatation during the transformation of small PAGs and the effect of anisotropic transformation deformation in causing deformation of the surrounding ferrite matrix in DP steels are evaluated.

To this end, a methodology is developed whereby the martensitic transformation-induced strains can be studied in DP steels as well as other multiphase steel microstructures containing martensite. The methodology includes four steps: (i) Analysis of the ferrite/martensite dual-phase microstructure, (ii) prior austenite grain reconstruction (iii) determination of martensitic transformation deformation, and (iv) calculation of transformation -induced strains in the ferrite matrix surrounding the martensite.

In previous modelling works concerning the transformation-induced deformation of ferrite in DP steels, PAG orientations were disregarded. In this study, the PAG orientations and morphology are obtained via PAG reconstruction from martensite regions of DP steel microstructure. The results of the PAG reconstruction and PTMC are then combined with the EBSD orientation data for the martensite in a unique way to estimate the variant-specific transformation deformation required for performing micromechanical calculations. The calculated transformation-induced strains in ferrite are further compared with experimental EBSD KAM and GND measurements of the same.

The results show regions of relatively large deformation in ferrite very close to the phase boundaries in experimental EBSD KAM and GND density maps as well as simulated ferrite strain maps. However, not all regions of large deformation in experimental and simulated results necessarily coincide. This may be because the influence of martensite formation below the experimentally observed surface of the specimen is not considered in this study. Moreover, a different martensite variant may be present at a location than predicted using calculations.

The assumption of isotropic or anisotropic transformation deformation in the microme-

chanical calculations affects the distribution of transformation-induced strains in ferrite. The transformation-induced deformation of ferrite is determined primarily by prior austenite and ferrite grain shapes along with the anisotropy of martensitic transformation deformation. It is also shown that neglecting the shear deformation associated with martensitic transformation under the assumption of isotropic dilatation results in a significant underestimation of transformation-induced strains in ferrite.

REFERENCES

[1] V. Atreya, J. S. Van Dokkum, C. Bos, and M. J. Santofimia, "Effect of the anisotropy of martensitic transformation on ferrite deformation in Dual-Phase steels," *Materials & Design*, vol. 219, p. 110 805, 2022, ISSN: 02641275. DOI: 10.1016/j.matdes.2022.110805.

[2] J. M. Moyer and G. S. Ansell, "The Volume Expansion Accompanying the Martensite Transformation in Iron-Carbon Alloys," *Metallurgical Transactions A*, vol. 6, no. September, pp. 1785–1791, 1975. DOI: 10.1007/BF02642308.

[3] J. S. Bowles and J. K. Mackenzie, "The crystallography of martensite transformations I," *Acta Metallurgica*, vol. 2, no. 1, pp. 129–137, 1954, ISSN: 00016160. DOI: 10.1016/0001-6160(54)90102-9.

[4] A. Ramazani, K. Mukherjee, U. Prahl, and W. Bleck, "Transformation-induced, geometrically necessary, dislocation-based flow curve modeling of dual-phase steels: Effect of grain size," *Metallurgical and Materials Transactions A: Physical Metallurgy and Materials Science*, vol. 43, no. 10, pp. 3850–3869, 2012, ISSN: 10735623. DOI: 10.1007/s11661-012-1196-3.

[5] A. Ramazani, K. Mukherjee, A. Schwedt, P. Goravanchi, U. Prahl, and W. Bleck, "Quantification of the effect of transformation-induced geometrically necessary dislocations on the flow-curve modelling of dual-phase steels," *International Journal of Plasticity*, vol. 43, pp. 128–152, 2013, ISSN: 07496419. DOI: 10.1016/j.ijplas.2012.11.003.

[6] U. Liedl, S. Traint, and E. A. Werner, "An unexpected feature of the stress-strain diagram of dual-phase steel," *Computational Materials Science*, vol. 25, no. 1-2, pp. 122–128, 2002, ISSN: 09270256. DOI: 10.1016/S0927-0256(02)00256-2.

[7] D. A. Korzekwa, D. K. Matlock, and G. Krauss, "Dislocation substructure as a function of strain in a dual-phase steel," *Metallurgical Transactions A*, vol. 15, no. 6, pp. 1221–1228, 1984, ISSN: 03602133. DOI: 10.1007/BF02644716.

[8] S. Li, C. Guo, L. Hao, Y. Kang, and Y. An, "In-situ EBSD study of deformation behaviour of 600 MPa grade dual phase steel during uniaxial tensile tests," *Materials Science and Engineering A*, vol. 759, no. March, pp. 624–632, 2019, ISSN: 09215093. DOI: 10.1016/j.msea.2019.05.083.

[9] T. Sakaki, K. Sugimoto, and T. Fukuzato, "Role of internal stress for the initial yielding of Dual-Phase steels.," *Acta Metallurgica*, vol. 31, pp. 455–460, 1983. DOI: 10.1016/b978-1-4832-8423-1.50076-6.

[10] D. L. Bourell and A. Rizk, "Influence of martensite transformation strain on the ductility of dual-phase steels," *Acta Metallurgica*, vol. 31, no. 4, pp. 609–617, 1983, ISSN: 00016160. DOI: 10.1016/0001-6160(83)90051-2.

[11] C. Tasan, M. Diehl, D. Yan, M. Bechtold, F. Roters, L. Schemmann, C. Zheng, N. Peranio, D. Ponge, M. Koyama, K. Tsuzaki, and D. Raabe, "An overview of Dual-Phase steels: Advances in microstructure-oriented processing and micromechanically guided design," *Annual Review of Materials Research*, vol. 45, no. 1, pp. 391–431, 2015, ISSN: 1531-7331. DOI: 10.1146/annurev-matsci-070214-021103.

[12] R. G. Davies, "Early stages of yielding and strain aging of a Vanadium-containing Dual-Phase steel," *Metallurgical Transactions A*, vol. 10A, 1979. DOI: https://doi.org/10.1007/BF02812021.

[13] J. Kadkhodapour, S. Schmauder, D. Raabe, S. Ziaei-Rad, U. Weber, and M. Calcagnotto, "Experimental and numerical study on geometrically necessary dislocations and non-homogeneous mechanical properties of the ferrite phase in dual phase steels," *Acta Materialia*, vol. 59, no. 11, pp. 4387–4394, 2011, ISSN: 13596454. DOI: 10.1016/j.actamat.2011.03.062.

[14] C. Du, J. P. Hoefnagels, S. Kölling, M. G. Geers, J. Sietsma, R. Petrov, V. Bliznuk, P. M. Koenraad, D. Schryvers, and B. Amin-Ahmadi, "Martensite crystallography and chemistry in dual phase and fully martensitic steels," *Materials Characterization*, vol. 139, no. October 2017, pp. 411–420, 2018, ISSN: 10445803. DOI: 10.1016/j.matchar.2018.03.011.

[15] S. Takaki, K. Fukunaga, J. Syarif, and T. Tsuchiyama, "Effect of Grain Refinement on Thermal Stability of Metastable Austenitic Steel," *Materials Transactions*, vol. 45, no. 7, 2004. DOI: http://dx.doi.org/10.2320/matertrans.45.2245.

[16] C. Celada-Casero, J. Sietsma, and M. J. Santofimia, "The role of the austenite grain size in the martensitic transformation in low carbon steels," *Materials and Design*, vol. 167, 2019. DOI: 10.1016/j.matdes.2019.107625.

[17] J. S. Bowles and J. K. Mackenzie, "The crystallography of martensite transformations III. Face-centred cubic to body-centred tetragonal transformations," *Acta Metallurgica*, vol. 2, no. 2, pp. 224–234, 1954, ISSN: 00016160. DOI: 10.1016/0001-6160(54)90163-7.

[18] C. M. Wayman, "The phenomenological theory of martensite crystallography: Interrelationships," *Metallurgical and Materials Transactions A*, vol. 25, no. 9, pp. 1787–1795, 1994, ISSN: 10735623. DOI: 10.1007/BF02649029.

[19] H. Moulinec and P. Suquet, "A numerical method for computing the overall response of nonlinear composites with complex microstructure," *Computer Methods in Applied Mechanics and Engineering*, vol. 157, no. 1-2, pp. 69–94, 1998, ISSN: 00457825. DOI: 10.1016/S0045-7825(97)00218-1. arXiv: 2012.08962.

[20] L. Ryde, "Application of EBSD to analysis of microstructures in commercial steels Application of EBSD to analysis of microstructures in commercial steels," *Material Science and Technology*, vol. 0836, 2006. DOI: 10.1179/174328406X130948.

[21] F. Bachmann, R. Hielscher, and H. Schaeben, "Texture analysis with MTEX- Free and open source software toolbox," *Solid State Phenomena*, vol. 160, pp. 63–68, 2010, ISSN: 10120394. DOI: 10.4028/www.scientific.net/SSP.160.63.

[22] F. Niessen, T. Nyyssönen, A. A. Gazder, and R. Hielscher, "Parent grain reconstruction from partially or fully transformed microstructures in MTEX," *Journal of Applied Crystallography*, vol. 55, pp. 180–194, 2022, ISSN: 16005767. DOI: 10.1107/S1600576721011560. arXiv: 2104.14603.

[23] G. Miyamoto, N. Takayama, and T. Furuhara, "Accurate measurement of the orientation relationship of lath martensite and bainite by electron backscatter diffraction analysis," *Scripta Materialia*, vol. 60, no. 12, pp. 1113–1116, 2009, ISSN: 13596462. DOI: 10.1016/j.scriptamat.2009.02.053.

[24] T. Nyyssönen, M. Isakov, P. Peura, and V. T. Kuokkala, "Iterative Determination of the Orientation Relationship Between Austenite and Martensite from a Large Amount of Grain Pair Misorientations," *Metallurgical and Materials Transactions A: Physical Metallurgy and Materials Science*, vol. 47, no. 6, pp. 2587–2590, 2016, ISSN: 10735623. DOI: 10.1007/s11661-016-3462-2.

[25] T. Nyyssönen, P. Peura, and V. T. Kuokkala, "Crystallography, Morphology, and Martensite Transformation of Prior Austenite in Intercritically Annealed High-Aluminum Steel," *Metallurgical and Materials Transactions A: Physical Metallurgy and Materials Science*, vol. 49, no. 12, pp. 6426–6441, 2018, ISSN: 10735623. DOI: 10.1007/s11661-018-4904-9.

[26] H. Bhadeshia, *Worked Examples in the Geometry of Crystals*, Second. London: The institute of Metals, 1991. DOI: 10.1524/zkri.1991.195.1-2.155.

[27] P. M. Kelly and J. Nutting, "The martensite transformation in carbon steels," *Proceedings of the Royal Society of London. Series A. Mathematical and Physical Sciences*, vol. 259, no. 1296, pp. 45–58, 1960, ISSN: 0080-4630. DOI: 10.1098/rspa.1960.0210.

[28] Z. Nishiyama, *Martensitic Transformation*. Academic Press, Inc., 1972, p. 480, ISBN: 9780323148818.

[29] X. F. Gu, T. Furuhara, and W. Z. Zhang, "PTCLab: Free and open-source software for calculating phase transformation crystallography," *Journal of Applied Crystallography*, vol. 49, no. April, pp. 1099–1106, 2016, ISSN: 16005767. DOI: 10.1107/S1600576716006075.

[30] H. Kitahara, R. Ueji, M. Ueda, N. Tsuji, and Y. Minamino, "Crystallographic analysis of plate martensite in Fe-28.5 at.% Ni by FE-SEM/EBSD," *Materials Characterization*, vol. 54, no. 4-5, pp. 378–386, 2005, ISSN: 10445803. DOI: 10.1016/j.matchar.2004.12.015.

[31] H. Kitahara, R. Ueji, N. Tsuji, and Y. Minamino, "Crystallographic features of lath martensite in low-carbon steel," *Acta Materialia*, vol. 54, no. 5, pp. 1279–1288, 2006, ISSN: 13596454.

[32] L. Sharma, R. H. Peerlings, M. G. Geers, and F. Roters, "Microstructural influences on fracture at prior austenite grain boundaries in dual-phase steels," *Materials*, vol. 12, no. 22, pp. 1–22, 2019, ISSN: 19961944. DOI: 10.3390/ma12223687.

[33] V. Atreya, C. Bos, and M. J. Santofimia, "Understanding ferrite deformation caused by austenite to martensite transformation in dual phase steels," *Scripta Materialia*, vol. 202, p. 114 032, 2021, ISSN: 13596462. DOI: 10.1016/j.scriptamat.2021.114032.

[34] V. A. Lobodyuk, Y. Y. Meshkov, and E. V. Pereloma, "On Tetragonality of the Martensite Crystal Lattice in Steels," *Metallurgical and Materials Transactions A: Physical Metallurgy and Materials Science*, vol. 50, no. 1, pp. 97–103, 2019, ISSN: 10735623. DOI: 10.1007/s11661-018-4999-z. [Online]. Available: https://doi.org/10.1007/s11661-018-4999-z.

[35] M. Kamaya, "Assessment of local deformation using EBSD: Quantification of accuracy of measurement and definition of local gradient," *Ultramicroscopy*, vol. 111, no. 8, pp. 1189–1199, 2011, ISSN: 03043991. DOI: 10.1016/j.ultramic.2011.02.004.

[36] R. Hielscher, T. Nyyssönen, F. Niessen, and A. A. Gazder, "The variant graph approach to improved parent grain reconstruction," *Materialia*, vol. 22, no. March, p. 101 399, 2022, ISSN: 2589-1529. DOI: 10.1016/j.mtla.2022.101399.

[37] W. Pantleon, "Resolving the geometrically necessary dislocation content by conventional electron backscattering diffraction," *Scripta Materialia*, vol. 58, no. 11, pp. 994–997, 2008, ISSN: 13596462. DOI: 10.1016/j.scriptamat.2008.01.050.

[38] A. H. Pham, T. Ohba, S. Morito, and T. Hayashi, "Effect of Chemical Composition on Average γ/α' Orientation Relationship in Carbon and Low Alloy Steels," *Materials Today: Proceedings*, vol. 2, S663–S666, 2015, ISSN: 22147853. DOI: 10.1016/j.matpr.2015.07.371.

[39] A. Saha Podder and H. K. Bhadeshia, "Thermal stability of austenite retained in bainitic steels," *Materials Science and Engineering A*, vol. 527, no. 7-8, pp. 2121–2128, 2010, ISSN: 09215093. DOI: 10.1016/j.msea.2009.11.063.

[40] R.-M. Rodriguez and I. Gutiérrez, "Unified Formulation to Predict the Tensile Curves of Steels with Different Microstructures," *Materials Science Forum*, vol. 426-432, pp. 4525–4530, 2003, ISSN: 1662-9752. DOI: 10.4028/www.scientific.net/MSF.426-432.4525.

[41] S. A. Kim and W. L. Johnson, "Elastic constants and internal friction of martensitic steel, ferritic-pearlitic steel, and α-iron," *Materials Science and Engineering A*, vol. 452-453, pp. 633–639, 2007, ISSN: 09215093. DOI: 10.1016/j.msea.2006.11.147.

[42] A. Ramazani, K. Mukherjee, H. Quade, U. Prahl, and W. Bleck, "Correlation between 2D and 3D flow curve modelling of DP steels using a microstructure-based RVE approach," *Materials Science and Engineering A*, vol. 560, pp. 129–139, 2013, ISSN: 09215093. DOI: 10.1016/j.msea.2012.09.046.

[43] P. M. Kelly, "Crystallography of lath martensite in steels," *Materials Transactions, JIM*, vol. 33, no. 3, pp. 235–242, 1992, ISSN: 09161821. DOI: 10.2320/matertrans1989.33.235.

[44] F. Maresca and W. A. Curtin, "The austenite/lath martensite interface in steels: Structure, athermal motion, and in-situ transformation strain revealed by simulation and theory," *Acta Materialia*, vol. 134, pp. 302–323, 2017, ISSN: 13596454. DOI: 10.1016/j.actamat.2017.05.044.

6

INFLUENCE OF SELF-ACCOMMODATION IN MARTENSITE ON THE TRANSFORMATION-INDUCED DEFORMATION OF FERRITE

This chapter is based on the scientific article: V. Atreya, C. Bos, and M. J. Santofimia, "Influence of self-accommodation in martensite on the transformation-induced deformation of ferrite in DP steels." (To be submitted). Parts of this chapter were also presented at the International Conference on Martensitic Transformation (ICOMAT), March 13-18, 2022, S. Korea.

It was reported in Chapter 4 that the DP steel specimen with the highest martensite volume fraction shows no transformation-induced deformation of ferrite. This was attributed to the decrease in the carbon content of martensite and an increase in self-accommodation due to the formation of more variants. In this chapter, the effect of self-accommodation on transformation-induced deformation of ferrite in DP steels was further investigated via modelling and verified using previously published EBSD experimental data. The martensitic transformation was simulated using a 3D RVE cube with spherical austenite at the centre. Austenite transformation into martensite was mimicked by imposing appropriate transformation deformation on austenite. The resulting strain state of the ferrite matrix was calculated using micromechanical calculations using the approach presented in Chapter 5. The calculations revealed that the average von-Mises equivalent strain in ferrite decreases as more and more variants form from a PAG and reaches a minimum when all twenty-four variants form. An increase in the number of variants leads to a more localised strain field in ferrite. This is because of a decrease in the effective shear magnitude of the PAG, which cancels out completely when all twenty-four variants are formed.

6.1. INTRODUCTION

As discussed in Chapter 2, the austenite to martensite phase transformation results in a hierarchical microstructure. The basic structural unit, called lath, can have one of the 24 Kurdjumov-Sachs (K-S) spatial orientations known as variants. The laths arrange themselves in groups called sub-blocks, blocks and packets depending on their orientation [1], [2]. All 24 K-S variant orientations with corresponding closed packed/bain groups were described in 2.1 [3].

In Chapter 4, it was revealed via EBSD experiments that the martensitic transformation can result in two distinct types of deformation modes in ferrite grains of dual-phase (DP) steels: type-I long-range and type-II short-range deformation. While type-I deformation penetrates deep into the interior of the ferrite grain (long-range) [4], type-II deformation occurs in the form of a small deformed region which runs along the phase boundaries (short-range) as shown in figure 4.3. It was also observed, as shown in figure 4.4, that with the formation of a drastically high volume fraction of martensite (0.93), the ferrite grains were devoid of either type of deformation.

This absence of transformation-induced deformation of ferrite in the DP steel specimen with high martensite volume fraction was attributed to the reduced carbon content in martensite and increased self-accommodation by a greater number of variants formed in relatively larger prior austenite grains (PAGs). Lesser carbon content decreases the magnitude of transformation deformation and makes the hierarchical microstructure finer. The number of variants formed within a PAG depends upon the PAG size (PAGS). Large PAGs exhibit all 24 variants, whereas it is not uncommon to observe that very small (less than 1 micron) sized PAGs transform into only a few variants [5], [6]. The formation of variants enables self-accommodation during martensitic transformation.

Self-accommodation occurs by the formation of different variants to reduce the volume average shear and thereby reduce the strain energy due to martensitic transformation as well. Morito et al. [7], [8] studied the self-accommodation in martensite by calculating the effective magnitude of transformation deformation for different variant combinations within a packet. They observed that the magnitude decreases with increasing variants and is minimum when all six variants are formed. Later, it was proven theoretically that when 24 variants form with equal volume fractions, the volume average shear tends to zero, thereby rendering the 'effective' magnitude of transformation deformation to be equal to isotropic dilatation [9]–[11].

It is therefore natural to hypothesize that the extent of self-accommodation in martensite also influences the transformation-induced deformation of the ferrite in DP steels. In this study, the influence of self-accommodation in martensite due to variant organization on the transformation-induced deformation of ferrite is investigated using experimental data available from literature and micromechanical modelling. Virtual DP microstructures are created with different combinations of variants which form from a PAG. The transformation-induced strain in the ferrite matrix is calculated using micromechanical modelling. The result is compared with the ferrite deformation field obtained from experimental EBSD orientation measurements.

6.2. EXPERIMENTAL PROCEDURE

The material used and the experimental procedure for this study are the same as used in Chapter 4. Thus they are only described briefly here. Cold-rolled steel with composition Fe-0.14C-1.8Mn-0.24Si by weight % and with an initial microstructure consisting of pearlite and ferrite was cut into a specimen of dimensions 10 mm x 4 mm x 2 mm using electrical discharge machining. Using a Bähr DIL A/D dilatometer, the specimen was heated at 5 °/s and kept at various intercritical temperatures to obtain ferrite-martensite dual-phase microstructures. The specimens were identified using the names IC750, IC775 and IC800 where 'IC' denotes inter-critical and the last three digits denote the intercritical temperature in °C.

The specimens were ground using SiC abrasive papers and subsequently polished using 3 and 1 μm diamond paste. Further, electropolishing was carried out using Struers A2 electrolyte at 35V, 277K for 6s. EBSD measurements were made on a Zeiss Ultra 55 scanning electron microscope (SEM) using the Edax Pegasus XM 4 Hikari EBSD system. The step size of the scan was 50 nm. The EBSD scans were analysed using the TSL OIM version 7 software. The grain average image quality (GAIQ) measure was used to distinguish martensite from ferrite regions [4], [12]. The identified martensite data points were used as input for the PAG reconstruction.

6.3. THEORY AND MODELLING PROCEDURE

6.3.1. PAG RECONSTRUCTION

Prior austenite grain (PAG) reconstruction was carried out on EBSD orientation data of all specimens for estimating PAG morphologies, PAG sizes and the martensite variants formed within them. The reconstruction was performed using Mtex, a freely available Matlab toolbox [13], [14]. Only the measurement points corresponding to martensite were considered for reconstruction. The PAG reconstruction is also carried out for an EBSD scan of a fully martensitic microstructure with composition Fe-0.3C-3.6Mn-1.5Si (wt.%) available from the literature [15]. The procedure for PAG reconstruction along with the corresponding theory is elaborated in Chapter 5 (section 5.2.2).

6.3.2. MICROMECHANICAL SIMULATIONS

To calculate the transformation-induced strain in the ferrite matrix of virtual DP steel microstructures, calculations are performed using the freely available code CraFT 1.2.0 based on the micromechanical model proposed by Moulinec and Suquet [16]. The procedure for carrying out the simulations is described in brief in Chapter 5 (section 5.2.4) and A. The analysis here is performed on a 3-dimensional DP virtual microstructure with spatial discretization in x, y, and z-direction being 200 x 200 x 200 units. The virtual microstructure consists of a spherical prior austenite grain of radius 25 units at the centre, surrounded by the ferrite matrix. This particular microstructural setup is chosen to disregard the effect of PAG or variant shapes on the transformation-induced deformation of ferrite. The selection of length scale units can be arbitrary and does not affect the outcome.

A combination of two martensite variants is assumed to form within the PAG with an equal volume fraction as shown in Figure 6.1. Two scenarios are considered: (i) The formation of two variants that take the form of two hemispheres (Figure 6.1(a)), and (ii) The formation of two variants that are randomly distributed within the PAG (Figure 6.1(b)). This last consideration means that any discrete point in the PAG is assigned one of the two variant orientations while keeping the overall volume fraction for both variants the same. The random distribution was chosen to avoid making any assumptions about the variant morphologies and can be extended to mimic the formation of all twenty-four variants.

The variant-specific anisotropic transformation deformation matrices are obtained using the PTMC theory [17], [18] assuming a carbon content of 0.14 wt.% in austenite/martensite (same as that in specimen IC800). Subsequently, variant-specific transformation eigenstrain tensors are calculated. Eigenstrains are the strains that develop in the material in the absence of external mechanical stress. The eigenstrains are then applied to the spherical austenite to mimic its transformation into multiple martensitic variants. Subsequently, induced strains in ferrite are calculated using the micromechanical model [16]. For martensite, the constitutive relation is applied on strain from which the transfor-

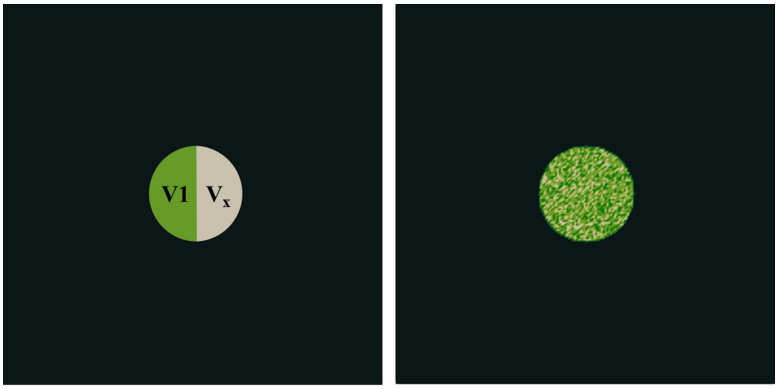

Figure 6.1: Cross-section of a 3D RVE containing spherical prior austenite in a 'black' ferrite matrix. (a) V1 and V_x are the martensite variants formed after transformation. V1 corresponds to 1st variant according to K-S OR. V_x can be any other variant. (b) V1 and V_x are randomly distributed inside the sphere.

mation eigenstrain is already subtracted. This is because phase transformation in itself does not cause stress in martensite, rather it is a resistance to shape change and volume increase offered by surrounding ferrite which causes stress in martensite.

The thermal strain is considered in this study but only for the ferrite phase [19], that too with an assumption that the linear coefficient of thermal expansion does not change with decreasing temperature during quenching. Determining the thermal strains for martensitic variants requires an estimate of instantaneous carbon content and transformation temperature of the transforming austenite, which is out of the scope of the current study.

6.4. RESULTS

6.4.1. EXPERIMENTS

TRANSFORMATION-INDUCED FERRITE DEFORMATION OBSERVED THROUGH EBSD ORIENTATION MAPPING

The difference in the deformed state of ferrite can be observed from the kernel average misorientation (KAM) maps, which were presented in Chapter 4, figure 4.2. Higher KAM values result from increased crystal misorientations due to plastic deformation and provide an indirect estimate of in-grain deformation [20]. Figure 4.3(a) showed both type-I LR and type-II SR deformation in ferrite grains of IC750 indicated by higher KAM values, while figure 4.3(b) shows the absence of any transformation-induced deformation in ferrite grains of IC800. It is also noteworthy that the misorientations in the martensite of IC800 are also lower than in IC750, as evident by the lower frequency of the red-coloured regions in full EBSD maps.

Figure 6.2(a) shows the misorientation distributions in the ferrite regions of the three DP steel specimens. Specimens IC750 and IC775 have a higher frequency of larger misorientation angles in the range of 0.5°-1.5°. Figure 6.2(b) shows the misorientation distributions in the martensite region of the specimens which follows the same trend as in figure 6.2(a). The average misorientation of both ferrite and martensite in IC800 is lower than that of IC750 and IC775 as shown in figure 6.3, with error bars representing the standard deviation.

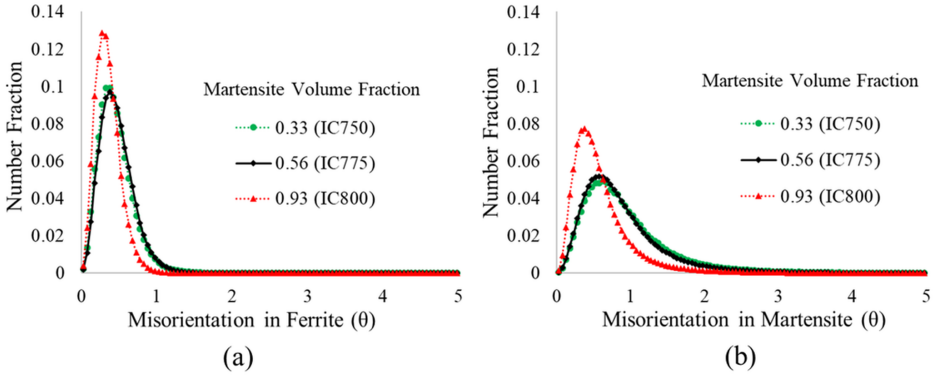

Figure 6.2: Misorientation distribution of (a) Ferrite and (b) Martensite regions of the three DP steel specimens

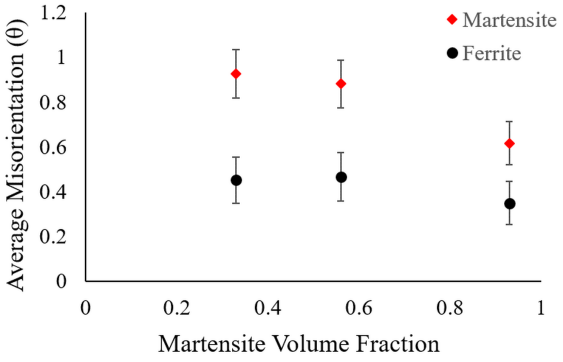

Figure 6.3: Average misorientation of ferrite and martensite regions in the DP steel specimens.

6.4.2. MODELLING

DEPENDENCE OF TRANSFORMATION SHEAR AND DILATATION ON CARBON CONTENT IN MARTENSITE

A possible explanation for the absence of type I or II deformation in the ferrite of specimen IC800 is the reduction in the carbon content of martensite with increasing martensite volume fraction. The shear and dilatation magnitudes for different austenite/martensite

carbon content and single variant formation were calculated as per classical PTMC theory using the freely available software PTCLab [21]. The results of the calculations are shown in figure 6.4. It is evident that as the carbon content in austenite/martensite increases, the unidirectional dilatation, which is responsible for the volume change during transformation, also increases. Similar findings have also been obtained via experiments and are reported in the literature [22]. Figure 6.4 also shows that the shear magnitude decreases with increasing carbon content. There are no experimental measurements of only the shear magnitude in literature to verify this finding.

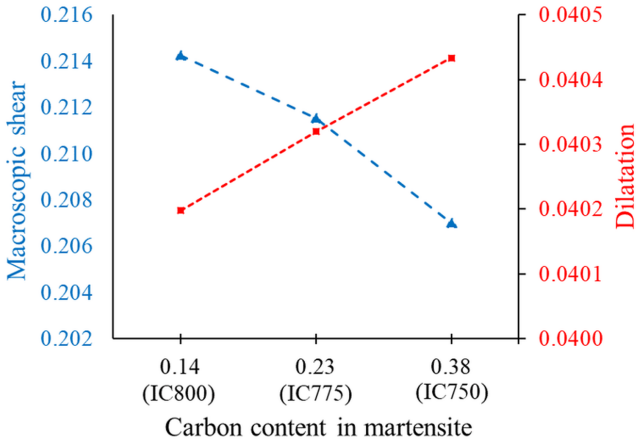

Figure 6.4: Variation of dilatation and macroscopic shear magnitude with carbon content (wt.%) in martensite calculated for a single variant formation using the classical PTMC theory.

PAG VARIANT DENSITY CALCULATED VIA PAG RECONSTRUCTION

PAG reconstruction was performed on the martensitic regions of the three DP steel specimens along with the fully martensitic steel microstructure (0.3 wt.% carbon) data available from the literature [15]. The number of martensitic variants within PAGs was plotted against the PAG size (effective diameter). The total number of PAGs considered for the analysis was 404, 432, 390 and 1111 for IC750, IC775, IC800 and fully martensitic steel respectively. In general, it was observed that the total number of variants formed increases with the PAG size as shown in figure 6.5. The graph for the fully martensitic steel also shows this trend, and as expected, the number of variants formed reaches an upper limit of 24 when the PAGS is large enough.

EFFECT OF DIFFERENT VARIANT COMBINATIONS ON TRANSFORMATION-INDUCED STRAIN IN FERRITE

To understand the effect of self-accommodation by martensitic variants on transformation-induced deformation of ferrite, the strain state of ferrite was calculated resulting from spherical austenite transforming into martensite in a 3D RVE. The average von-Mises

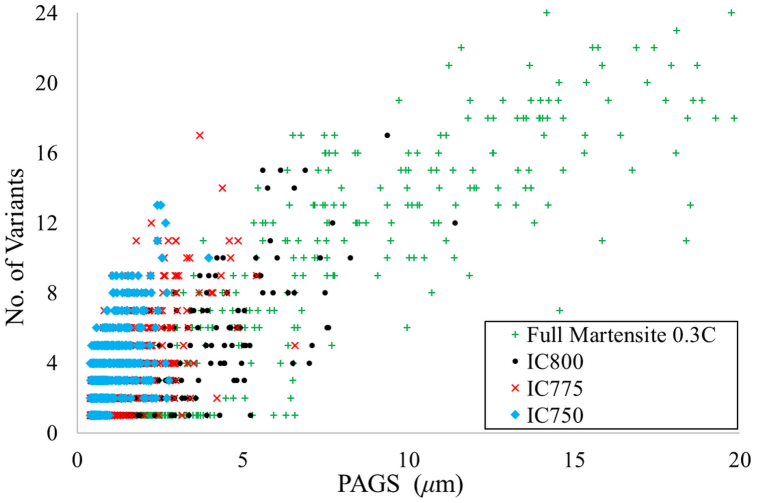

Figure 6.5: Number of variants in a PAG vs the size of that PAG.

equivalent strain in the ferrite matrix for different variant combinations was calculated using a setup similar to figure 6.1(a) and the results are shown in figure 6.6(a). All variant combinations result in a lower average von-Mises strain in the ferrite matrix compared to the case where a single variant, V1, is formed.

The average von-Mises strain is highest in variant combinations V1/V8, V1/V16 and V1/V24 and lowest in variant combinations V1/V6, V1/V9 and V1/V17. Within a packet, there are six different values for average deformation corresponding to six variants. The same values are repeated for other packets, albeit in a different sequence.

The average von-Mises equivalent strain in the ferrite matrix for multi-variant combinations was calculated using a setup similar to figure 6.1(b) and the results are shown in figure 6.6(b). It can be seen that if the number of variants within a PAG increases, the average von-Mises strain of ferrite keeps on decreasing. However, the decrease is less drastic after a combination of six variants (V1:V6) is formed.

To evaluate the adequacy of using randomly distributed variants within the PAG, the average strain in ferrite due to two-variant combinations occupying equal volume hemispheres (figure 6.1(a)) was compared with the case of two-variant combinations, randomly distributed in the PAG (figure 6.1(b)). The average von-Mises strains calculated were found to be of similar magnitude. This indicates that the shape of the variant may be of minor consequence for estimating transformation-induced deformation of ferrite, as long as the volume fraction and orientation of the variant considered are accurate.

Figure 6.7 shows the von-Mises equivalent strain maps for ferrite in the case of different two-variant combinations within a PAG. The strain maps are shown for the X, Y and Z

cross-sections of the 3D cubic RVE, passing through the centre. The deformation becomes more localized with certain specific variant combinations like V1/V6. It is also noteworthy that the value of strain close to the phase boundary is largest for V1/V6 even though the average strain as per figure 6.6(b) is lower.

Figure 6.8 shows the von-Mises strain maps for variant combinations containing three or more randomly distributed variants. The notation ':' denotes the presence of all intermediate variants in equal volume fractions. The strain field in ferrite becomes highly localized with the increasing number of variants. In the case of variants V1:V6 and V1:V24, the high-strain region becomes localized near the phase boundary.

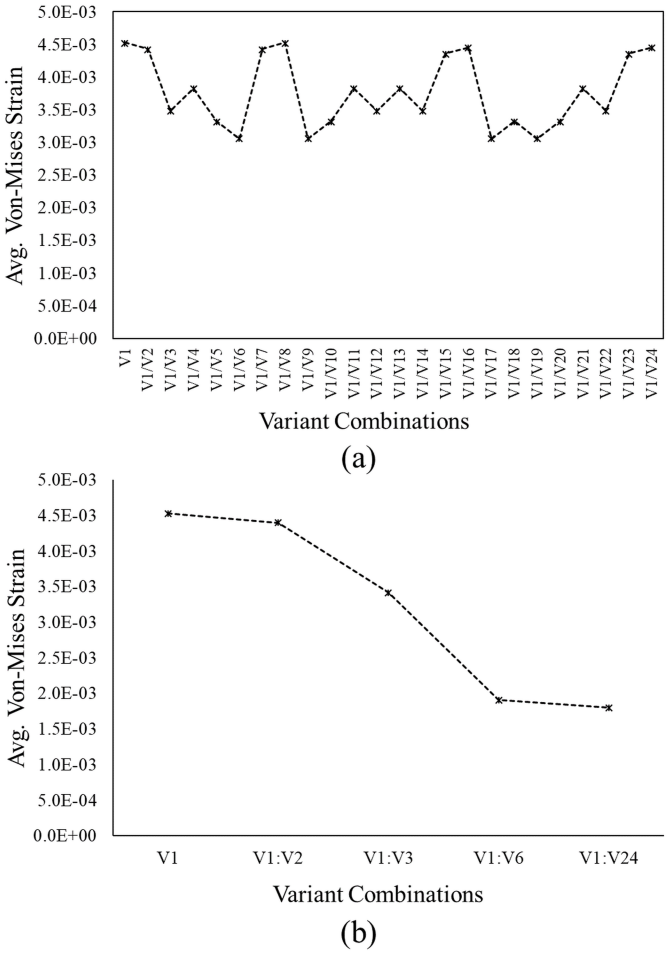

Figure 6.6: (a) Average von-Mises strain in ferrite phase of the RVE due to a single variant formation (V1) compared with combinations of two variants (b) The decrease in the von-Mises strain with an increasing number of variants. The symbol ':' denotes all variants in between.

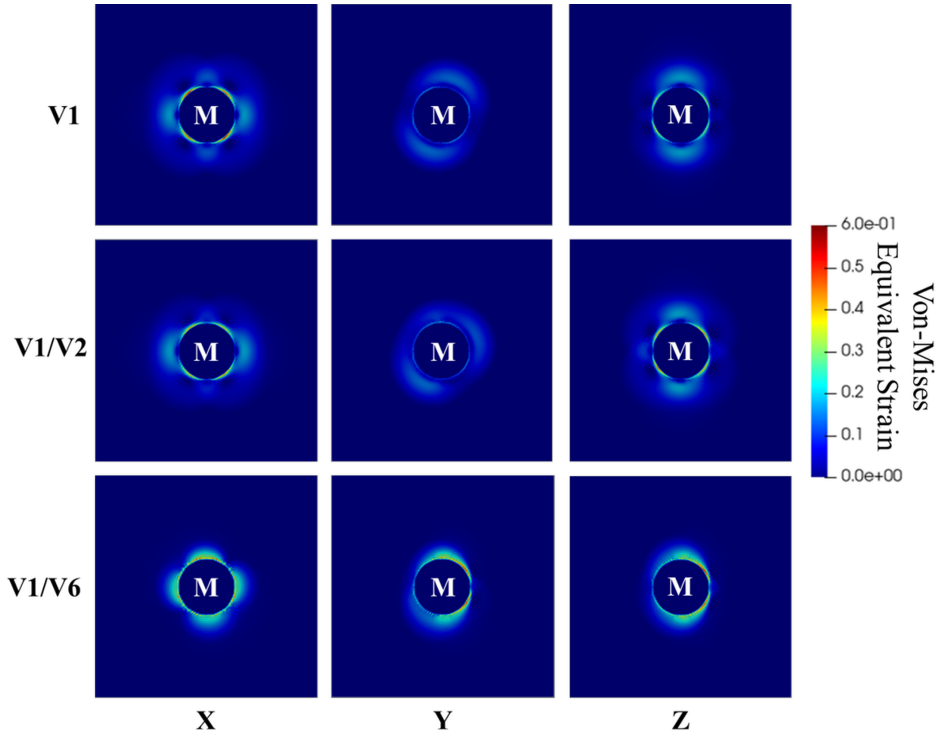

Figure 6.7: von-Mises equivalent strain maps for single variant formation (V1) and variant combinations (V1/V2 and V1/V6) in a cross-section of 3D RVE normal to X, Y and Z axis respectively.

6.5. DISCUSSION

6.5.1. INFLUENCE OF CARBON CONTENT IN MARTENSITE ON TRANSFORMATION DILATATION AND SHEAR MAGNITUDES

Figure 6.4 shows that the decrease in dilatation magnitude from specimen IC750 to IC775 is similar to its decrease from specimen IC775 to IC800. The decrease in dilatation magnitude is less than 1% in both cases. It was also illustrated in Chapter 4 that specimens IC750 and IC775 both exhibit similar magnitude of type-II deformation of ferrite. If the dilatation alone was responsible for type-II deformation, it can not explain the absence of any transformation-induced deformation of ferrite in specimen IC800. A more plausible reason could be that the increased self-accommodation in the martensite of specimen IC800 results in the apparent lack of any transformation-induced deformation of ferrite.

Figure 6.4 also shows that as per PTMC, the shear magnitude for single variant formation increases with decreasing carbon content. Theoretically, this should result in the largest transformation-induced deformation in the ferrite of the IC800 specimen. However, no conclusions can be made based on this observation due to a lack of experimental data in

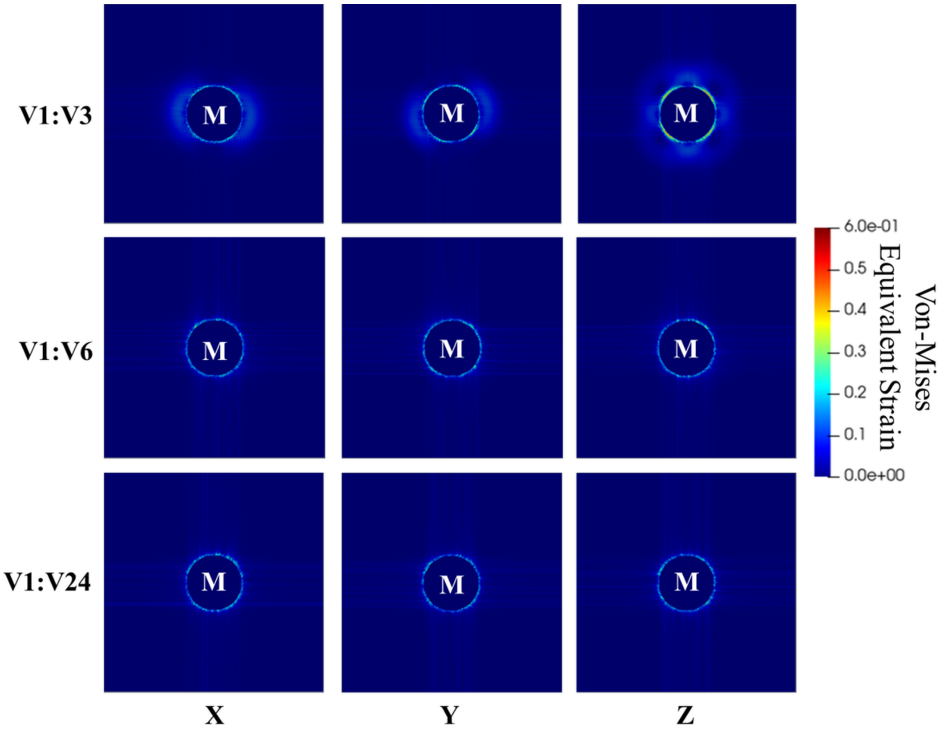

Figure 6.8: von-Mises equivalent strain maps for multiple variant formation (V1:V3), (V1:V6) and (V1:V24) in a cross-section of 3D RVE normal to X, Y and Z axis respectively. The symbol ':' denotes all variants in between.

the literature to verify PTMC's prediction regarding the variation of shear magnitude with carbon content in low-carbon martensite.

6.5.2. INCREASED SELF-ACCOMMODATION DUE TO HIGHER VARIANT DENSITY IN LARGE PAGS

Figure 6.5 shows that the number of variants formed from a PAG increase with increasing PAGS. Clearly, among the DP steel specimens, IC800 contains the largest PAGs. PAGs which constitute six or more martensitic variants cover an area fraction of 0.33, 0.46, and 0.55 of the total martensite surface area for specimens IC750, IC775, and IC800 respectively. Hence, the majority of the martensite regions belong to a large PAG in IC800. 50% of the PAGs in contact with ferrite comprise six or more variants. Perhaps due to increased self-accommodation in martensite, there is no measurable deformation in the ferrite of the IC800 specimen.

Some small PAGs were also present in the neighbourhood of ferrite grains in the IC800 specimen. Their effect on ferrite grains in the form of type I or type II deformation was

not observed. The apparent small PAGs may be part of bigger PAGs in 3-dimensions, which comprise more than 6 variants.

6.5.3. EFFECTIVE TRANSFORMATION-DEFORMATION DUE TO SELF- ACCOMMODATION IN MARTENSITE

Morito et al. [7], [8] illustrated that the magnitude of transformation deformation reaches a minimum when 3 martensite variants belonging to different bain groups are formed and remains the same even if all 6 variants belonging to the packet are formed in a PAG. Accordingly, the transformation-induced deformation of ferrite should also show a minimum when 3 variants are formed in a PAG. However, we see in figure 6.6(b) and figure 6.8 that the average, as well as local strain in ferrite, decreases further when six or twenty-four variants are formed.

In theory, the cumulative shear of a PAG transformation into martensite is negligible if only a packet is formed with all six variants inside it and becomes zero if all 24 variants are formed [9]–[11]. This is what is closer to the results of the simulation shown in figure 6.6(b) and figure 6.8, where it can be seen that both the average and local distribution of V1:V6 and V1:V24 cases do not differ much. Specifically for IC800, the transformation deformation matrix for variant 1 can be written as:

$$\begin{bmatrix} 0.99029 & -0.03929 & 0.03175 \\ 0.03175 & 1.1285 & 0.09033 \\ -0.02762 & -0.11181 & 0.92141 \end{bmatrix}$$

The average transformation deformation matrix for the formation of all 24 variants in equal volume is:

$$\begin{bmatrix} 1.0134 & 0 & 0 \\ 0 & 1.0134 & 0 \\ 0 & 0 & 1.0134 \end{bmatrix}$$

where the shear components have vanished and the result is just an isotropic dilation of magnitude 0.0134, equal to isotropic dilatation calculated for IC800 (=0.0402/3) using classical PTMC. Therefore, for IC800, it seems plausible that due to the formation of a higher number of variants in larger PAGs, the effective magnitude of transformation deformation is reduced since the shear of different variants cancels out.

6.5.4. THE ROLE OF MARTENSITE SUB-STRUCTURE IN CAUSING DEFORMATION OF FERRITE MATRIX

Apart from increased self-accommodation, the coarse martensite sub-structure in the IC800 specimen also seems to cause minimal deformation of the ferrite matrix. It was reported in Chapter 4 (section 4.3.2) that with decreasing carbon content in martensite, the sub-structure of martensite becomes coarser with an average block size of 0.08 μm^2 in

IC750 to 0.35 μm^2 in IC800. The KAM values are calculated for misorientation values less than 4°, which exclude all variant boundary misorientation such as sub-block, block, and packet boundary, showing that within the sub-blocks and laths the martensite in IC800 is less deformed than in IC750 or IC775. This indicates that the extent of plastic accommodation within martensite decreases with decreasing carbon content. The martensitic transformation causes similar variations of plastic accommodation in martensite as well as in ferrite as revealed by variations in misorientation distributions and misorientation averages as shown in figures 6.2 and 6.3.

6.5.5. COMPARISON OF SIMULATED STRAIN FIELDS WITH THE EXPERIMENTALLY OBSERVED DEFORMATION OF FERRITE GRAINS

As stated in Chapter 4, the width of the deformed ferrite region which represents type II SR deformation lies in the range of 0.1-0.5 μm for both specimen IC750 and IC775. Chapter 5 showed that the variation in the extent of transformation-induced deformation depends upon PAG morphology and orientation along with martensite variant orientation. This chapter illustrates that self-accommodation due to martensite variant organisation also influences the transformation-induced deformation of ferrite.

In the case where three or fewer variants are formed, high-magnitude strains reach a greater distance into the ferrite grain interior from the phase boundary. The strain field becomes localised with an increasing number of variants formed as shown in figure 6.8. The strain field appears to be uniform and in the form of a very thin layer around the spherical martensite when six variants (V1:V6) or twenty-four variants form (V1:V24). Since specimen IC800 possesses the highest area fraction belonging to large PAGs, self-accommodation explains the absence of transformation-induced deformation in IC800.

In Chapter 4, it was mentioned that a small PAG may transform into a martensite variant having a close-packed plane parallel (CPPP) relation with adjacent ferrite, which results in type I LR deformation. Even in the absence of the CPPP relationship, the transformation of a small PAG into a single martensite variant will result in a larger spatial extent of transformation-induced deformation as compared to multi-variant transformation.

6.6. CONCLUSIONS

In this study, the effect of martensite sub-structure and variant organization on transformation - induced deformation of ferrite in DP steels was investigated via modelling and verified using previously published EBSD experimental data. PAG reconstruction was performed on martensite regions to obtain the variant density in PAGs which determines the extent of self-accommodation. It was found that the number of variants formed increases with PAGS. The DP steel specimen IC800 consists of relatively large PAGs and it shows the highest self-accommodation as evident by the lack of transformation-induced deformation of ferrite.

It was also observed that the variations in plastic accommodation in martensite due to the transformation can be an indication of variations in plastic accommodation in the ferrite matrix. The misorientation distribution and the average misorientation of the ferrite matrix follow the same trend as those of martensite in DP steel specimens. This means that with varying carbon content, martensitic transformation produces similar variations in the extent of plastic accommodation in both martensite and ferrite.

The martensitic transformation was simulated by a 3D RVE cube with spherical austenite at the centre. The transformation of austenite into martensite was mimicked by imposing appropriate transformation deformation on austenite. The resulting strain state of the ferrite matrix was calculated using micromechanical calculations. The calculations revealed that the average von-Mises equivalent strain in ferrite decreases as more and more variants form from a PAG and reaches a minimum when all twenty-four variants form. An important assumption in this study was that all variants formed have equal volume fractions. With more variants, the ferrite strain field becomes more localized. This is because of a decrease in the effective shear magnitude of the PAG, which cancels out completely when all twenty-four variants are formed.

REFERENCES

[1] H. Kitahara, R. Ueji, N. Tsuji, and Y. Minamino, "Crystallographic features of lath martensite in low-carbon steel," *Acta Materialia*, vol. 54, no. 5, pp. 1279–1288, 2006, ISSN: 13596454.

[2] G. Miyamoto, N. Iwata, N. Takayama, and T. Furuhara, "Mapping the parent austenite orientation reconstructed from the orientation of martensite by EBSD and its application to ausformed martensite," *Acta Materialia*, vol. 58, no. 19, pp. 6393–6403, 2010, ISSN: 13596454. DOI: 10.1016/j.actamat.2010.08.001.

[3] T. Furuhara, T. Chiba, T. Kaneshita, H. Wu, and G. Miyamoto, "Crystallography and Interphase Boundary of Martensite and Bainite in Steels," *Metallurgical and Materials Transactions A: Physical Metallurgy and Materials Science*, vol. 48, no. 6, pp. 2739–2752, 2017, ISSN: 10735623. DOI: 10.1007/s11661-017-4064-3.

[4] V. Atreya, C. Bos, and M. J. Santofimia, "Understanding ferrite deformation caused by austenite to martensite transformation in dual phase steels," *Scripta Materialia*, vol. 202, p. 114 032, 2021, ISSN: 13596462. DOI: 10.1016/j.scriptamat.2021.114032.

[5] S. Takaki, K. Fukunaga, J. Syarif, and T. Tsuchiyama, "Effect of Grain Refinement on Thermal Stability of Metastable Austenitic Steel," *Materials Transactions*, vol. 45, no. 7, 2004. DOI: http://dx.doi.org/10.2320/matertrans.45.2245.

[6] C. Du, J. P. Hoefnagels, S. Kölling, M. G. Geers, J. Sietsma, R. Petrov, V. Bliznuk, P. M. Koenraad, D. Schryvers, and B. Amin-Ahmadi, "Martensite crystallography and chemistry in dual phase and fully martensitic steels," *Materials Characterization*, vol. 139, no. October 2017, pp. 411–420, 2018, ISSN: 10445803. DOI: 10.1016/j.matchar.2018.03.011.

[7] S. Morito, H. Tanaka, R. Konishi, T. Furuhara, and T. Maki, "The morphology and crystallography of lath martensite in Fe-C alloys," vol. 51, pp. 1789–1799, 2003. DOI: 10.1016/S1359-6454(02)00577-3.

[8] S. Morito, H. Yoshida, T. Maki, and X. Huang, "Effect of block size on the strength of lath martensite in low carbon steels," *Materials Science and Engineering A*, vol. 438-440, no. SPEC. ISS. Pp. 237–240, 2006, ISSN: 09215093. DOI: 10.1016/j.msea.2005.12.048.

[9] L. Qi, A. G. Khachaturyan, and J. W. Morris, "The microstructure of dislocated martensitic steel: Theory," *Acta Materialia*, vol. 76, pp. 23–39, 2014, ISSN: 13596454. DOI: 10.1016/j.actamat.2014.04.038.

[10] C. C. Kinney, K. R. Pytlewski, A. G. Khachaturyan, and J. W. Morris, "The microstructure of lath martensite in quenched 9Ni steel," *Acta Materialia*, vol. 69, pp. 372–385, 2014, ISSN: 13596454. DOI: 10.1016/j.actamat.2014.01.058.

[11] D. Sun, Z. Guo, and J. Gu, "The microstructure and crystallography of lath martensite with Greninger-Troiano orientation relationship in a Fe-12.8Ni-1.5Si-0.22%C steel," *Materials Characterization*, vol. 181, no. March, p. 111 501, 2021, ISSN: 10445803. DOI: 10.1016/j.matchar.2021.111501.

[12] L. Ryde, "Application of EBSD to analysis of microstructures in commercial steels Application of EBSD to analysis of microstructures in commercial steels," *Material Science and Technology*, vol. 0836, 2006. DOI: 10.1179/174328406X130948.

[13] F. Bachmann, R. Hielscher, and H. Schaeben, "Texture analysis with MTEX- Free and open source software toolbox," *Solid State Phenomena*, vol. 160, pp. 63–68, 2010, ISSN: 10120394. DOI: 10.4028/www.scientific.net/SSP.160.63.

[14] F. Niessen, T. Nyyssönen, A. A. Gazder, and R. Hielscher, "Parent grain reconstruction from partially or fully transformed microstructures in MTEX," *Journal of Applied Crystallography*, vol. 55, pp. 180–194, 2022, ISSN: 16005767. DOI: 10.1107/S1600576721011560. arXiv: 2104.14603.

[15] V. Atreya, "Unraveling the Role of Carbon on the Strengthening Mechanisms of Low Mn-Si Martensitic Steels," M.S. thesis, Delft University of Technology, 2017.

[16] H. Moulinec and P. Suquet, "A numerical method for computing the overall response of nonlinear composites with complex microstructure," *Computer Methods in Applied Mechanics and Engineering*, vol. 157, no. 1-2, pp. 69–94, 1998, ISSN: 00457825. DOI: 10.1016/S0045-7825(97)00218-1. arXiv: 2012.08962.

[17] J. S. Bowles and J. K. Mackenzie, "The crystallography of martensite transformations I," *Acta Metallurgica*, vol. 2, no. 1, pp. 129–137, 1954, ISSN: 00016160. DOI: 10.1016/0001-6160(54)90102-9.

[18] C. M. Wayman, "The phenomenological theory of martensite crystallography: Interrelationships," *Metallurgical and Materials Transactions A*, vol. 25, no. 9, pp. 1787–1795, 1994, ISSN: 10735623. DOI: 10.1007/BF02649029.

[19] A. Saha Podder and H. K. Bhadeshia, "Thermal stability of austenite retained in bainitic steels," *Materials Science and Engineering A*, vol. 527, no. 7-8, pp. 2121–2128, 2010, ISSN: 09215093. DOI: 10.1016/j.msea.2009.11.063.

[20] M. Kamaya, A. J. Wilkinson, and J. M. Titchmarsh, "Quantification of plastic strain of stainless steel and nickel alloy by electron backscatter diffraction," *Acta Materialia*, vol. 54, no. 2, pp. 539–548, 2006, ISSN: 13596454. DOI: 10.1016/j.actamat.2005.08.046.

[21] X. F. Gu, T. Furuhara, and W. Z. Zhang, "PTCLab: Free and open-source software for calculating phase transformation crystallography," *Journal of Applied Crystallography*, vol. 49, no. April, pp. 1099–1106, 2016, ISSN: 16005767. DOI: 10.1107/S1600576716006075.

[22] J. M. Moyer and G. S. Ansell, "The Volume Expansion Accompanying the Martensite Transformation in Iron-Carbon Alloys," *Metallurgical Transactions A*, vol. 6, no. September, pp. 1785–1791, 1975. DOI: 10.1007/BF02642308.

7

Conclusions

This thesis is an attempt to understand the deformation of the ferrite matrix resulting from austenite to martensite phase transformations in Dual-phase (DP) steels via experimental characterisation and numerical modelling. The cumulative martensitic phase transformation strain consists of dilatation and shear components, and its accommodation in the microstructure causes the deformation of the surrounding ferrite matrix. This alters the local mechanical properties of the ferritic matrix, which in turn influences the global mechanical properties of DP steel. Hence, for the rapid development of DP steels with application-specific mechanical properties, it is pertinent to experimentally characterise the transformation-induced deformation of ferrite and develop accurate models to predict the same.

This thesis starts with a review of the state-of-the-art experimental and modelling techniques and a discussion about the gaps in the understanding of transformation-induced deformation of ferrite. Next, a combined framework of cellular-automata-based microstructure evolution model and micromechanics is shown to be helpful in studying the effect of transformation-induced deformation of ferrite on the global mechanical behaviour of DP steels. For experimental characterisation, electron backscatter diffraction (EBSD) measurements are performed, where attention is paid to the less explored influence of crystallographic orientations of martensite variants and ferrite grains on the transformation-induced deformation of ferrite. Subsequently, the importance of considering the anisotropy of martensitic phase-transformation strain is illustrated using a novel methodology comprising sequential experimental and numerical research on DP steels to quantify transformation-induced strains in ferrite. Towards the end, the influence of the degree of self-accommodation in martensite due to the formation of variants on transformation-induced deformation of ferrite is investigated and discussed. Key takeaways from the chapters of this PhD thesis are summarised in the following section.

7.1. KEY TAKEAWAYS

- The martensitic transformation-induced deformation of ferrite in DP steels plays an important role in determining the overall mechanical behaviour of DP steels. At the onset of this thesis, state-of-the-art analytical and numerical techniques for modelling the transformation-induced deformation of ferrite are critically assessed. It is concluded that in order to arrive at a realistic estimation of the transformation-induced ferrite deformation field, the modelling approach should consider the influence of crystallographic, morphological and compositional characteristics of martensite on the transformation-induced deformation of ferrite.

- The modelling technique based on the ‘core and mantle’ approach, where transformation-induced plastically deformed regions of ferrite are modelled as an interphase layer of strain-hardened ferrite, is adequate for a qualitative prediction of the overall mechanical behaviour of DP steels. However, in this approach, the local variations

in spatial extent and magnitude of interphase layer hardening as a function of local microstructural features are required to be known beforehand. No quantitative estimates of the influence of such features on the interphase layer exist which can be extended to the whole microstructure. Therefore, EBSD experiments were carried out to identify and study in detail the influence of these microstructural features on the transformation-induced deformation of ferrite.

- There are two types of deformation observed in ferrite grains: a type I long-range (LR) deformation that covers the majority of the ferrite grain area, and a type II short-range (SR) deformation in the form of a deformed ferrite region at the ferrite/martensite phase boundaries. When PAGS is small, austenite may transform into martensitic variants having a (110) CPPP relationship with neighbouring ferrite. This enables effective relaxation of transformation stresses by relatively easy deformation of ferrite and results in type I LR deformation. It was observed that most ferrite grains with type I LR deformation also possess a (110) CPPP relationship with several surrounding martensite variants. In the absence of a (110) CPPP relationship, type II SR deformation was observed.

- In previous studies on modelling the transformation-induced deformation of ferrite, the anisotropy of transformation deformation is ignored. Rather, isotropic dilatation alone is considered to induce the deformation of the ferritic matrix. It is shown in this study that the assumption of isotropic dilatation, which neglects the shear deformation associated with martensitic transformation, results in a significant underestimation of transformation-induced strains in ferrite. A four-step methodology is developed which also takes into account the PAG orientation and morphology while calculating the transformation-induced strains in ferrite.

- The higher the number of variants which form in a PAG, the less deformation it causes in the surrounding ferrite matrix upon transformation. The highest number of variants are observed to form in large PAGS. When three or fewer variants are formed, the ferrite deformation is relatively large. But as the number of variants increases, the ferrite deformation localises. This is because of a decrease in the effective shear magnitude of transformation, which cancels out completely when all twenty-four variants are formed from a PAG. Therefore, if the PAGS is large leading to a high degree of self-accommodation, neither type I LR nor type II SR deformation is observed in the surrounding ferrite matrix.

7.2. APPLICATION OF THIS STUDY

As discussed in Chapter 2, a cellular-automata-based microstructure evolution model combined with a suitable micromechanical model can be an effective way to model the transformation-induced deformation of ferrite. Figure 7.1(a) shows a 2D representative volume element (RVE) of DP steel containing 50 vol.% ferrite, obtained using the CA-based

microstructural evolution model. The details of the model can be found in the literature [1], [2] and Chapter 2. The RVE shows martensitic variants in form of laths. Different colours of martensitic laths represent the twenty-four variants which are formed from a single PAG. In reality, every martensitic variant contains numerous laths and the shape of a variant region is quite different from that of a lath.

The RVE was used as an input to the micromechanical model, which allows for the definition of the eigenstrains in specific grains or phases and calculates the resulting strains/stresses in the remaining microstructure [3]. Here, the eigenstrains were calculated for every variant using the prior austenite grain (PAG) orientation and phenomenological theory of martensite crystallography (PTMC), assuming the carbon content in martensite to be 0.2 wt.%. The complete procedure along with the material properties and boundary conditions used is elaborated in Chapter 5. Figure 7.1(b) shows the transformation-induced strain in ferrite calculated using the aforementioned micromechanical model. The martensite in the figure is masked by black colour for better visibility of strains in ferrite.

As per the author's knowledge, the calculation of transformation-induced deformation of ferrite for RVEs with realistic martensitic microstructure has not been reported previously. The ferrite strain map such as in figure 7.1(b) can also be calculated for 3D DP RVEs. If the hierarchical microstructure of martensite in the form of sub-blocks, blocks and packets is also incorporated in the RVEs, it can be used to calculate transformation-induced strain maps with more accuracy for any multi-phase steel microstructure containing martensite. Furthermore, the effect of transformation-induced strains/stresses on the overall mechanical behaviour of RVE can be studied, for example, by simulating a virtual uniaxial tensile test on a DP steel RVE with pre-existing transformation-induced strains/stresses in ferrite.

7.3. RECOMMENDATIONS FOR FUTURE WORKS

Although this work presents a complete framework to calculate transformation-induced strains in ferrite of DP steels for both virtual and real microstructures, the following improvements can be made in the models used in order to increase the robustness and versatility of the predictions.

7.3.1. USING FINITE-STRAIN AND CRYSTAL PLASTICITY BASED MICROMECHANICAL MODEL

In this study, a small-strain formulation was used where the second-order terms from the definition of finite strain are neglected. Therefore any significant transformation-induced rotation in the material contributes to the error in calculated transformation-induced strains. Moreover, isotropic plasticity and linear hardening were assumed for ferrite. However, the extent and magnitude of transformation-induced strains within the ferrite

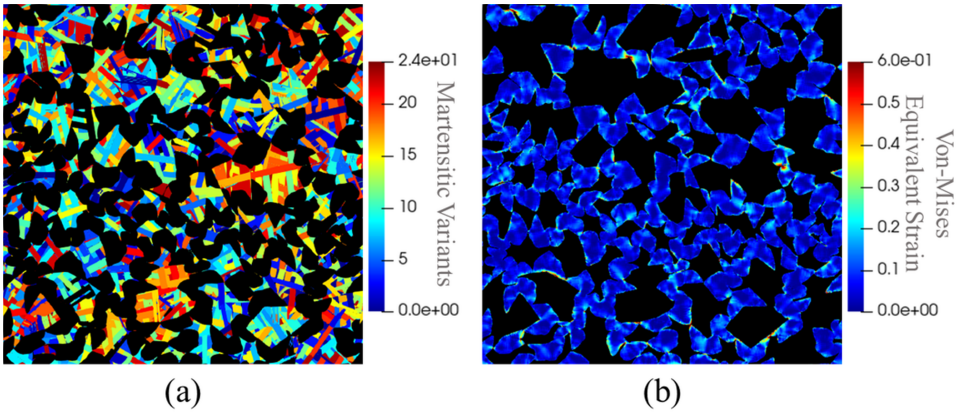

Figure 7.1: (a) A Dual-phase (DP) representative volume element (RVE) showing ferrite in black and twenty-four martensitic variants in different colours (b) Transformation-induced strains in ferrite. The martensite is masked by black colour.

grains must depend upon the orientation of its slip planes. Therefore, for accurate quantitative modelling of transformation-induced deformation of ferrite, a finite-strain and crystal plasticity-based micromechanical model is desirable. With the increased complexity of the micromechanical model and by incorporating finite strains in the calculations, the challenge then would be to ensure that the iterative solution scheme converges into a solution.

7.3.2. PRIOR AUSTENITE GRAIN RECONSTRUCTION BASED ON 3D EBSD MEASUREMENTS

In this study, the transformation-induced deformation of ferrite is characterised via EBSD experiments, in which the measurement is performed on the surface of the specimen. The disadvantage of 2D measurement is that the contribution of the martensite which is below the observed surface to the transformation-induced deformation of the observed ferrite grain can not be ascertained. For this, EBSD measurements performed in conjugation with serial sectioning along one of the specimen axes are required. Although time-consuming and difficult to perform, this kind of 3D EBSD measurements on DP steel specimens have been reported in previous studies [4].

For using 3D EBSD data to validate the 3D modelling results, a procedure for 3D reconstruction of PAGs is required. As explained in Chapter 5, the calculation of the transformation shape strain of every observed variant on the EBSD map requires PAG orientations obtained via reconstruction and the use of PTMC. As per the author's knowledge, no such software/algorithm yet exists that possesses the capability to reconstruct PAGs in 3D.

7.3.3. LOCAL VARIATIONS IN TRANSFORMATION STRAIN AND ORIENTATION RELATIONSHIPS BASED ON THE CARBON CONTENT OF MARTENSITE

During the manufacturing of DP steels, prior to the quenching step which transforms austenite into martensite, the austenite grains at different locations in the microstructure can have a different carbon content. The magnitude of transformation deformation depends upon the carbon content of austenite. Also, it is well known that the habit plane of martensite (which is parallel to the shear component and perpendicular to the dilation component of the transformation deformation) varies according to the carbon content of transforming austenite [5], [6]. Moreover, observed orientation relationships gradually change from K-S to N-W with the increasing carbon content of austenite [7]. Local variations in the aforementioned quantities can be incorporated into the models if the carbon content of prior austenite is known. While simulating microstructure evolution, it is possible to use models which track the carbon concentration of PAGs. However, it is difficult to ascertain the carbon concentration of all observed PAGs from an EBSD scan, which presents a major challenge in PAG reconstruction and the use of PTMC.

REFERENCES

[1] C. Bos, M. G. Mecozzi, and J. Sietsma, "A microstructure model for recrystallisation and phase transformation during the dual-phase steel annealing cycle," *Computational Materials Science*, vol. 48, no. 3, pp. 692–699, 2010, ISSN: 09270256. DOI: 10.1016/j.commatsci.2010.03.010.

[2] C. Bos, M. G. Mecozzi, D. N. Hanlon, M. P. Aarnts, and J. Sietsma, "Application of a three-dimensional microstructure evolution model to identify key process settings for the production of dual-phase steels," *Metallurgical and Materials Transactions A: Physical Metallurgy and Materials Science*, vol. 42, no. 12, pp. 3602–3610, 2011, ISSN: 10735623. DOI: 10.1007/s11661-011-0696-x.

[3] H. Moulinec and P. Suquet, "A numerical method for computing the overall response of nonlinear composites with complex microstructure," *Computer Methods in Applied Mechanics and Engineering*, vol. 157, no. 1-2, pp. 69–94, 1998, ISSN: 00457825. DOI: 10.1016/S0045-7825(97)00218-1. arXiv: 2012.08962.

[4] M. Calcagnotto, D. Ponge, E. Demir, and D. Raabe, "Orientation gradients and geometrically necessary dislocations in ultrafine grained dual-phase steels studied by 2D and 3D EBSD," *Materials Science and Engineering A*, vol. 527, no. 10-11, pp. 2738–2746, 2010, ISSN: 09215093. DOI: 10.1016/j.msea.2010.01.004.

[5] P. M. Kelly and J. Nutting, "The martensite transformation in carbon steels," *Proceedings of the Royal Society of London. Series A. Mathematical and Physical Sciences*, vol. 259, no. 1296, pp. 45–58, 1960, ISSN: 0080-4630. DOI: 10.1098/rspa.1960.0210.

[6] C. M. Wayman, "The phenomenological theory of martensite crystallography: Interrelationships," *Metallurgical and Materials Transactions A*, vol. 25, no. 9, pp. 1787–1795, 1994, ISSN: 10735623. DOI: 10.1007/BF02649029.

[7] K. Zhang, P. Liu, W. Li, F. C. Ma, and Y. H. Rong, "Quantitative Analysis of the Crystallographic Orientation Relationship Between the Martensite and Austenite in Quenching – Partitioning – Tempering Steels," *Acta Metallurgica Sinica (English Letters)*, vol. 31, no. 6, pp. 659–667, 2018, ISSN: 21941289. DOI: 10.1007/s40195-017-0683-3.

A

APPENDIX

THE MICROMECHANICAL MODEL

The macroscopic behaviour of a homogenized elastic composite is given as:

$$\boldsymbol{S} = \mathscr{C} : \boldsymbol{E}, \tag{A.1}$$

where $\mathscr{C}$ is the effective elastic moduli, $\boldsymbol{S}$ and $\boldsymbol{E}$ are the averages of stress field, $\boldsymbol{\sigma}(\boldsymbol{x})$, and strain field, $\boldsymbol{\epsilon}(\boldsymbol{x})$, respectively, which are computed as the solution of following problem:

$$\begin{cases} \boldsymbol{\sigma}(\boldsymbol{x}) = \mathscr{C}^{\mathrm{r}} : \boldsymbol{\epsilon}(\boldsymbol{x}), & \\ \boldsymbol{\epsilon}(\boldsymbol{x}) = \boldsymbol{\epsilon}\left(\boldsymbol{u}^{+}(\boldsymbol{x})\right) + \boldsymbol{E}, & \forall \boldsymbol{x} \in V \\ \nabla \cdot \boldsymbol{\sigma}(\boldsymbol{x}) = 0, & \forall \boldsymbol{x} \in V \\ \boldsymbol{u}^{+} \text{ is periodic}, & \boldsymbol{\sigma} : \hat{\boldsymbol{n}} \text{ is anti-periodic}, \end{cases} \tag{A.2}$$

where $\mathscr{C}^{\mathrm{r}}$ is the elastic moduli tensor in phase r, $\boldsymbol{\epsilon}\left(\boldsymbol{u}^{+}(\boldsymbol{x})\right)$ is the polarization field of strain and V is the periodic volume. To solve a set of equations A.2, a fast fourier transform (FFT) based method is developed by H. Moulinec and P. Suquet [1] is used. The problem A.2 is then replaced by an auxiliary problem which includes a linear homogenous elastic body of stiffness $\mathscr{C}^{0}$ under a polarization field $\boldsymbol{\tau}(\boldsymbol{x})$.

$$\begin{cases} \boldsymbol{\sigma}(\boldsymbol{x}) = \mathscr{C}^0 : \boldsymbol{\epsilon}(\boldsymbol{x}) + \boldsymbol{\tau}(\boldsymbol{x}), & \\ \boldsymbol{\tau}(\boldsymbol{x}) = \left(\mathscr{C}^r - \mathscr{C}^0\right) : \boldsymbol{\epsilon}(\boldsymbol{x}), & \\ \boldsymbol{\epsilon}(\boldsymbol{x}) = \boldsymbol{E} - \Gamma^0 * \boldsymbol{\tau}(\boldsymbol{x}), & \forall \boldsymbol{x} \in V \\ \nabla \cdot \sigma(\boldsymbol{x}) = 0, & \forall \boldsymbol{x} \in V \\ \boldsymbol{u}^+ \text{ is periodic}, & \boldsymbol{\sigma} : \hat{\boldsymbol{n}} \text{ is anti-periodic}, \end{cases} \tag{A.3}$$

with the periodic Green's operator Γ^0 associated with $\mathscr{C}^0$ and $*$ the convolution product. The Γ^0 operator is explicitly known in fourier space. In the current work, $\boldsymbol{\epsilon}(\boldsymbol{x})$ is initialized with values of transformation eigenstrains for martensitic variants $\boldsymbol{\epsilon}^*(\boldsymbol{x})$. The isotropic transformation eigenstrain, $\boldsymbol{\epsilon}^{*,\text{iso}}$ is given by $(\delta/3)\,\boldsymbol{\epsilon}_{ii}$, where δ is given by equation 5.11, while anisotropic transformation eigenstrains are calculated from deformation gradient matrix $\mathbf{Z}$ obtained via PTMC theory using the definition of Green-Lagrange strain:

$$\boldsymbol{\epsilon}^{*,\text{aniso}}(\boldsymbol{x}) = \frac{1}{2}\left[\mathbf{Z}(\boldsymbol{x})^{\mathrm{T}} \cdot \mathbf{Z}(\boldsymbol{x}) - \mathrm{I}\right], \tag{A.4}$$

where I is the identity matrix. Subsequently, $\boldsymbol{\epsilon}^*(\boldsymbol{x})$ is used to calculate the polarization field $\boldsymbol{\tau}(\boldsymbol{x})$ which is held constant. Problem A.3 is then solved iteratively. The convergence is reached when error e is below a specified value:

$$e = \frac{\left(\langle \| \nabla \cdot \sigma \|^2 \rangle\right)^{\frac{1}{2}}}{\| \langle \sigma \rangle \|}, \tag{A.5}$$

The elastic-plastic von-Mises materials obey the following linear hardening law:

$$\begin{cases} \boldsymbol{\sigma} = \mathscr{C}^{\mathrm{r}}\left(\boldsymbol{\epsilon} - \boldsymbol{\epsilon}_{\mathrm{p}}\right), \\ \dot{\boldsymbol{\epsilon}}_{\mathrm{p}} = \dfrac{3}{2}\,\dot{p}\,\dfrac{\boldsymbol{\sigma}_{\mathrm{d}}}{\boldsymbol{\sigma}_{\mathrm{vM}}} \text{ where } p = \dfrac{2}{3}\sqrt{\boldsymbol{\epsilon}_{\mathrm{p}} \cdot \boldsymbol{\epsilon}_{\mathrm{p}}}, \\ \sigma_{\mathrm{vM}} \geq \sigma_{\mathrm{Y}}, \end{cases} \tag{A.6}$$

where $\boldsymbol{\epsilon}_{\mathrm{p}}$ is the deviatoric plastic strain, $\boldsymbol{\sigma}_{\mathrm{d}}$ and σ_{vM} are the deviatoric stress and von-Mises equivalent stress respectively, p is the hardening parameter and σ_{Y} is the yield strength.

ACKNOWLEDGEMENTS

As the journey of pursuing a PhD inches towards its conclusion, all the attention is usually focused on a single individual. However, it's the behind-the-scene collaborative effort of several people which has resulted in the research work compiled in this thesis. First and foremost, I offer my heartfelt gratitude to Prof. Dr. M. J. Santofimia and Dr. ir. C.Bos for providing me with the opportunity to work on this PhD project. The encouragement, support, freedom and trust they provided me throughout the project have been instrumental in shaping me into the confident independent researcher that I am today.

I would like to thank Tata Steel, Ijmuiden and the material innovation institute (M2i) for conceptualising and bringing to fruition the Digitally Enhanced New Steel (DENS) Development programme, of which my PhD project was a part. This provided an excellent platform for close collaborations and discussions among several fellow PhD researchers involved in the project and experts at Tata Steel. The time spent at several DENS conferences provided valuable feedback and learning. Being an M2i PhD Researcher, participating in yearly M2i conferences was exciting and provided immense exposure to me as a young researcher.

This incredible journey of PhD would not have been possible without coming in contact with some amazing folks. I am highly indebted to Jan and Arthur for the time they spent with me on the coding and scientific discussions, and most importantly for showing how pushing the boundaries of understanding can be fun. The journey of PhD was full of ups and downs. It was the people with whom I had the pleasure to interact on daily basis, who helped me grow not only as a researcher but also as a person. I will miss sharing the DENS office space with Jhon, Arthur, Xiaohui, Jesús and Pablo. I will fondly remember numerous pleasant interactions with my fellow researchers Jithin, Farnaz, Vitória, Soroush, Pablo, Jaji, Aravind, Gaojie, Emiliano, Daniel, Rutger, Javier, Alfonso, Sudheendra, Wei and Konstantina. I also thank my colleagues from DENS programme Vitesh, Sharan, Lei, Vahid, Mahdi and Shahrzad for being a part of this beautiful journey and making it worth remembering.

I would like to thank Piet Kok (now retired) and Eisso Atzema from Tata Steel for very helpful discussions during the initial stages of the project. I also thank Monika Krugla from Tata Steel, and Nico Geerlofs, technical staff of the MSE laboratory, for helping me with the experimental work. An additional challenge during the PhD was confronting the Covid-19 pandemic, which reduced social contact to a minimum for over a year. I feel blessed to have a small coterie of friends from my masters, Nirmal, Sambit, Varun,

and friends from India, Pradyumn, Ankit and Jayant, who have been there in thick and thin and provided the much-needed support system in challenging times, distances notwithstanding.

In the end, I want to offer my heartiest gratitude to my family. Without their support, trust and sacrifices, it would not have been possible for me to be where I am today. To my dear wife and my best friend, Bhavya, thank you for being the pillar of support in my life since I was a teenager. I thank my parents – their enthusiasm and encouragement for their children to achieve the best possible life often hid the struggles they had to face. To my dear sister, Niyati, thank you for always being my biggest cheerleader and a bundle of joy for the whole family.

CURRICULUM VITÆ

Vibhor ATREYA

Born on September 15, 1991 in Meerut, India.

PROFESSIONAL EXPERIENCE

06.2022-Present	Process Simulation Engineer Bosch Transmission Technology BV, Tilburg, the Netherlands
04.2018-05.2022	PhD Researcher Delft University of Technology, the Netherlands
01.2017-04.2017	Industrial Internship (within Masters) Tata Steel Europe, Ijmuiden, the Netherlands
06.2014-09.2014	Graduate Engineer Trainee SKF India Limited, Pune, India
08.2013-12.2013	Industrial Internship (within Bachelors) Tata Technologies Limited, Pune, India

EDUCATION

04.2018-05.2022	PhD in Material Science and Engineering Delft University of Technology, the Netherlands
09.2015-08.2017	Master of Science in Mechanical Engineering (Track: Materials Engineering and Applications) Delft University of Technology, the Netherlands
08.2009-05.2014	Master of Science in Biological Sciences Bachelor of Engineering in Mechanical Engineering Birla Institute of Technology & Science, Goa, India

EXTRACURRICULAR ACTIVITIES

07.2016-12.2016	Teacher, eVidyaloka Trust, India Interactive online classes for the children via the digital classrooms set up in rural India.

LANGUAGES

Hindi	Native
English	Full Professional Proficiency
Dutch	Beginner's level (A1/A2)

LIST OF PUBLICATIONS

5. **V. Atreya**, C. Bos, and M. J. Santofimia, "Characterisation and modelling of transformation-induced deformation of ferrite: A Review." To be submmitted for publication.

4. **V. Atreya**, C. Bos, and M. J. Santofimia, "Influence of self-accommodation in martensite on the transformation-induced deformation of ferrite in DP steels." To be submmitted for publication.

3. **V. Atreya**, J. S. Van Dokkum, C. Bos, and M. J. Santofimia, "Effect of the anisotropy of martensitic transformation on ferrite deformation in Dual-Phase steels", *Materials & Design*, vol. 219, p. 110805, 2022 (2022).

2. **V. Atreya**, C. Bos, and M. J. Santofimia, "Understanding ferrite deformation caused by austenite to martensite transformation in dual phase steels", *Scripta Materialia*, vol. 202, p. 114 032, 2021.

1. **V. Atreya**, C. Bos, and M. J. Santofimia, "Cellular Automata modelling of plastic deformation in ferrite during martensite formation in Dual-Phase steels", in *Proceedings of the 8th International Conference on Modeling and Simulation of Metallurgical Processes in Steelmaking (STEELSIM 2019)*, Toronto, Canada, 2019.

List of Conference Presentations

5. **V. Atreya**, J. S. Van Dokkum, C. Bos, and M. J. Santofimia, "Effect of variant selection on martensitic transformation induced deformation of ferrite in Dual-phase steels", International Conference on Martensitic Transformation (ICOMAT), March 13-18, 2022, S. Korea - **Oral presentation**.

4. **V. Atreya**, C. Bos, and M. J. Santofimia, "Using martensitic crystallography to determine transformation-induced deformation of ferrite in dual-phase steels", Material Science & Technology (MS&T) Technical Meeting and Exhibition, October 17-20, 2021, Columbus, Ohio, USA - **Oral presentation**.

3. **V. Atreya**, C. Bos, and M. J. Santofimia, "Effect of martensite island size on transformation induced deformation of ferrite in DP steels", Material Science and Engineering (MSE) Congress, September 22-25, 2020, Darmstadt, Germany - **Oral presentation**.

2. **V. Atreya**, C. Bos, and M. J. Santofimia, "EBSD evaluation of martensitic transformation induced deformations in ferrite grains in DP steel microstructures", European Congress and Exhibition on Advanced Materials and Processes (EUROMAT), September 1-5, 2019, Stockholm, Sweden - **Oral presentation**.

1. **V. Atreya**, C. Bos, and M. J. Santofimia, "Cellular Automata modelling of plastic deformation in ferrite during martensite formation in Dual-Phase steels", 8th International Conference on Modeling and Simulation of Metallurgical Processes in Steelmaking (STEELSIM), August 11-15, 2019, Toronto, Canada - **Oral presentation**.